FIELD STUDY AND TESTS OF SEVERAL ONE-DIMENSIONAL SEDIMENT-TRANSPORT COMPUTER MODELS FOR POOL 20, MISSISSIPPI RIVER

by

Tatsuaki Nakato & John L. Vadnal

July 1981

Submitted to

GREAT-II Dredging Requirements Work Group
U.S. Army Corps of Engineers
Rock Island District
Rock Island, Illinois

ABSTRACT

To test the applicability of various one-dimensional sediment-transport numerical models of movable-bed channels to Pool 20 of the Mississippi River, detailed field data were first collected, and several numerical models were subsequently evaluated using these field data.

Chapter I describes the detailed results from a sediment sampling field study conducted in 1978 near Buzzard Island (RM 347-55) in Pool 20 of the Mississippi River. Variations in the longitudinal and transverse distributions are presented for various flow quantities and sediment characteristics, and are analyzed in connection with the prevalent shoaling problem in the Buzzard Island study reach.

Chapter II evaluates the performance of four mathematical simulation models which used the data from a complimentary field study conducted in 1976 to establish the initial conditions when predicting the 1978 conditions. The four models evaluated were: (1) the HEC-6 model provided by the Hydrologic Engineering Center, U.S. Army Corps of Engineers; (2) the SUSR and (3) UUWSR models employed at the Colorado State University; and (4) the CHAR2 model used by the Sogreah consulting firm in Grenoble, France.

ACKNOWLEDGMENTS

The authors wish to extend their gratitude to the persons (listed by group or organization) whose contributions enabled the sediment field study and subsequent analyses of various mathematical models. First, from the U.S. Army Corps of Engineers, Rock Island District, to Messrs. Marvin Martens, William Koellner, and Satyesh Nanda who assisted in the compilation of hydrologic, geomorphic, and sediment data involving the Mississippi River study reach. From the U.S. Geological Survey Office in Iowa City, Iowa, to Mr. Wilbur J. Matthes Jr., without his involvement and their equipment the field study would not have been possible. From the Iowa Institute of Hydraulic Research, the University of Iowa, to Mr. Dale Harris and his staff, particularly, Mr. James R. Goss, in addition to the secretaries responsible for typing the report drafts and revisions. A special thanks to the Institute Director, Dr. John F. Kennedy, for his critical review of the report, to Dr. Arthur R. Giaquinta, for editing the manuscript, and to Mr. Charles P. Robison for proof-reading the manuscript. From the Weeg Computer Center, the University of Iowa, to Mr. David W. Webb, for his computer programming consultation. Finally, to the authors and providers of the mathematical models evaluated: Drs. Y.H. Chen and D.B. Simons, for the two Colorado State University models; Dr. J.A. Cunge, the Sogreah consulting firm, Grenoble, France, for the CHAR2 model; and Dr. Michael Gee, from the Hydrologic Engineering Center, Davis, California, whose recommendations and explanations enabled the HEC-6 model to be employed by the authors at the University of Iowa.

TABLE OF CONTENTS

LIST OF TABLES

LIST OF FIGURES

LIST OF SYMBOLS

a = distance above river bed to sampler intake nozzle when suspended-sediment sampler is at the lowest vertical position

A = cross-sectional area of channel

C = point-integrated local suspended-sediment concentration

$\bar{C}$ = mean suspended-sediment concentration averaged over depth

d = local flow depth

$\bar{d}$ = mean flow depth (A/W)

D_{50} = median size of bed sediment

$\bar{D}_{50}$ = mean median size of bed sediment

D_g = geometric mean size of bed sediment

q = water discharge per unit width (Q/W)

Q = water discharge

q_B = bed-load discharge per unit width (Q_B/W)

q_i = water discharge for i-th subsection of transect

q_s = suspended-load discharge per unit width (Q_s/W)

Q_B = bed-load discharge

Q_s = suspended-load discharge

Q_T = total sediment discharge (Q_B+Q_s)

q_{Bi} = bed-load discharge for i-th subsection of transect

q_{si} = suspended-load discharge for i-th subsection of transect

$\bar{q}$ = water discharge per unit width (q_i/W_i)

$\bar{q}_B$ = bed-load discharge per unit width (q_{Bi}/W_i)

$\bar{q}_s$ = suspended-load discharge per unit width (q_{si}/W_i)

S = slope of energy gradient

T = surface water temperature

u = local flow velocity

U = mean flow velocity (Q/A)

$\bar{u}$ = mean flow velocity at vertical

u_* = shear velocity

w = fall velocity of sediment particle

W = channel width

W_i = width of i-th subsection of transect

y = distance above river bed

z = Rouse number ($w/\beta\kappa u_*$)

Z = distance from right bank

β = ratio of ε_s to ε_m ($\varepsilon_s/\varepsilon_m$)

ε_m = diffusion coefficient for momentum

ε_s = diffusion coefficient for sediment

κ = Kármán constant

σ_g = geometric standard deviation of particle size

LIST OF U.S. CUSTOMARY SI CONVERSION FACTORS

To convert	to	multiply by
inches (in.)	millimeters (mm)	25.40
inches (in.)	centimeters (cm)	2.540
inches (in.)	meters (m)	0.0254
feet (ft)	meters (m)	0.305
miles (mi)	kilometers (km)	1.61
yards (yd)	meters (m)	0.91
cubic inches (cu in.)	cubic centimeters (cm^3)	16.4
cubic feet (cu ft)	cubic meters (m^3)	0.028
cubic yards (cu yd)	cubic meters (m^3)	0.765
pounds (lb)	kilograms (kg)	0.453
tons (ton)	kilograms (kg)	1000.0

FIELD STUDY AND TESTS OF SEVERAL ONE-DIMENSIONAL SEDIMENT-TRANSPORT COMPUTER MODELS FOR POOL 20, MISSISSIPPI RIVER

I. 1978 FIELD STUDY AND DATA PRESENTATION

A. Introduction. The field study was conducted to obtain detailed information concerning the flow and sediment-transport characteristics along the Mississippi River reach near Buzzard Island (river mile (RM) 349-51). The location of the study reach is shown in figure I-A.1. The field data collected during the study were obtained to help explain and lead to a better understanding of the river processes that create a shoaling problem in the vicinity of the downstream tip of Buzzard Island. There are several related adverse consequences of this shoaling problem. Foremost is the adverse effect that the shoaling has on the navigation channel. Significant rises in the bed elevation due to sediment deposition can obstruct barge traffic within the navigation channel, which must then be dredged to maintain the required 9-ft depth along the passageway. The cost of dredging has risen sharply in recent years, making dredging an expensive means of alleviating the shoaling problem. Another problem that must then be faced pertains to the disposal of the dredged material. This dredged material must be disposed of in accordance with the standards established by the various environmental and conservation agencies, so as not to be detrimental to the surrounding environment or wildlife.

There are three general features of the Mississippi River (MR) in the study reach that lead to the shoaling problem. First, the flow bifurcates at two locations near the downstream tip of Buzzard Island. The bifurcation of flow reduces the main channel flow and diminishes the sediment-transport capacity of the river. Second, the river widens in the shoaling area, which decreases the mean flow velocity and diminishes the sediment-transport capacity. Finally, the thalweg crosses the river in this reach. This so-called "cross-over" reach lacks the strong secondary currents that are produced in river bends which significantly

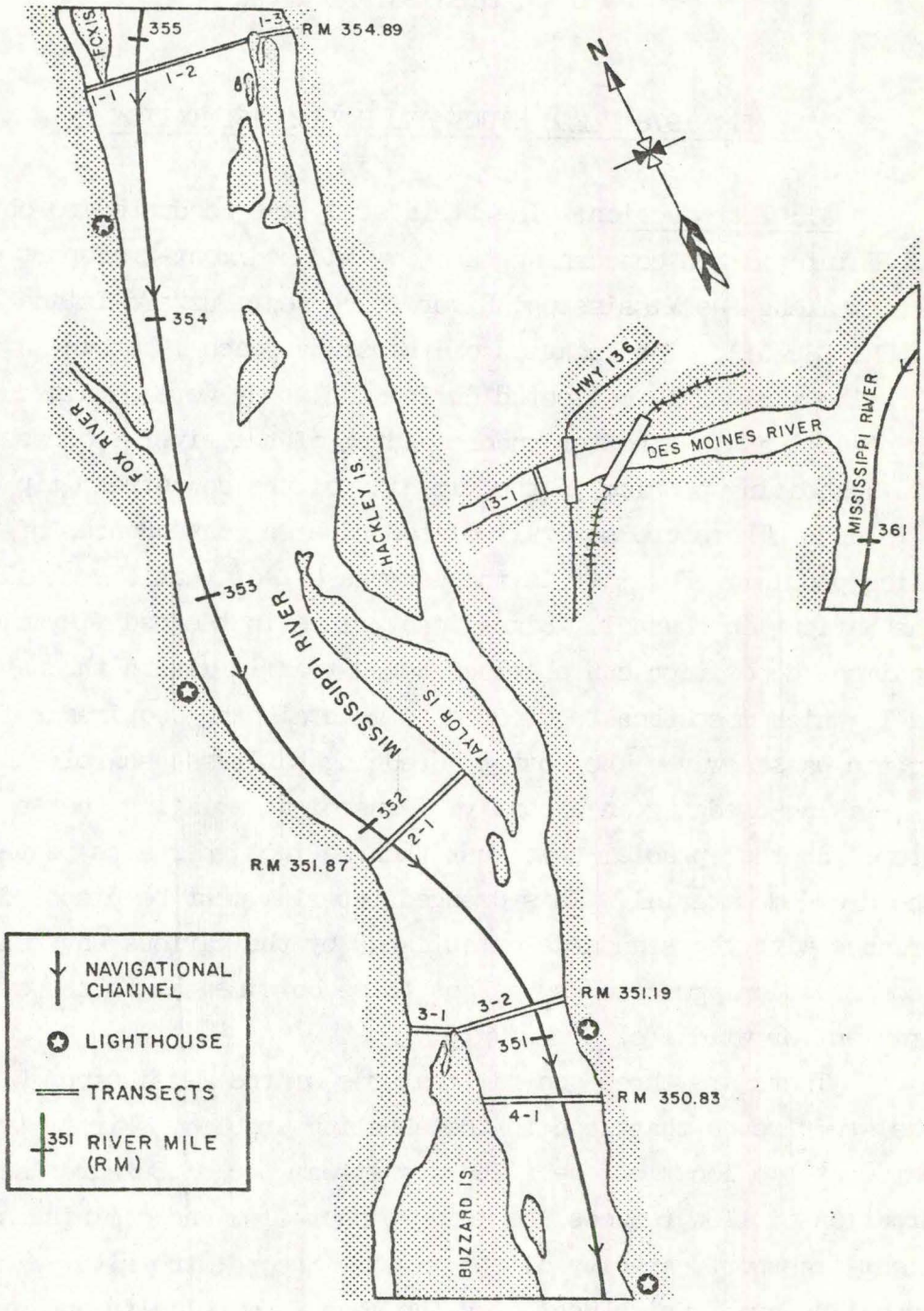

Figure I-A.1 Buzzard Island study reach

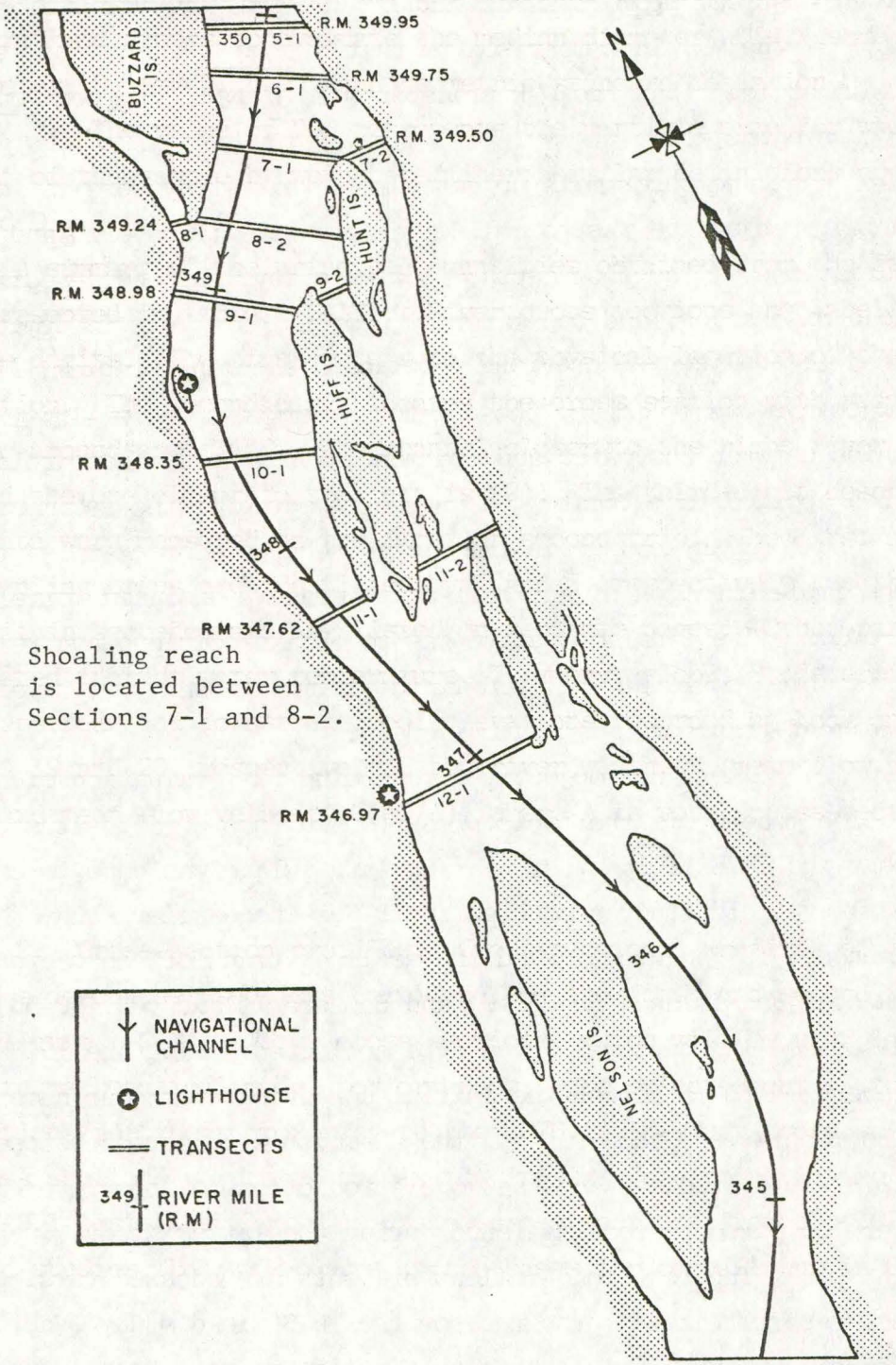

Note: Shoaling reach is located between Sections 7-1 and 8-2.

Figure I-A.1 (cont'd)

increase the sediment-transport capacity of the flow. The sediment being deposited in the study reach is thought to originate primarily from the Des Moines River (DMR), whose confluence with the MR is roughly 10 mi upstream from Buzzard Island. The smaller energy slope and velocity of the MR, in comparison to that of the DMR, are unable to carry the sediment load that the DMR transports to the MR, and sediment deposition occurs downstream.

The three main objectives of this study were as follows. The primary objective was to collect data on the transverse and streamwise variations of the flow depth, flow velocity, suspended-sediment and bed-load discharges, and bed-material properties. This information could be used to analyze the previously metioned shoaling problem. The second objective was to employ these data to formulate power-law relationships between the water and sediment discharges. These relationships were then applied to estimate the change expected in the sediment discharge as a result of any change in the flow discharge, for example, the effect of the implementation of any corrective measure designed to relieve the shoaling problem. The final objective was to obtain complete and reliable field data which could be utilized in the formation and testing of mathematical sediment-transport simulation models.

The final objective, regarding the evaluation of numerical simulation models, is the topic presented in Chapter II. It should be mentioned that the 1978 field study near Buzzard Island was done to complement an earlier field study conducted in 1976. The earlier study (Nakato and Kennedy, 1977) investigated the sediment transport characteristics of the MR near Fox Island (RM 355-6) and Buzzard Island (RM 449-50). As will be discussed in Chapter II, the data collected during the 1976 field study were used to establish the initial conditions for four numerical models. The models were then run for the 28-month time period between the 1976 and 1978 field studies, and the model predictions of the river characteristics were compared to results found during the latter study.

The text that follows presents a condensed version of the original report that was prepared for the 1978 field study (Vadnal, 1978). Readers who desire further clarification or more detail concerning the various subjects discussed herein should refer to the original report.

B. Equipment and Field-Laboratory Procedure. Data collection on the MR was conducted from the Iowa Institute of Hydraulic Research (IIHR) 18-foot Jon-Boat. A Price AA bucket-type current meter was used to obtain flow velocities, while the bed-material, depth-integrated suspended-sediment, and bed-load samples were collected using a US BM-54, US P-61, and Helley-Smith sampler, respectively. Sediment samples were taken at eight verticals that were fairly evenly spaced across the main-channel cross sections of the MR, while typically 3 or 4 verticals were sufficient for sampling the side-channel sections and the DMR. Consequently, these verticals established an identical number of subsections at each cross section for which the flow and sediment discharge characteristics would be determined. In addition to the sediment samples, flow velocities were measured at each vertical at two-tenths and eight-tenths of the flow depth, which were then averaged to obtain a mean subsection flow velocity. Detailed measurements of flow velocities and suspended-sediment concentrations were made at one vertical for each main-channel section in the MR and for the DMR.

Analyses of all sediment samples were performed at the IIHR according to recommended laboratory procedures (Guy, 1969). The analyses of the suspended-sediment samples gave the suspended-sediment concentrations, in parts per million (mg/l). Analyses of the bed-load samples gave the bed-load discharges and the bed-load particle-size graduations, while the bed-material analyses gave the bed-material particle-size distributions. The results of the particle-size analyses of all the bed-material samples collected during the two trips of the 1978 field study are tabulated in Appendix A.

C. Presentation and Discussion of Field Data.

1. Data analysis. Locations of twelve sampling sections were chosen in an arrangement that would enable the determination of the flow and sediment characteristics of the MR in the Buzzard Island study reach. Two data-collecting trips which gathered a total of 961 sediment samples were made during the 1978 field study: the first trip during 26 June - 12 July and the second trip during 14-25 August. The total discharge at each cross section, Q, was determined by summing the products of each average subsection flow velocity and the subsection area, determined

from the cross-section plot. Similar procedures were used to compute the suspended-sediment discharge, Q_S, and bed-load discharge, Q_B. The resulting size distributions of the bed-material samples were plotted on semi-logarithmic graphs to evaluate the median diameter, D_{50}, geometric mean diameter, D_g ($= \sqrt{D_{84}D_{16}}$), and geometric standard deviation, σ_g ($= \sqrt{D_{84}/D_{16}}$). The value of D_{50} represents the particle size for which 50 percent of the sample by weight is finer; similar definitions apply to D_{84} and D_{16}.

A summary of the principal quantities obtained from the field data is presented in table I-C-1.1. River cross sections are labelled with three digits. The first refers to the physical location of the cross section. The second digit locates the cross section with regard to passage around an island. The channel closer to the right river bank is (1) and the one closer to the left is (2). The third digit describes whether data were measured on the first or second trip. The first and second sampling trips are identified by 1 and 2, respectively, as the third digit in sequence and are listed on separate pages. Other parameters listed include water temperature, T, energy slope, S (determined from the upstream and downstream pool elevations recorded at Lock and Dams (L&D) 19 and 20, respectively), top river width, W, mean flow depth, $\bar{d}$(=A/W), and mean flow velocity U(=Q/A), where A is total cross-section flow area.

2. Cross-section profiles. Cross-sectional profiles of the main- and side-channel sections compiled from the first and second trips are shown in figure I-C-2.1. Five cross sections, which will be used later to evaluate mathematical model performances, were selected out of the 12 cross sections for their proximity to the 1976 field-study cross sections. These cross sections were used to fix the initial conditions in the models. Table I-C-2.1 lists the locations of the cross sections from the 1976 and 1978 field studies that will serve as the bases for comparisons in Chapter II.

Table I-C-1.1 Summary of Principal Quantities Obtained from the Field Data(1st Trip)

Date	Sec. No.	T (°F)	S	W (ft)	$\bar{d}$ (ft)	U (ft/s)	Q (cfs)	Q_B (tons/day)	Q_s (tons/day)	$\bar{D}_{50}$ (mm)	D_g (mm)	σ_g
062678	1-1-1	77	7.125×10^{-5}	331	8.0	1.86	4,902	3	10,062	0.25	cannot determine	
062678	1-2-1	78	7.125×10^{-5}	2,799	12.6	3.06	107,869	497	96,110	0.65	0.80	2.16
062778	1-3-1	78	7.179×10^{-5}	482	8.0	2.89	11,208	2,762	4,847	0.39	0.43	1.44
062778	2-1-1	78	7.179×10^{-5}	2,556	12.3	3.38	106,559	4,932	53,965	0.50	0.54	1.69
062978	3-1-1	80	7.513×10^{-5}	669	5.2	2.34	8,076	28	6,186	0.61	0.59	1.58
062778	3-2-1	79	7.179×10^{-5}	2,575	15.1	3.04	117,870	3,700	47,598	0.45	0.45	1.66
062978	4-1-1	80	7.513×10^{-5}	2,159	18.4	3.57	142,010	1,832	180,058	0.54	0.76	2.52
063078	5-1-1	81	7.089×10^{-5}	2,064	19.3	3.40	135,596	1,317	154,829	0.56	2.37	7.08
070578	6-1-1	81	7.287×10^{-5}	2,172	18.0	3.16	123,949	414	118,541	0.54	0.56	1.71
070578	7-1-1	81	7.287×10^{-5}	2,257	14.0	3.22	101,830	1,958	89,467	0.61	0.70	2.12
070678	7-2-1	81	7.422×10^{-5}	801	9.3	2.16	16,155	102	13,280	0.38	0.40	1.53
070678	8-1-1	82	7.422×10^{-5}	410	10.0	2.24	9,173	1	6,126	0.36	0.39	1.38
070678	8-2-1	81	7.422×10^{-5}	2,625	13.6	3.04	108,694	681	75,436	0.52	0.57	1.79
070778	9-1-1	81	7.846×10^{-5}	2,375	13.7	2.98	96,800	630	62,925	0.53	0.61	1.98
070778	9-2-1	81	7.846×10^{-5}	722	11.8	3.55	30,271	77	22,956	0.61	0.74	1.97
071178	10-1-1	77	7.215×10^{-5}	2,290	15.7	3.23	115,767	712	123,647	0.57	0.72	2.10
071078	11-1-1	78	7.143×10^{-5}	1,398	22.9	3.71	118,558	733	188,646	0.47	0.34	2.15
071078	11-2-1	78	7.143×10^{-5}	1,752	11.8	3.12	64,772	864	91,454	0.60	0.72	2.04
071178	12-1-1	78	7.215×10^{-5}	2,871	17.1	3.25	159,183	516	202,245	0.46	0.52	1.73
062678	13-1-1	77	2.436×10^{-4}	545	7.4	3.51	14,120	833	62,770	0.85	0.93	2.46
062978	13-1-1	80	2.189×10^{-4}	571	8.6	3.75	18,444	74	149,178	0.51	0.55	1.73
071278	13-1-1	76	1.840×10^{-4}	574	9.3	2.17	11,574	7	9,547	0.68	0.76	2.17

Table I-C-1.1 (cont'd) (2nd Trip)

Date	Sec. No.	T (°F)	S	W (ft)	$\bar{d}$ (ft)	U (ft/s)	Q (cfs)	Q_B (tons/day)	Q_s (tons/day)	$\bar{D}_{50}$ (mm)	D_g (mm)	σ_g
081578	1-1-2	79	1.840×10^{-5}	295	5.2	0.29	445	0.02	61	0.36	0.38	1.58
081678	1-2-2	77	1.759×10^{-5}	2,749	10.0	1.77	48,687	27	4,351	0.58	0.70	2.07
081578	1-3-2	79	1.840×10^{-5}	492	6.1	1.76	5,273	81	658	0.44	0.49	1.49
081478	2-1-2	81	1.515×10^{-5}	2,523	10.5	1.79	47,257	9.4	5,014	0.56	0.58	1.74
081678	3-1-2	79	1.759×10^{-5}	646	2.5	0.98	1,604	0.3	161	0.74	0.77	2.39
081678	3-2-2	79	1.759×10^{-5}	2,585	14.1	1.29	46,899	2.8	3,657	0.45	0.49	1.60
081778	4-1-2	77	1.127×10^{-5}	2,251	14.6	1.20	39,283	5	2,296	0.46	0.52	1.68
081778	5-1-2	78	1.127×10^{-5}	1,978	16.7	1.15	38,077	0.5	2,781	0.49	0.62	3.20
081878	6-1-2	77	1.163×10^{-5}	2,133	16.1	1.16	39,790	3.2	4,046	0.49	0.53	2.14
082178	7-1-2	77	1.461×10^{-5}	2,231	13.5	1.48	44,509	30	13,458	0.50	0.60	1.81
082178	7-2-2	75	1.461×10^{-5}	774	6.4	0.81	4,010	0.07	467	0.35	0.35	1.41
082278	8-1-2	79	1.723×10^{-5}	371	6.8	0.54	1,363	0.3	243	0.54	0.62	1.94
082178	8-2-2	77	1.461×10^{-5}	2,595	12.0	1.48	46,400	21	8,523	0.49	0.61	2.64
082278	9-1-2	79	1.723×10^{-5}	2,316	10.7	1.24	30,703	1.4	4,281	0.46	0.53	1.85
082278	9-2-2	79	1.723×10^{-5}	686	9.4	1.18	7,592	0.3	669	0.51	0.52	1.39
082278	10-1-2	79	1.723×10^{-5}	2,267	10.9	1.12	27,469	1.7	3,651	0.49	0.57	1.96
082378	11-1-2	77	1.389×10^{-5}	1,365	19.1	1.03	26,840	1.5	2,565	0.53	2.72	9.38
082378	11-2-2	77	1.389×10^{-5}	1,722	8.0	0.93	12,747	0.1	992	0.50	0.53	1.56
082478	12-1-2	78	1.383×10^{-5}	2,710	12.7	1.24	42,727	3.4	4,188	0.54	0.66	1.95
081478	13-1-2	79	2.171×10^{-4}	554	3.0	0.96	1,575	1.6	397	0.53	0.62	1.87
082578	13-1-2	79	2.132×10^{-4}	551	2.9	0.66	1,058	0.04	131	0.48	0.47	2.02

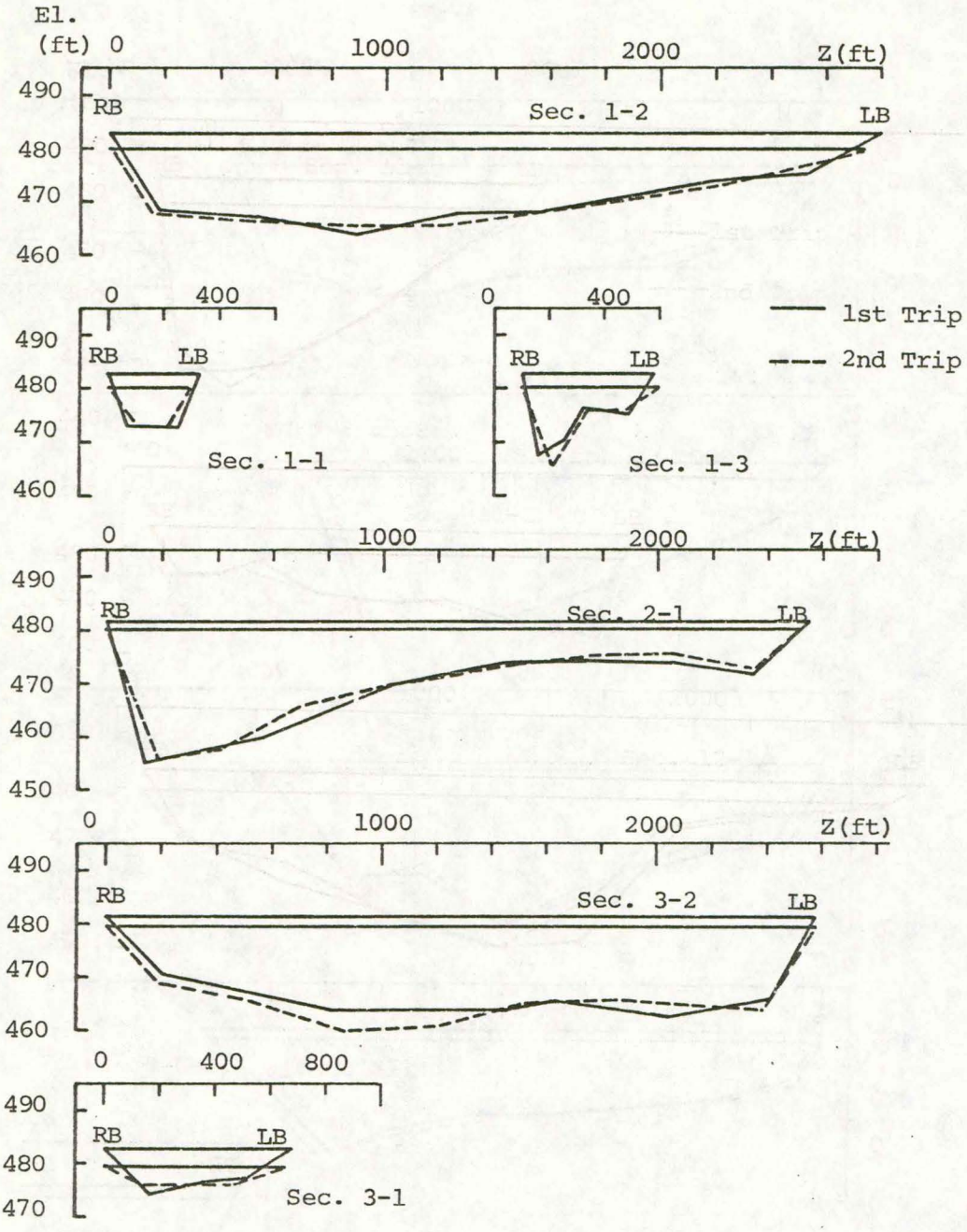

Figure I-C-2.1 Variations in the cross-sectional bed profiles

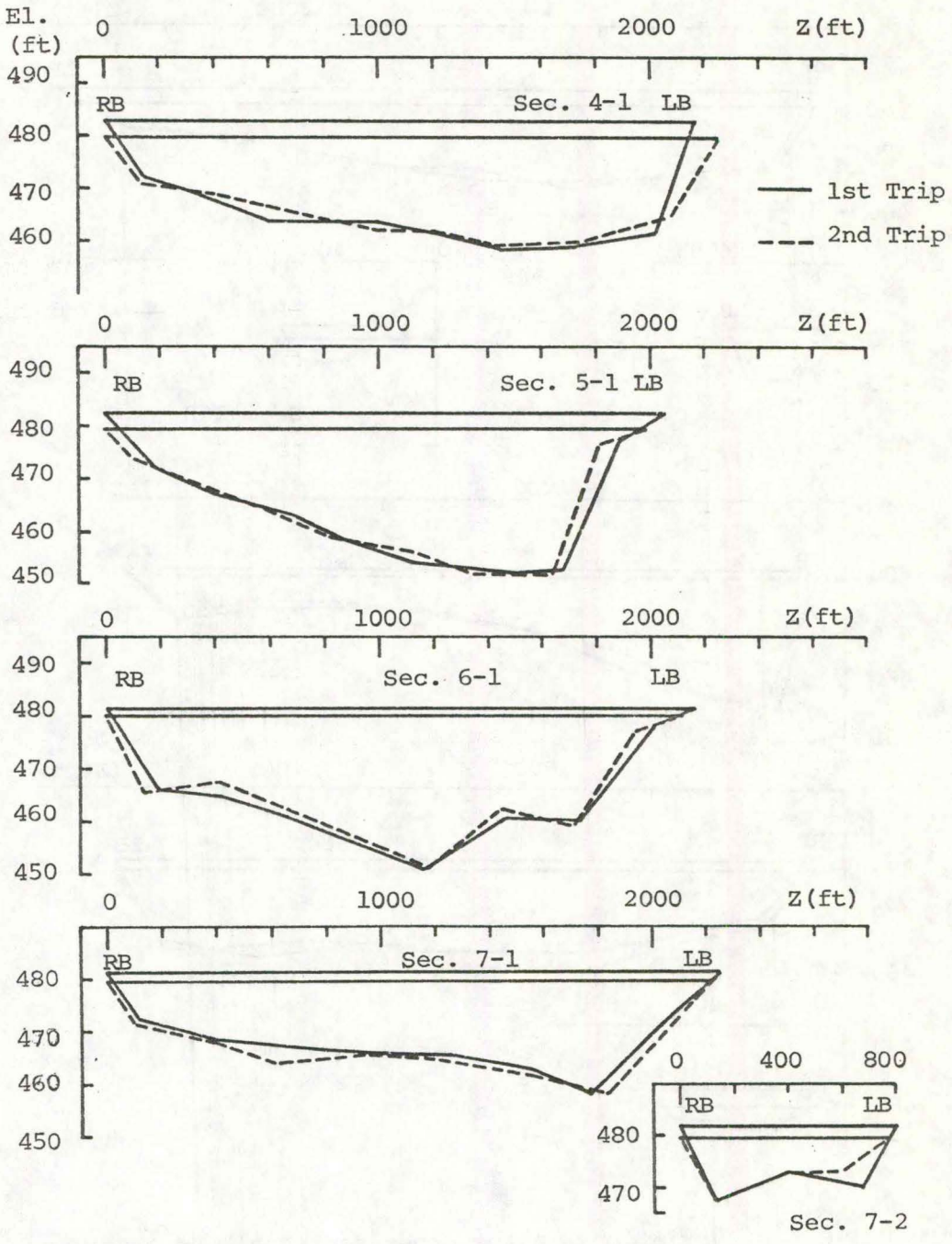

Figure I-C-2.1 (cont'd)

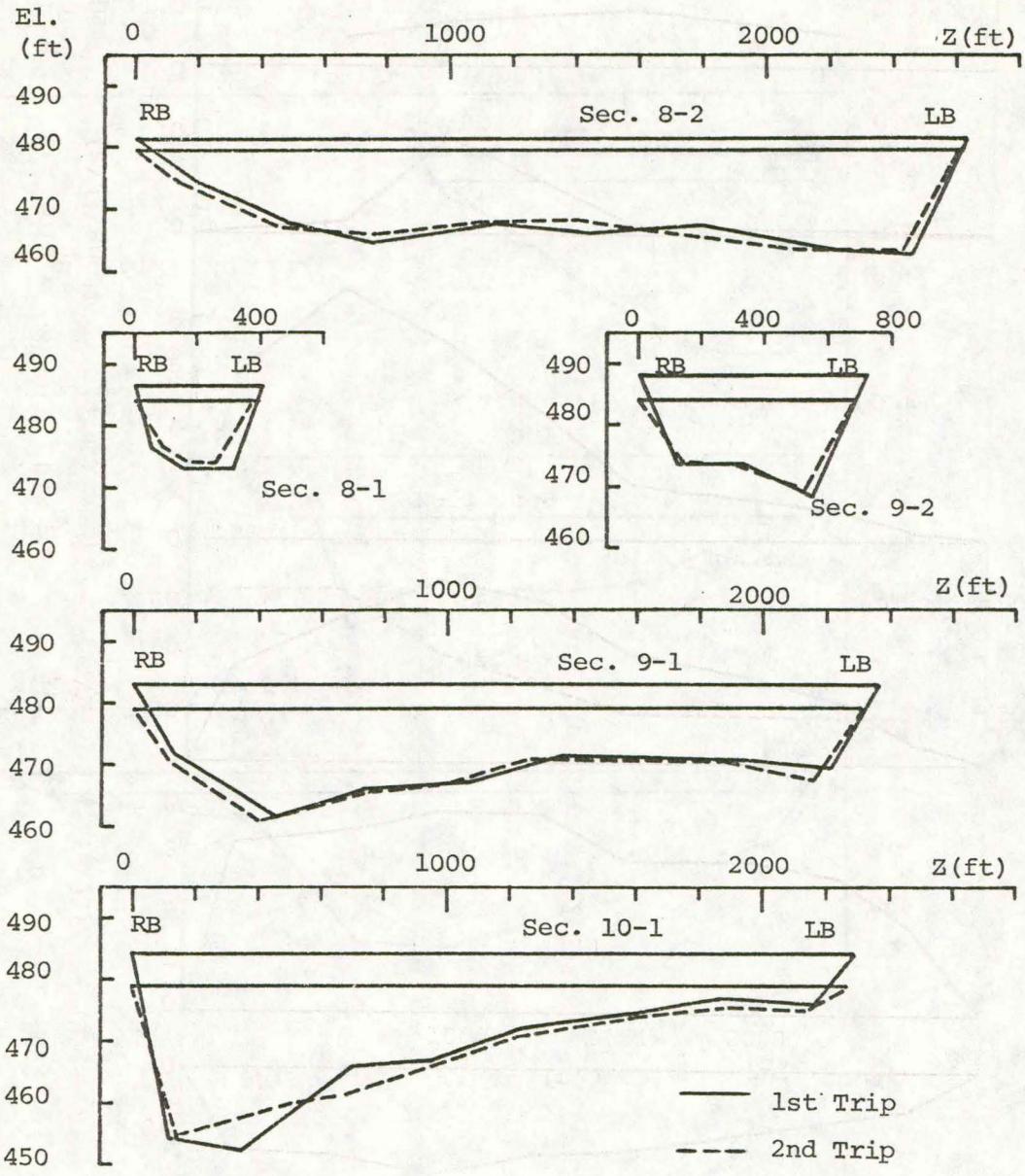

Figure I-C-2.1 (cont'd)

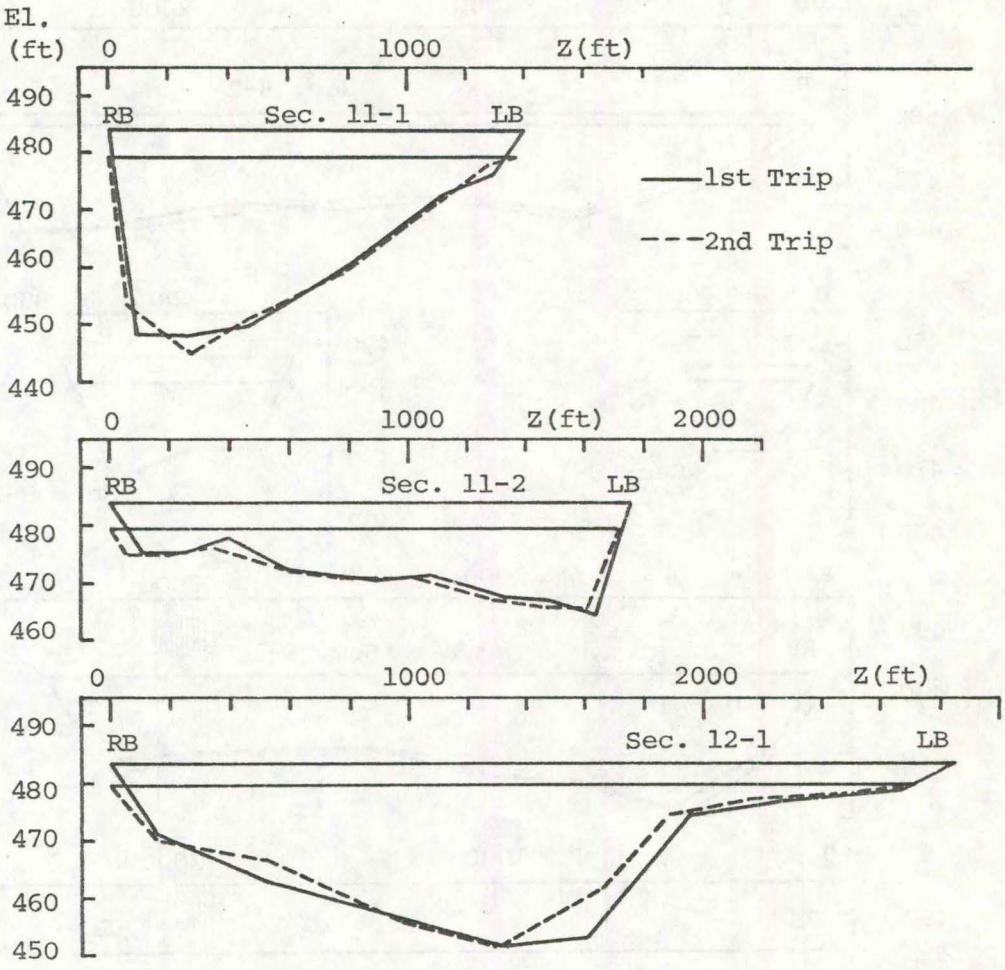

Figure I-C-2.1 (cont'd)

Table I-C-2.1

Comparable Cross Sections from the 1976 and 1978 Field Studies

1978	RM	1976	RM
1-2	354.89	3-2	354.93
6-1	349.75	5-1	349.82
7-1	349.50	6-1	349.45
8-2	349.24	7-2	349.29
9-1	348.98	8-1	348.96

3. Lateral distributions. Figures I-C-3.1 through I-C-3.26 present the lateral (cross-channel) variations in depth, d; mean flow velocity, $\bar{u}$; unit water discharge, $\bar{q}$; mean suspended-sediment concentration, $\bar{C}$; unit suspended-sediment discharge, $\bar{q}_s$; unit bed-load discharge, $\bar{q}_B$; and median bed-material diameter, D_{50}, obtained from the field data collected during both trips at the main-channel sections. Note again that when referring to any specific section (e.g., 1-2-1), the third number in the sequence denotes the trip number. All cross sections are plotted so that the right bank is on the left side of the figure, as if being viewed from downstream.

The lateral distributions determined for the first trip are shown in figures I-C-3.1 through I-C-3.13. Figure I-C-3.1 of section 1-2-1 shows a high mean concentration of suspended sediment near the right bank. This high concentration was caused by the confluence of the DMR and the MR roughly 6 mi upstream from this section. The large MR flow velocities swept the inflow from the DMR downstream without causing much cross-stream mixing. The DMR inflow carried a high concentration of suspended sediment (approximately 1,800 ppm when measured earlier on the same day). The river reach between the confluence and section 1-2-1 is fairly straight, so that lateral mixing due to curvature effects is minimal. The figure shows that the concentration of about 600 ppm near the right bank drops across the channel to a nearly constant concentration of about 200 ppm. Note that the concentration of roughly 600 ppm measured near the right bank was one-third of the concentration measured in the DMR. The concentration became almost uniform across the channel at the downstream section 3-2-1, as seen in figure I-C-3.3.

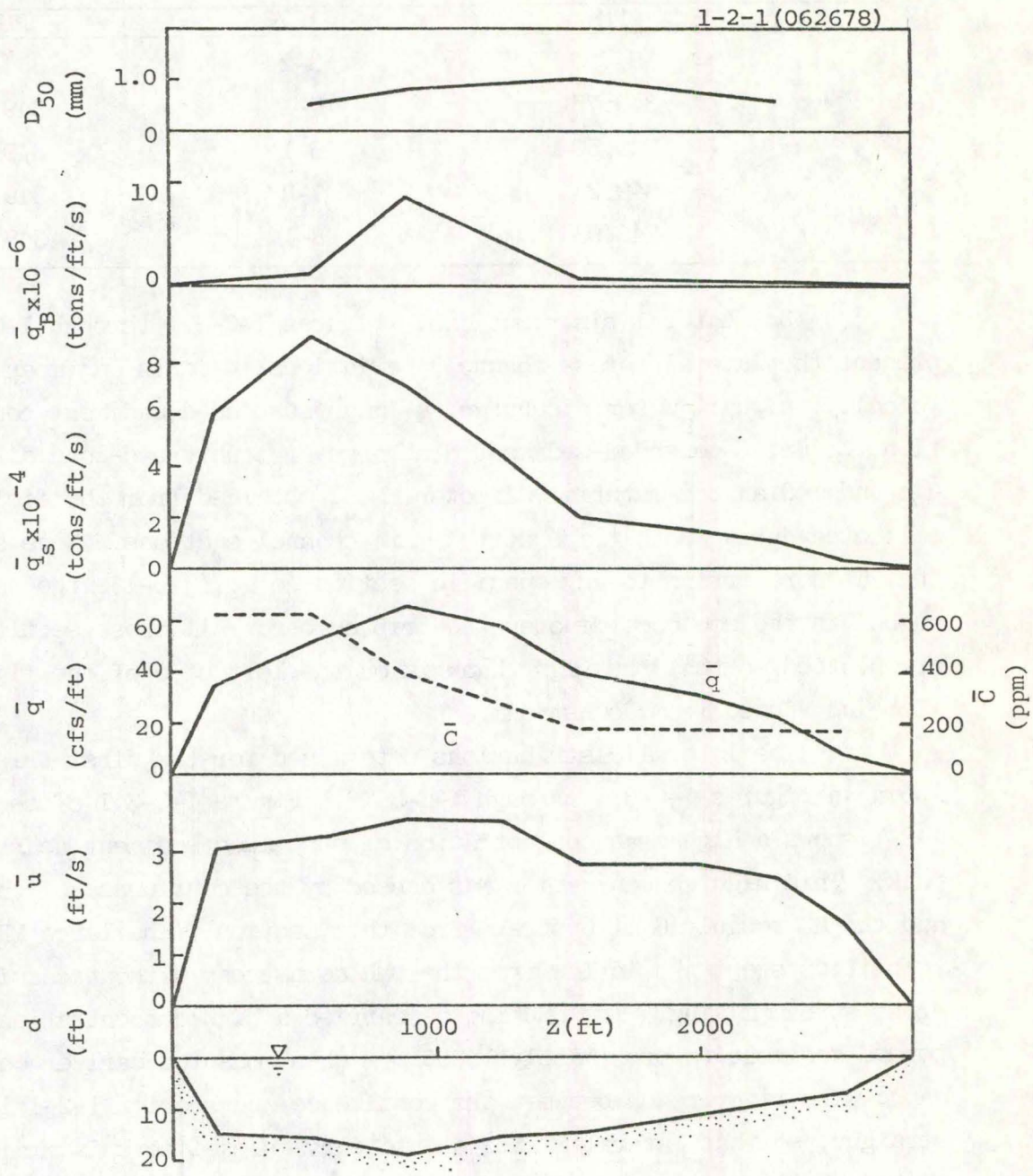

Figure I-C-3.1 Lateral distributions of d, $\bar{u}$, $\bar{q}$, $\bar{C}$, $\bar{q}_s$, $\bar{q}_B$, and D_{50} for section 1-2-1

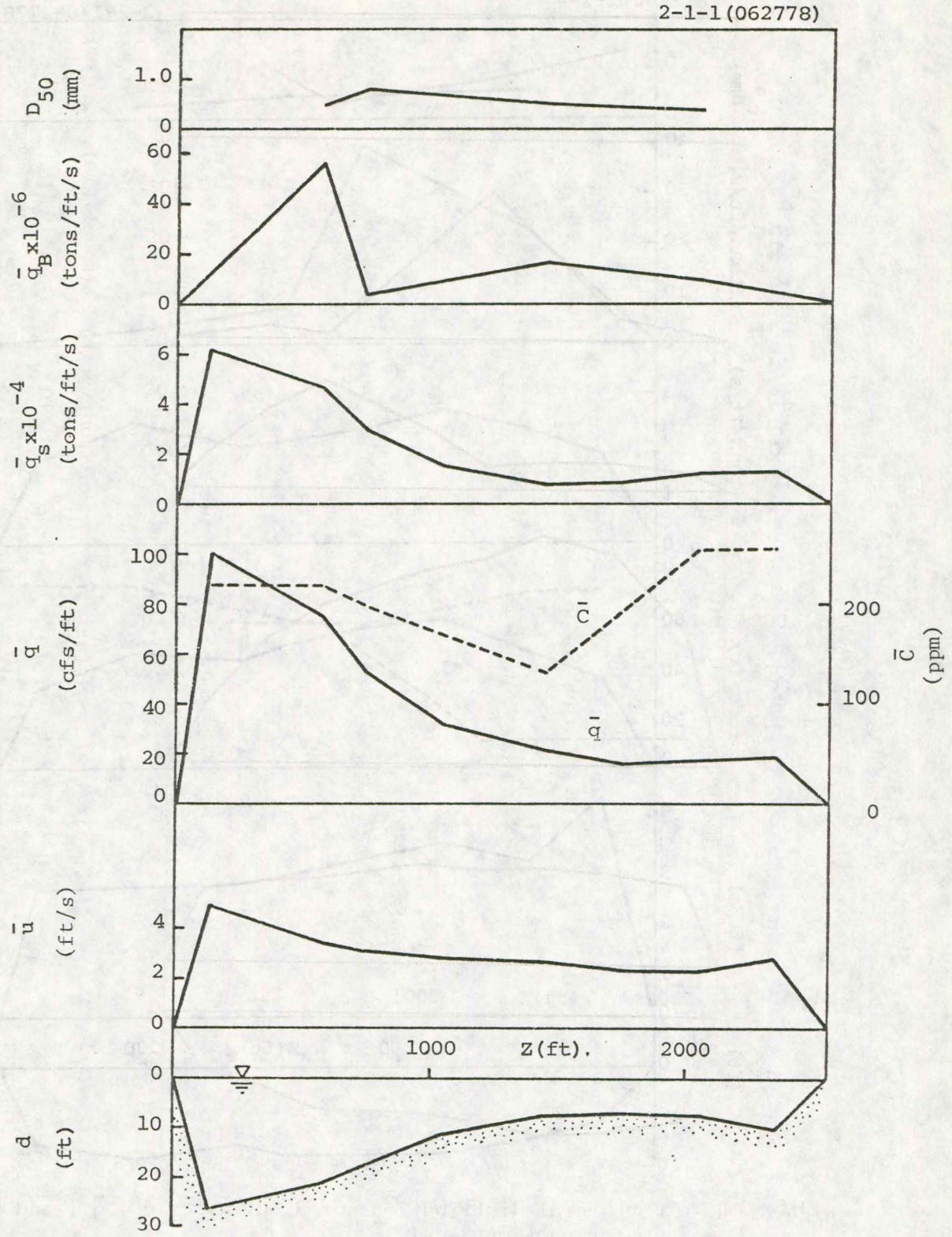

Figure I-C-3.2 Lateral distributions of d, $\bar{u}$, $\bar{q}$, $\bar{C}$, $\bar{q}_s$, $\bar{q}_B$, and D_{50} for section 2-1-1

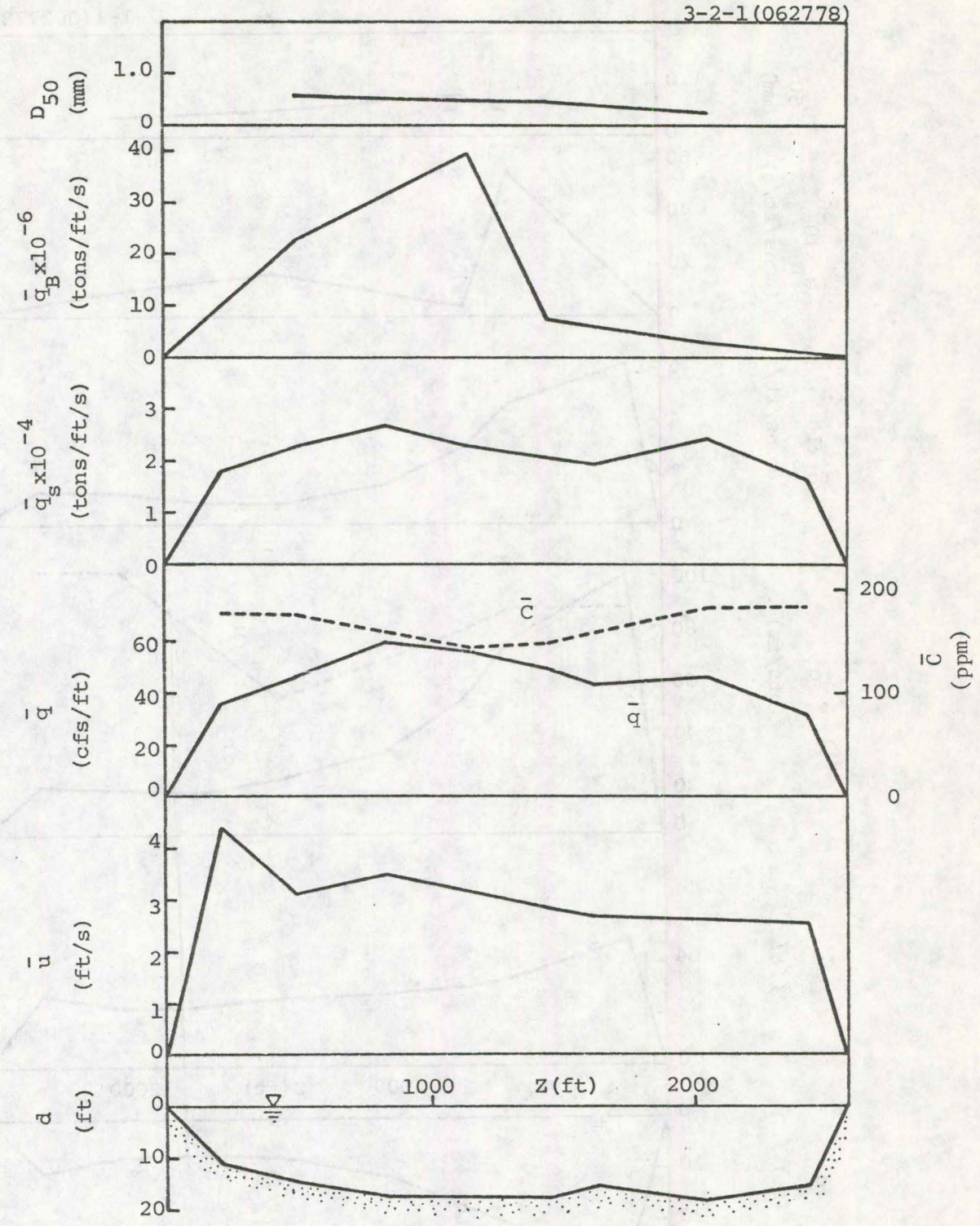

Figure I-C-3.3 Lateral distributions of d, $\bar{u}$, $\bar{q}$, $\bar{C}$, $\bar{q}_s$, $\bar{q}_B$, and D_{50} for section 3-2-1

The lateral distributions at section 2-1-1 are shown in figure I-C-3.2. This section was located downstream from a bend in the river. The centrifugal effect of the bend and secondary currents have carved a steep right bank. Note that the mean flow velocity near this bank for the first trip was almost 5 ft/s. The slight increases in depth and mean velocity near the left bank were due to the effect of the flow behind the small island downstream from Taylor Island. The large drop of mean concentration seen in the shallow center of the section was due to the bifurcation of flow downstream at section 3, where roughly 12 percent of the total suspended-sediment load occurred in the side channel section 3-1-1.

The lateral distributions at section 3-2-1 are shown in figure I-C-3.3. The right bank of this section is located on the upstream tip of Buzzard Island. Large flow velocities, over 4 ft/s near the right bank, produced a strong scouring action, making the tip unstable and washing large concentrations of sediment downstream. The cross-sectional profile of section 3-2 in figure I-C-2.1 shows that a lot of scouring had occurred near the right bank of the island between the first and second trips. During both trips, the tip of the island was wedge-shaped and had very steep banks.

The lateral distributions at section 4-1-1 in figure I-C-3.4 show extremely high suspended-sediment concentrations near the right bank, some of which were caused by the scouring action near the tip of Buzzard Island. However, the extent of the lateral dispersion of suspended sediment (seen to occur over 1000 ft in a longitudinal distance of 1900 ft between sections 3-2 and 4-1) seems unrealistic, so another sediment source, in addition to the scouring of the island, is presumed. Consequently, the major cause of the high sediment concentrations was most likely the suspended-sediment inflow from the DMR, approximately 10 mi upstream. A mean suspended-sediment concentration of 3,300 ppm for the DMR was measured approximately one hour after the sampling at section 4-1-1 was completed. Note that the mean suspended-sediment concentrations of roughly 1,100 ppm measured near the right bank of section 4-1-1 are one-third of the sediment concentration measured in the DMR. Note also the similar trend described for section 1-2-1. Although the unit flow discharge was high near the left bank, the unit suspended-sediment discharge was much

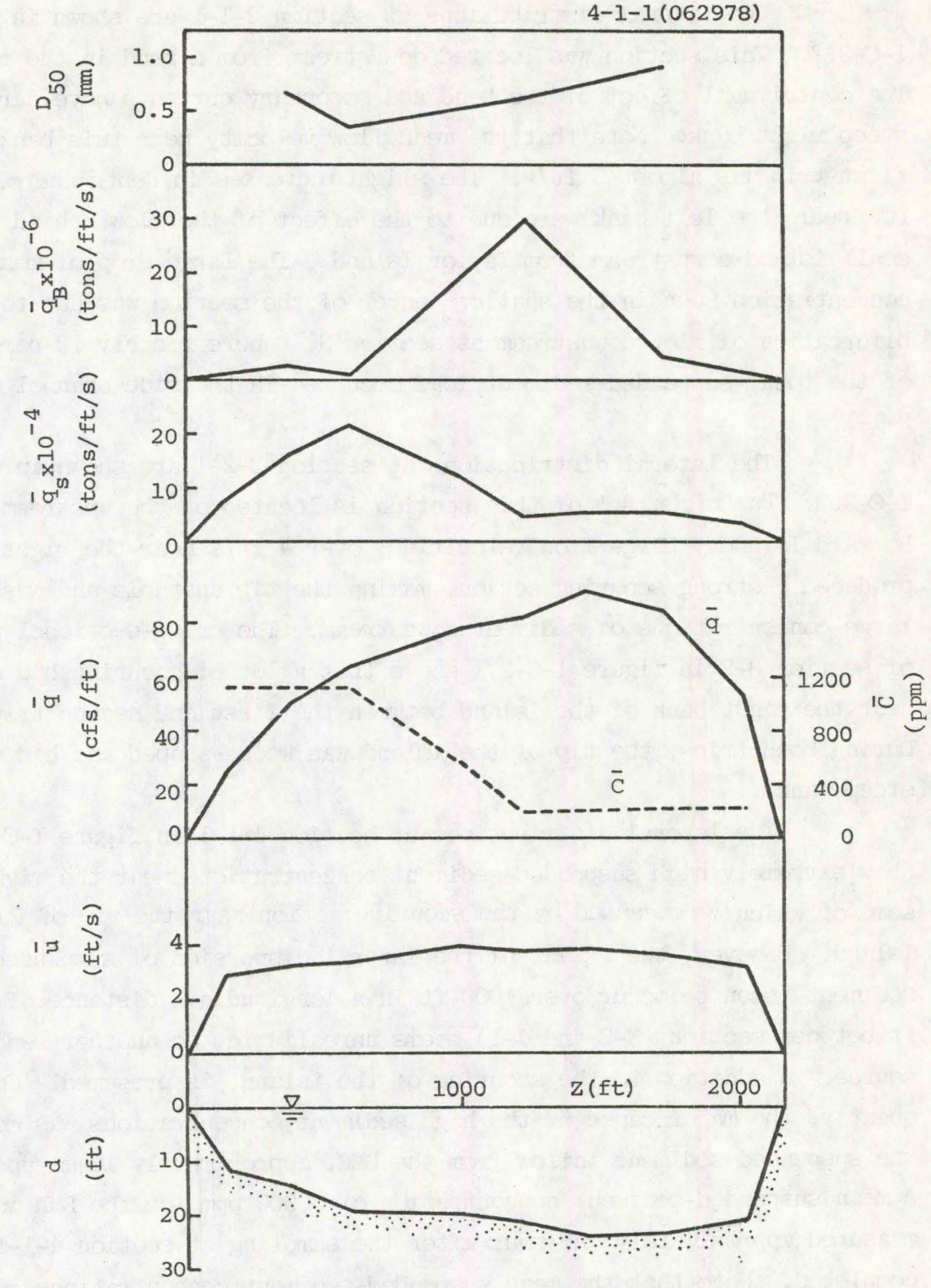

Figure I-C-3.4 Lateral distributions of d, $\bar{u}$, $\bar{q}$, $\bar{C}$, $\bar{q}_s$, $\bar{q}_B$, and D_{50} for section 4-1-1

larger near the right bank where the high mean concentrations were measured. These higher concentrations near the right bank continued for approximately two miles downstream, and finally became uniformly distributed across the transect at section 8-2-1. Note that the effect of the DMR sediment outflow was observed to extend roughly 12 mi downstream from the confluence.

Another pattern that developed in the first five sections was that the lateral distributions of unit bed load, $\bar{q}_B$, were all single-peaked, and the maximum values followed the navigation channel of the MR. The distributions became multi-peaked farther downstream, where the flow bifurcated at transects 7 and 9.

The lateral distributions at sections 5 through 8 are shown in figures I-C-3.5 through I-C-3.8. At these locations, the deepest parts of the cross sections consistently occurred near the left bank, away from the navigation channel which crosses the river to the right bank. The major bed-load movement at section 6-1-1, as shown in figure I-C-3.6, occurred in the right half of the section, especially in the region just beyond the submerged wing dam that extended from the left bank. The bed-load movement appeared restricted in the left half of the section while the flow velocities and unit flow discharges decreased quickly towards the left bank. Note the increase in the magnitude of the bed-load discharge from section 6-1-1 to 7-1-1 shown in figures I-C-3.6 and I-C-3.7, respectively, with a similar decrease in magnitude from section 7-1-1 to 8-2-1 in figures I-C-3.7 and I-C-3.8. Sections 6-1-1 and 7-1-1 were sampled on the same day, while section 8-2-1 was sampled on the following day. The reach between sections 6-1 and 7-1 will be discussed later concerning scouring, and the reach between sections 7-1 and 8-2 will be discussed with shoaling.

The bifurcation of flow occurring at transect 9 is apparent from figures I-C-3.7 and I-C-3.8 for sections 7-1-1 and 8-2-1, respectively. The largest values of depth, mean flow velocity, unit water discharge, and unit suspended-sediment discharge all occurred close to the left bank. Note that the navigation channel is along the right bank. Figure I-C-3.9 shows the lateral distribution at section 9-1-1, where the deepest part of the transect is near the right bank where the navigation channel

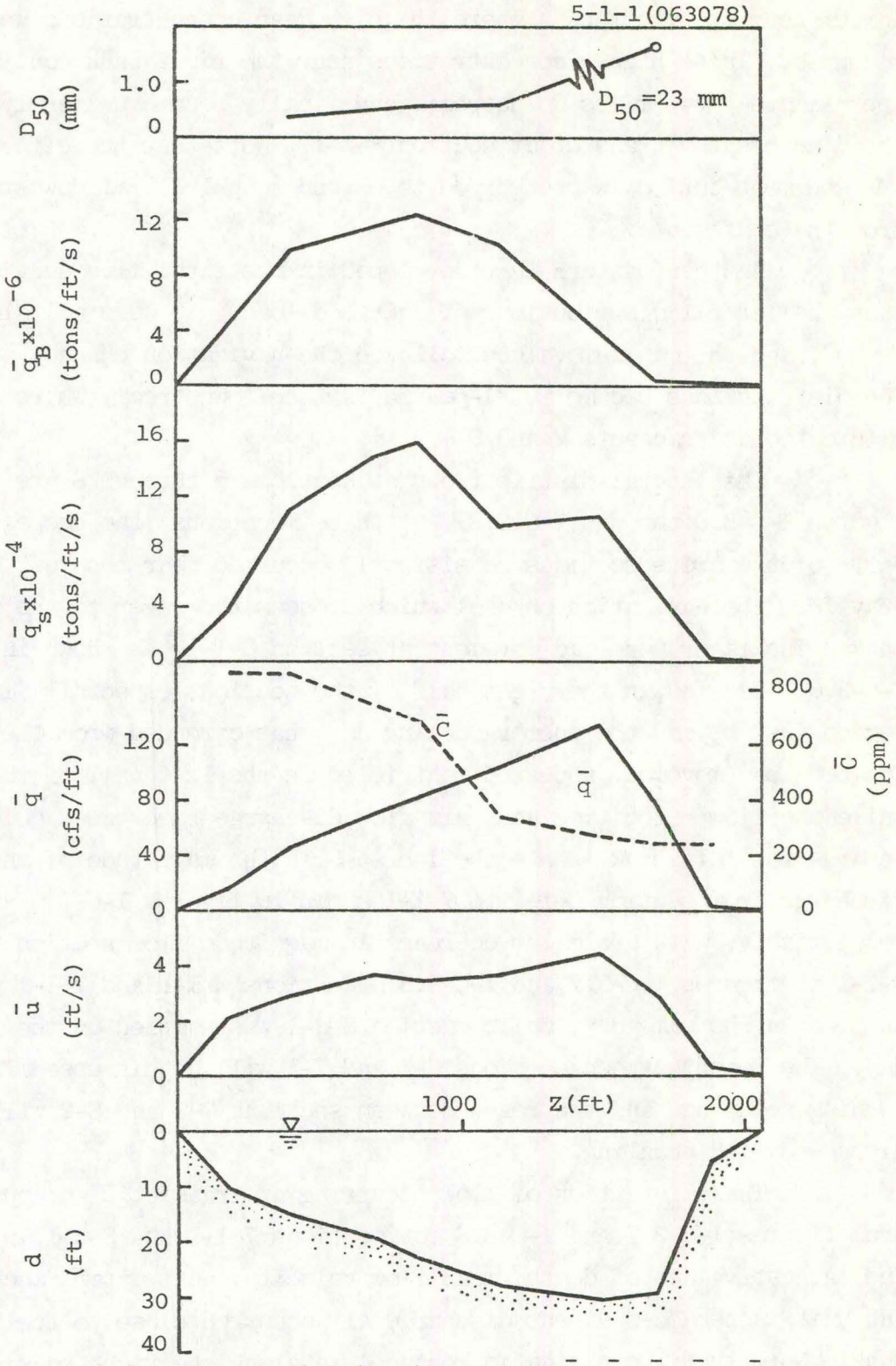

Figure I-C-3.5 Lateral distributions of d, $\bar{u}$, $\bar{q}$, $\bar{C}$, $\bar{q}_s$, $\bar{q}_B$, and D_{50} for section 5-1-1

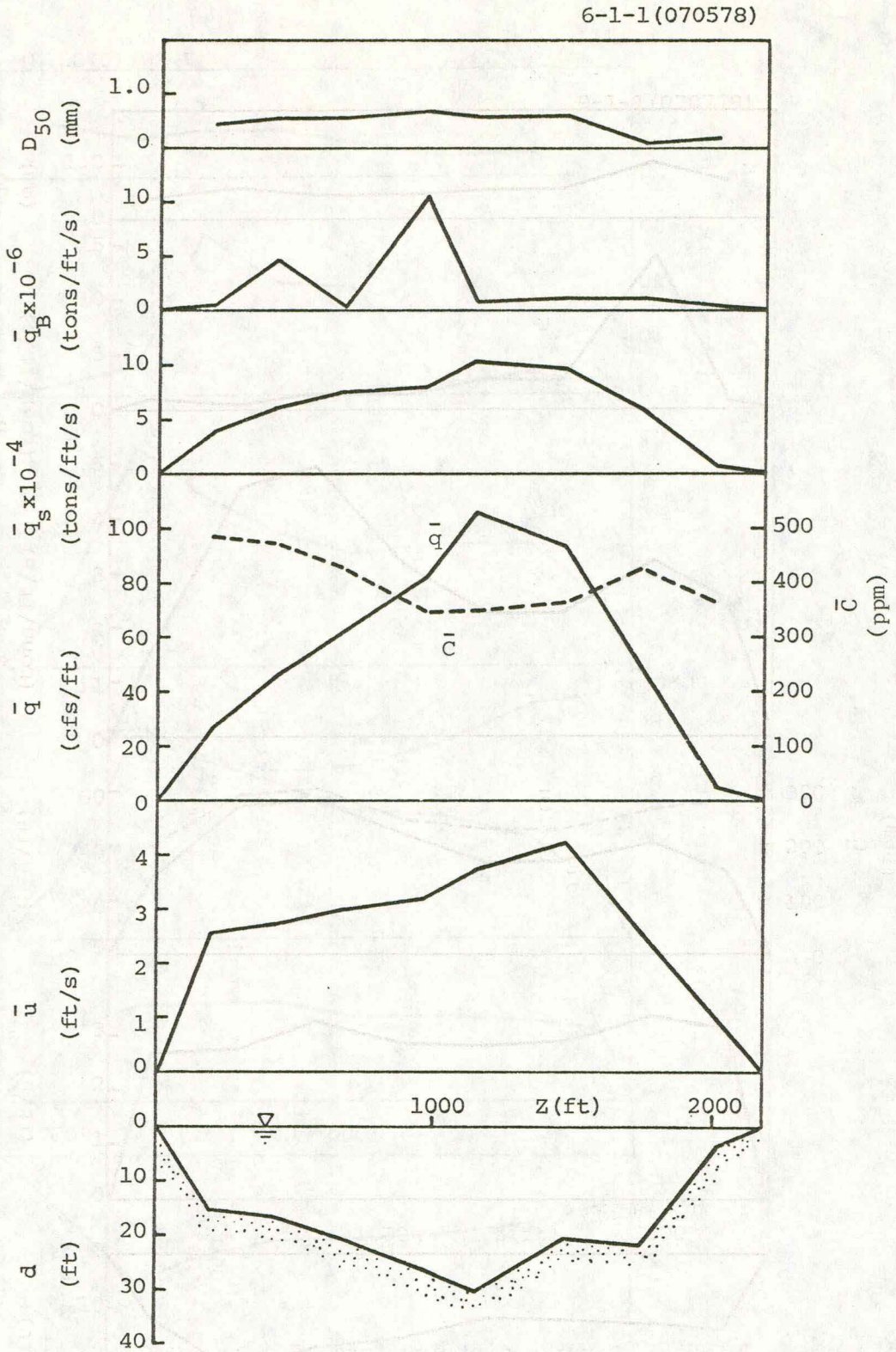

Figure I-C-3.6 Lateral distributions of d, $\bar{u}$, $\bar{q}$, $\bar{C}$, $\bar{q}_s$, $\bar{q}_B$, and D_{50} for section 6-1-1

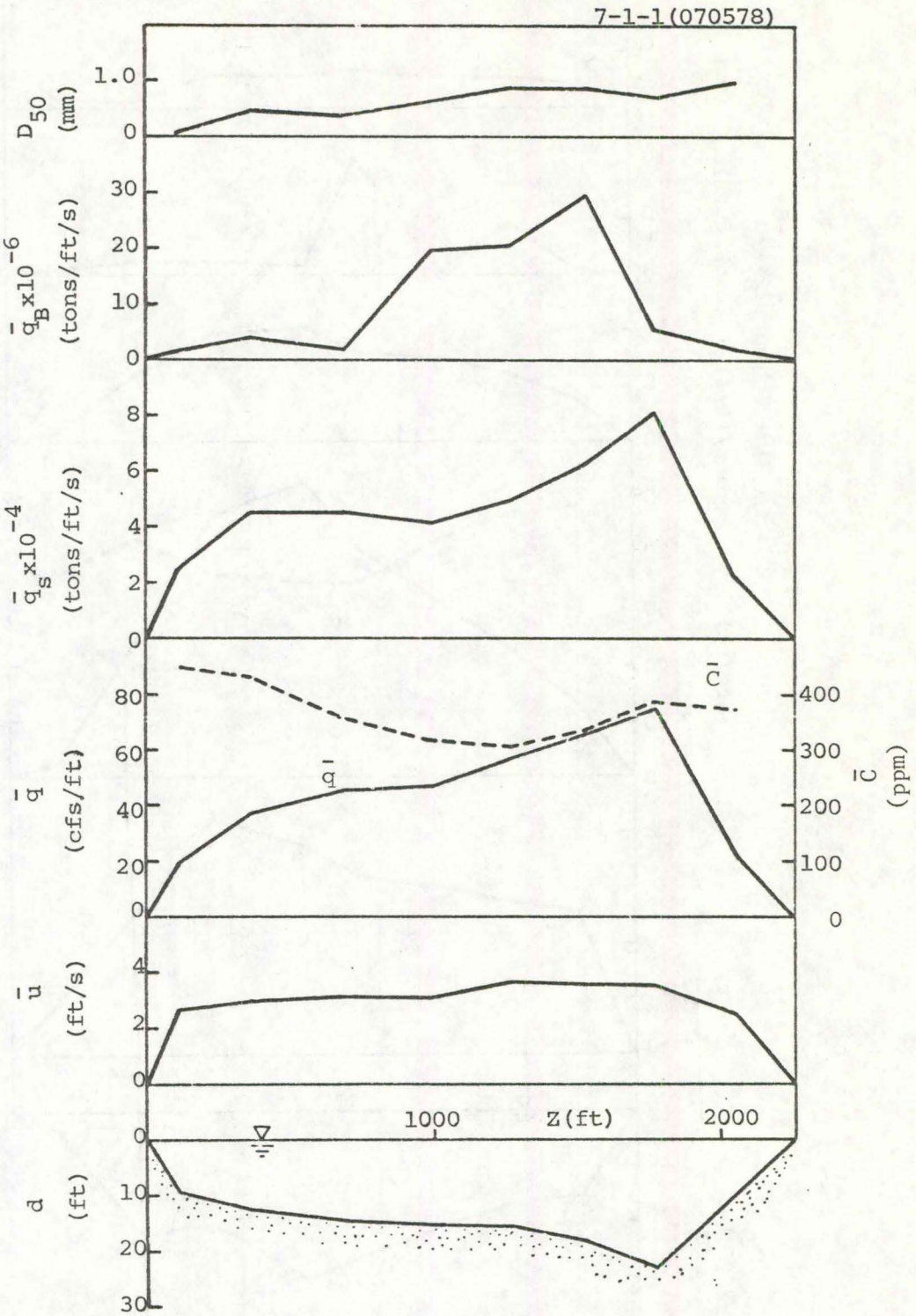

Figure I-C-3.7 Lateral distributions of d, $\bar{u}$, $\bar{q}$, $\bar{C}$, $\bar{q}_s$, $\bar{q}_B$, and D_{50} for section 7-1-1

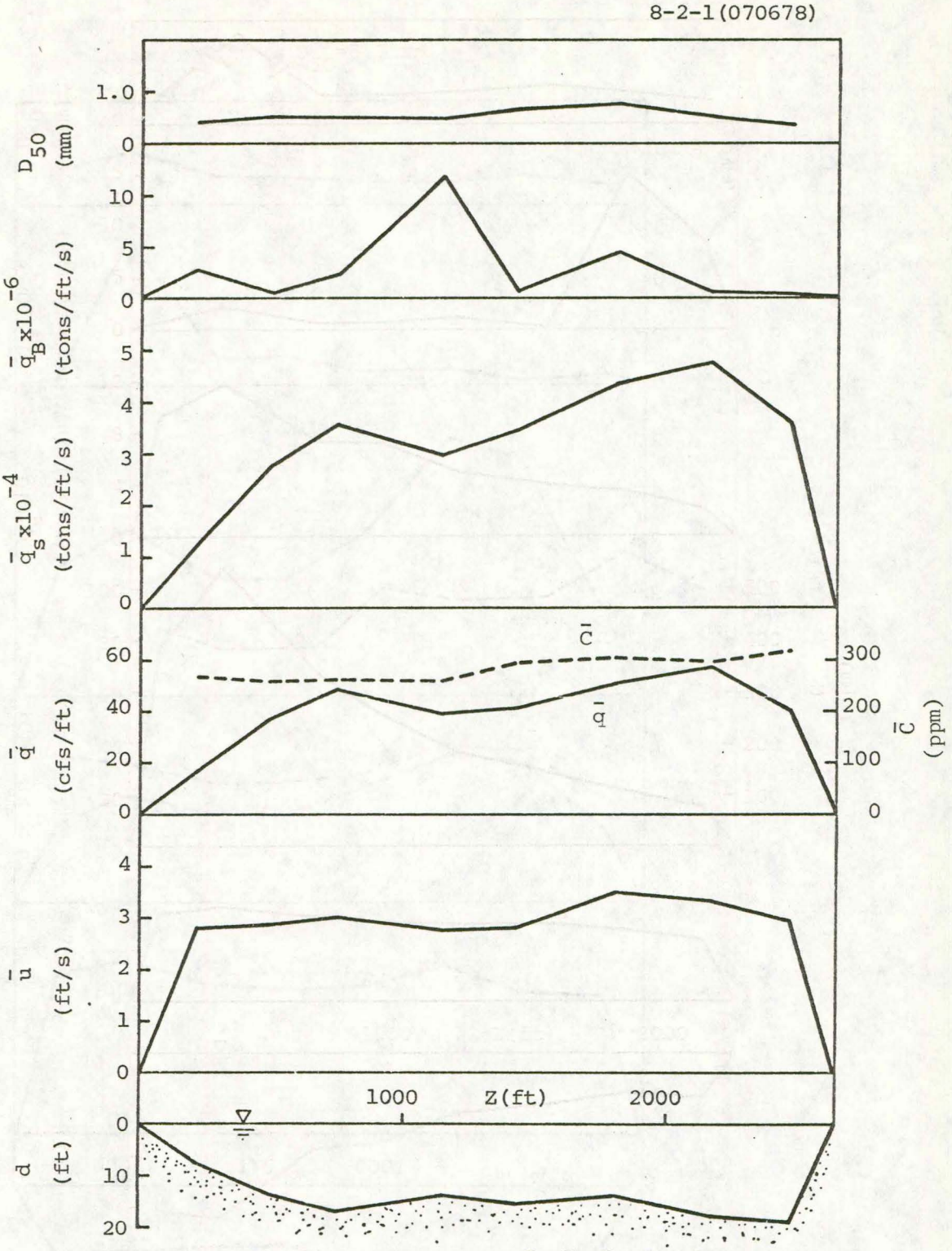

I-C-3.8 Lateral distributions of d, $\bar{u}$, $\bar{q}$, $\bar{C}$, $\bar{q}_s$, $\bar{q}_B$, and D_{50} for section 8-2-1

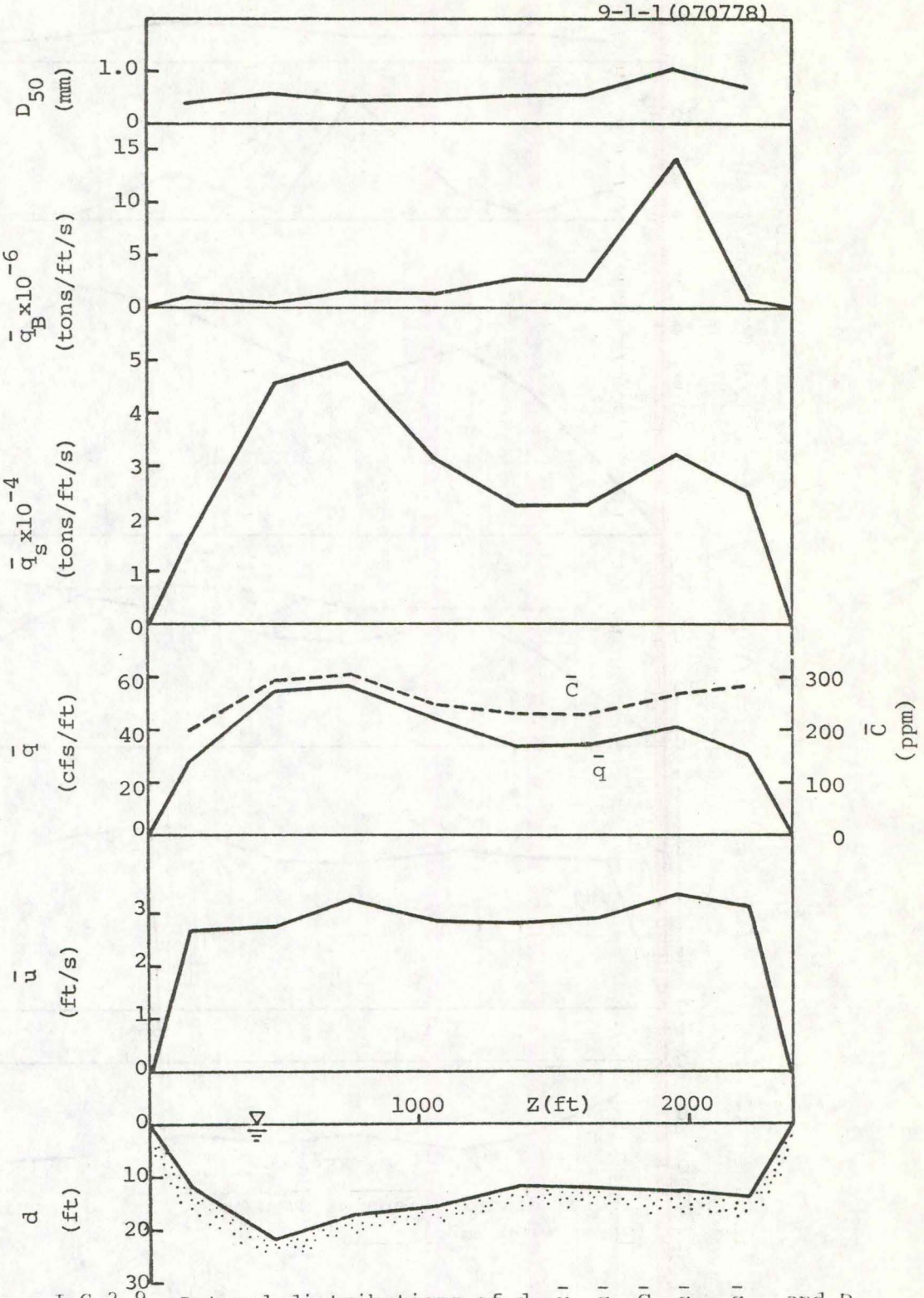

Figure I-C-3.9 Lateral distributions of d, $\bar{u}$, $\bar{q}$, $\bar{C}$, $\bar{q}_s$, $\bar{q}_B$, and D_{50} for section 9-1-1

is located. Table I-C-3.1 summarizes the percentages of water discharges and sediment discharges through side channels 7-2-1 and 9-2-1.

Table I-C-3.1

Water and Sediment Discharges at Sections 7 and 9

Section	Date	Q (cfs)	Q_S (tons/day)	Q_B (tons/day)
7-1-1	070578	101,830	89,467	1,958
7-2-1	070678	16,155 Q_2/Q_1=16%	13,280 Q_{s2}/Q_{s1}=15%	102 Q_{B2}/Q_{B1}=5%
9-1-1	070778	96,800	62,925	630
9-2-1	070778	30,271 Q_2/Q_1=31%	22,956 Q_{s2}/Q_{s1}=36%	77 Q_{B2}/Q_{B1}=12%

Figures I-C-3.9 and I-C-3.10, which depict sections 9-1-1 and 10-1-1, respectively, show that the maximum unit bed-load discharges occurred near the left bank. The flow was very turbulent near the upstream tip of Huff Island during the first trip. The splitting of the flow around Huff Island and the presence of a submerged wing dam extending from the left bank upstream from section 9-1 created turbulence which caused the large bed-load movement. The figure of section 10-1-1 shows that the mean velocity was fairly uniform across the transect, although the depth changed significantly. The maximum unit flow discharge occurred near the right bank where the channel was the deepest, but the largest flow concentrations and unit bed-load discharges were found in the shallower area near the left bank.

Figures I-C-3.11, I-C-3.12, and I-C-3.13 show the lateral distributions at sections 11-1-1, 11-2-1, and 12-1-1, respectively. The width of the main channel decreases considerably between sections 9-1 and 11-1, with a corresponding increase in flow depth. The figure of section 11-1-1 shows that depths of over 35 ft were measured near the right bank. As seen in figure I-A.1, section 11-2 could be treated as three smaller subsections. Flow from the two subsections nearer the right bank reentered the main channel upstream from section 12, but the flow through the subsection nearer the left bank continued along the back side of an island

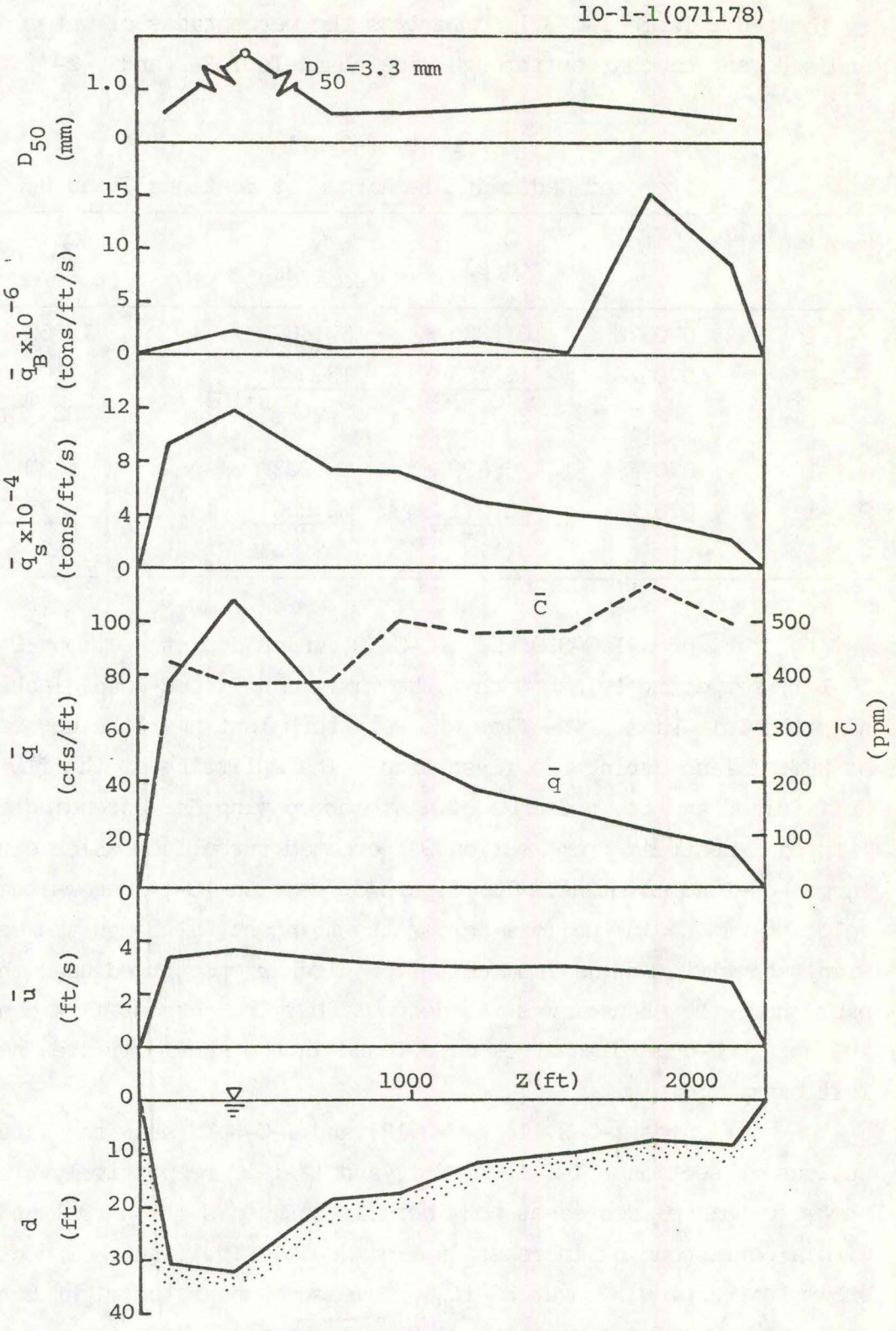

Figure I-C-3.10 Lateral distributions of d, $\bar{u}$, $\bar{q}$, $\bar{C}$, $\bar{q}_s$, $\bar{q}_B$, and D_{50} for section 10-1-1

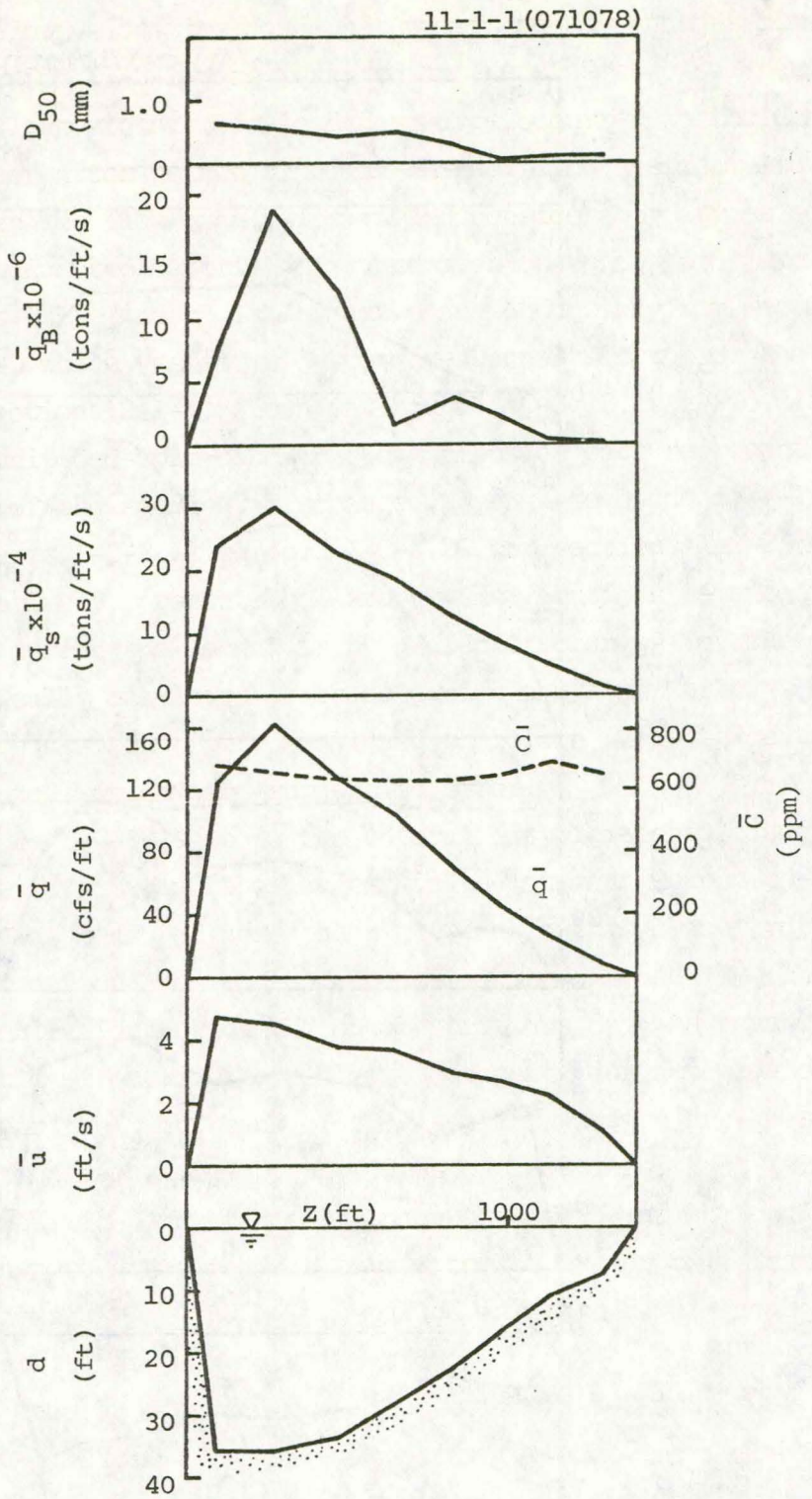

Figure I-C-3.11 Lateral distributions of d, $\bar{u}$, $\bar{q}$, $\bar{C}$, $\bar{q}_s$, $\bar{q}_B$, and D_{50} for section 11-1-1

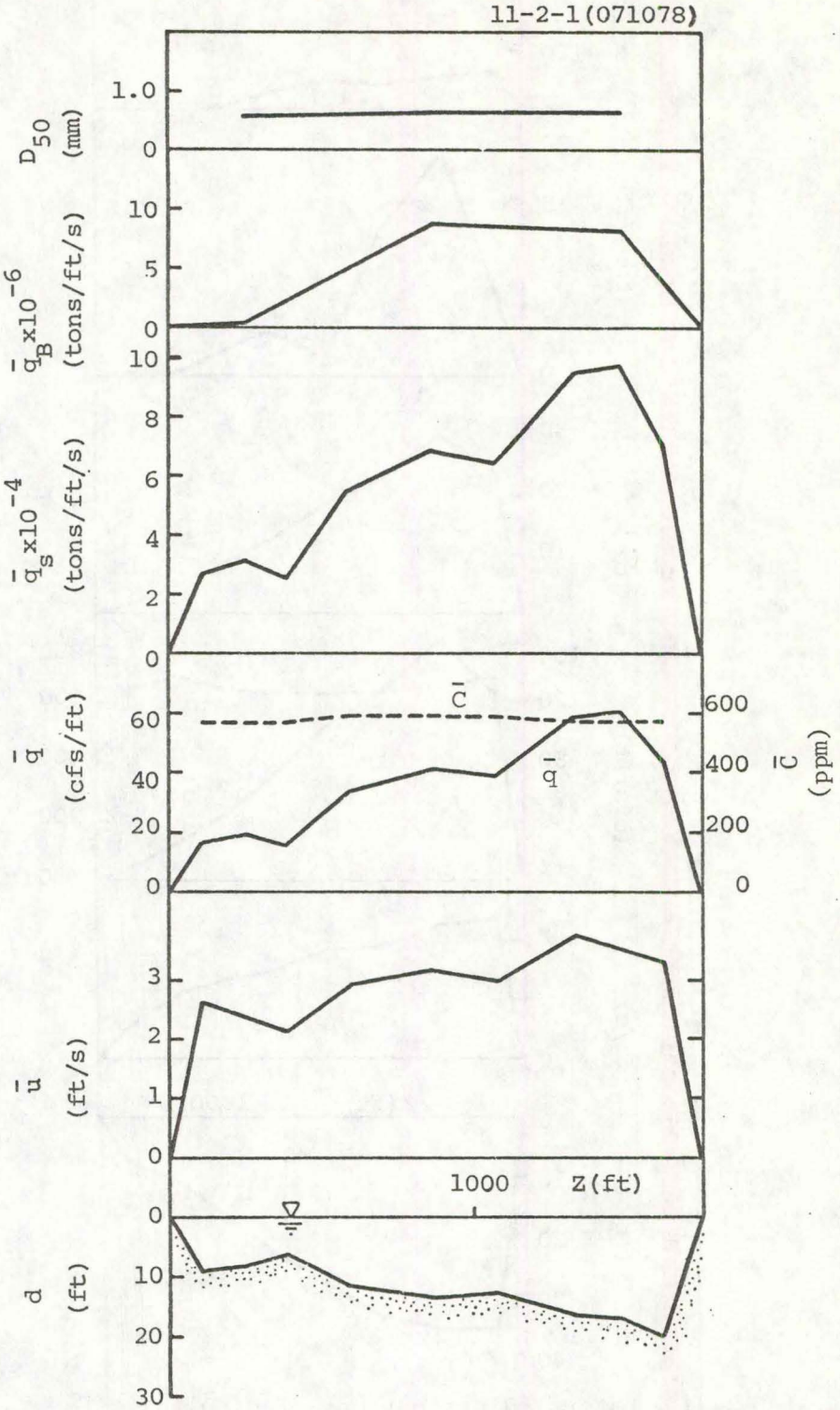

Figure I-C-3.12 Lateral distributions of d, $\bar{u}$, $\bar{q}$, $\bar{C}$, $\bar{q}_s$, $\bar{q}_B$, and D_{50} for section 11-2-1

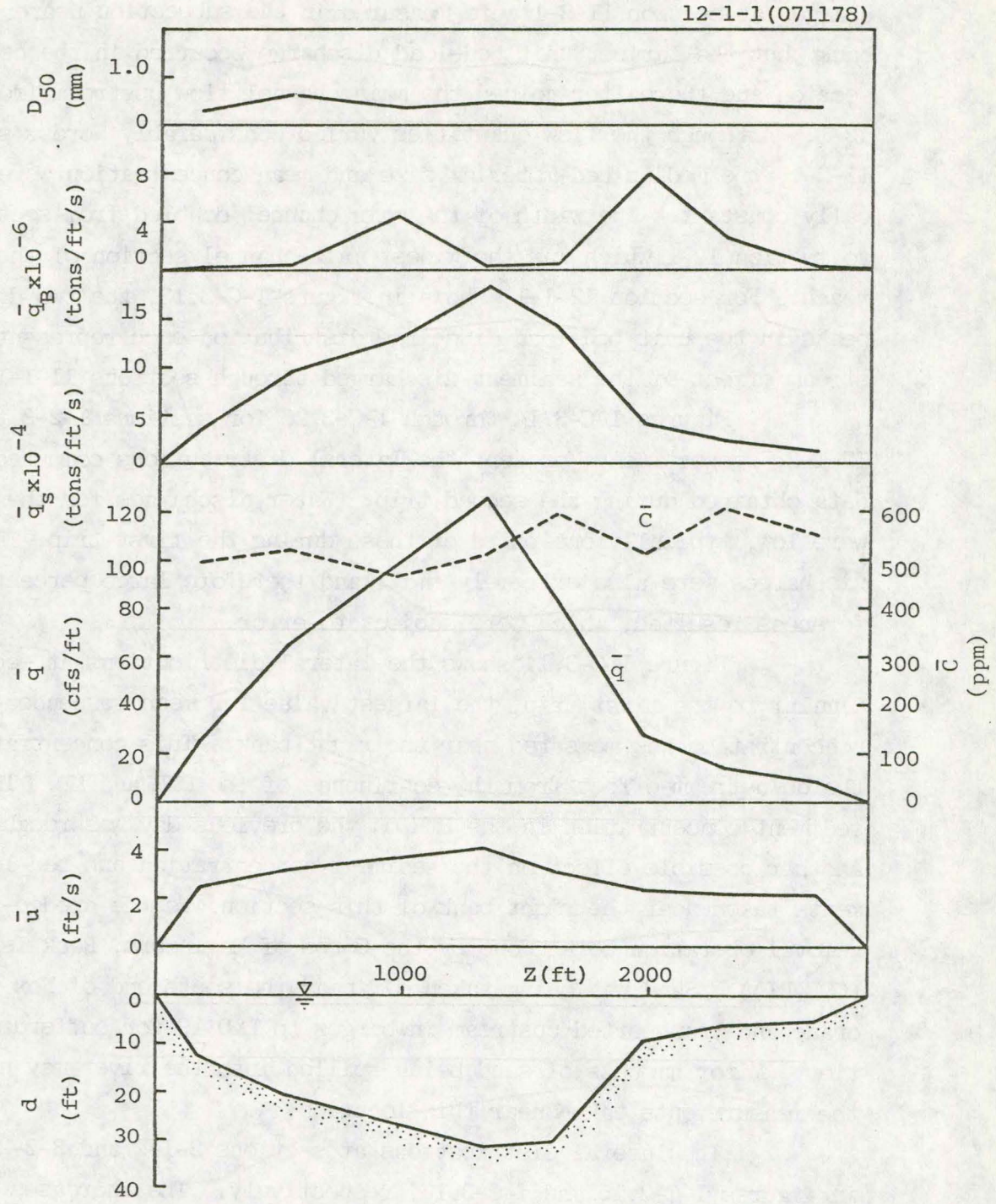

Figure I-C-3.13 Lateral distributions of d, $\bar{u}$, $\bar{q}$, $\bar{C}$, $\bar{q}_s$, $\bar{q}_B$, and D_{50} for section 12-1-1

and re-entered the main channel downstream from section 12. The largest depths, mean flow velocities, and unit water and suspended-sediment discharges at section 11-2-1 were measured in the subsection nearer the left bank, but the largest unit bed-load discharge occurred in the center subsection and thereafter joined the main channel flow upstream from section 12-1. Although the flow quantities varied considerably across section 11-2-1, the median bed-material size and mean concentration were practically constant. The width of the main channel doubled from section 11-1 to section 12-1 which was the widest main-channel section of the study reach. For section 12-1-1, shown in figure I-C-3.13, the two distinct peaks in the unit bed-load-discharge distribution each represent the downstream effect of the sediment discharged through sections 11-1-1 and 11-2-1.

Figures I-C-3.14 through I-C-3.26 for sections 1-2-2 through 12-1-2, respectively, present the lateral distributions computed from the data obtained during the second trip. Water discharges for the second trip were low, typically one-third of those during the first trip. Bed-load discharges were also extremely small and therefore large percentage differences resulted, which were subject to error.

Figure I-C-3.14 shows the lateral distributions at section 1-2-2. Similar to the first trip, the largest value for mean suspended-sediment concentration was measured near the right bank. This concentration was the downstream effect from the confluence of the DMR and MR. The mean sediment concentration in the DMR on the previous day was roughly 100 ppm. Another possible effect on the sediment concentration and bed-load measurements taken near the right bank of this section was the dredge-spoil-removal operation being done by the Corps of Engineers, Rock Island District (COE(RI)). Sand was being taken off near the south end of Fox Island by crane and transported upstream in barges to L&D 19 for cofferdam construction. Minor amounts of sand being spilled into the river may have affected the measurements taken near this location.

The lateral distributions at sections 2-1-2 and 3-2-2 are shown in figures I-C-3.15 and I-C-3.16, respectively. The increases in the depth, mean velocity, and unit bed-load discharge observed near the left bank of section 2-1-2 compared with section 1-2-2 were caused by the flow between the small downstream island and Taylor Island. The mean concentration was smaller in the center of the section, as was seen for the first

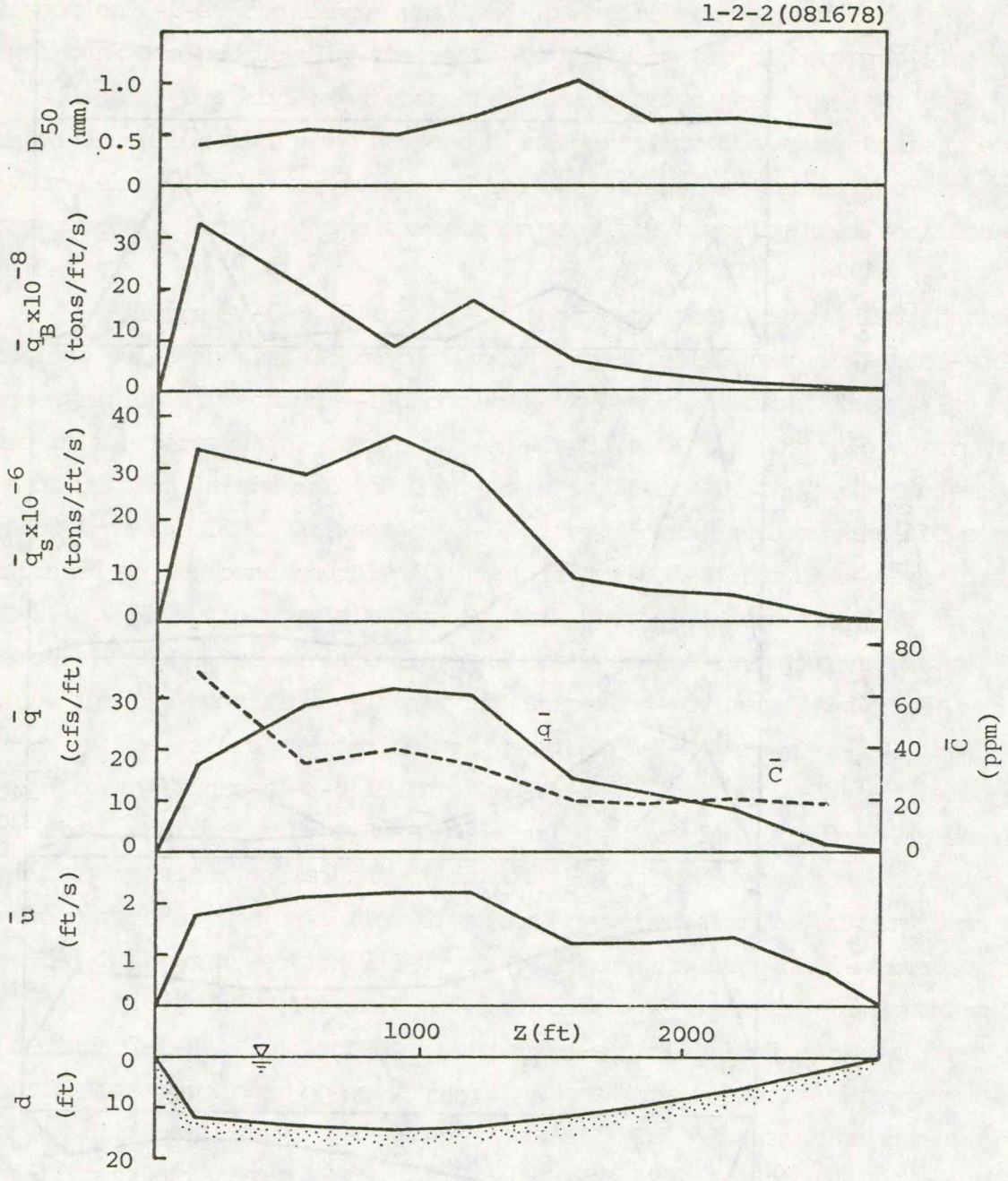

Figure I-C-3.14 Lateral distributions of d, $\bar{u}$, $\bar{q}$, $\bar{C}$, $\bar{q}_s$, $\bar{q}_B$, and D_{50} for section 1-2-2

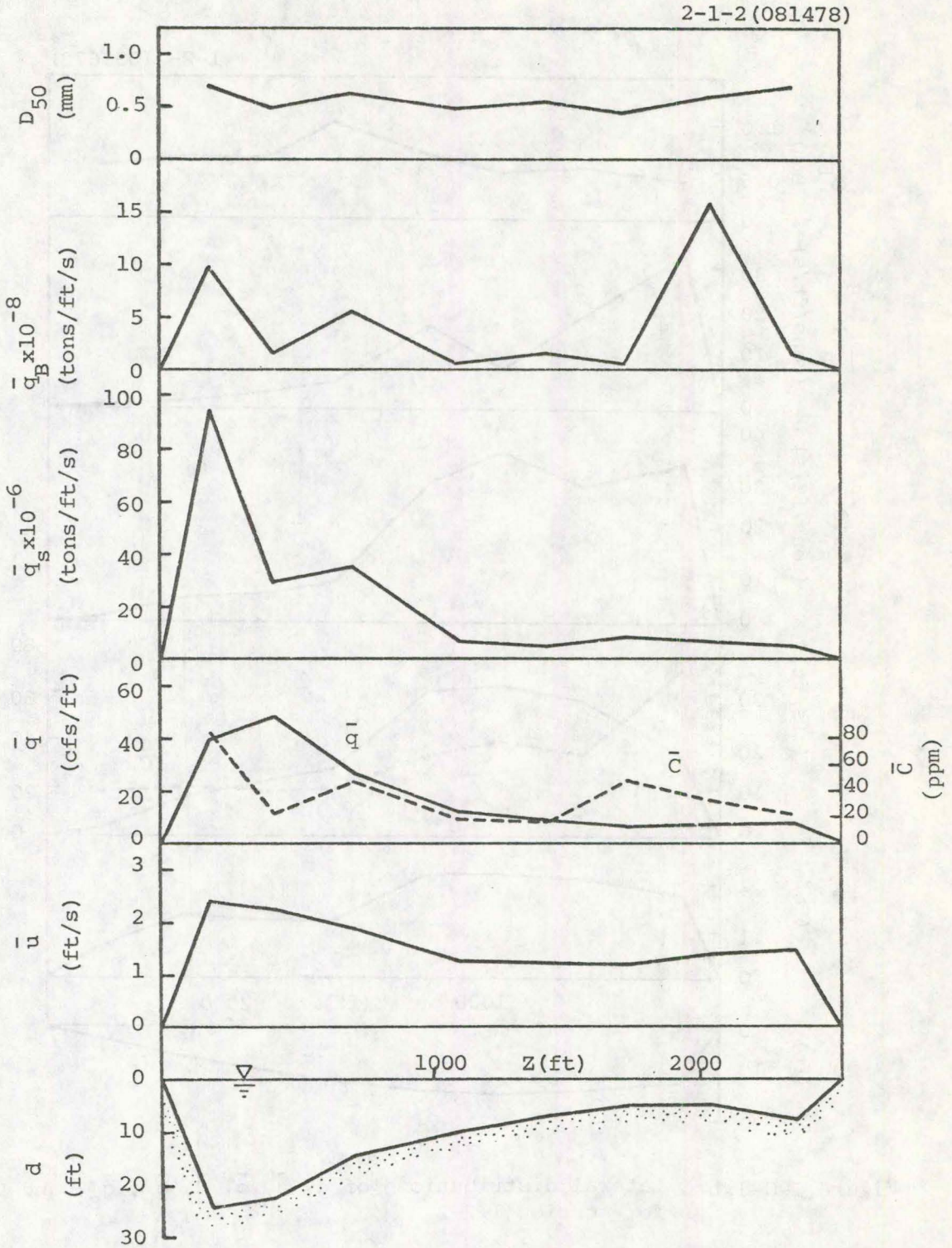

Figure I-C-3.15 Lateral distributions of d, $\bar{u}$, $\bar{q}$, $\bar{C}$, $\bar{q}_s$, $\bar{q}_B$, and D_{50} for section 2-1-2

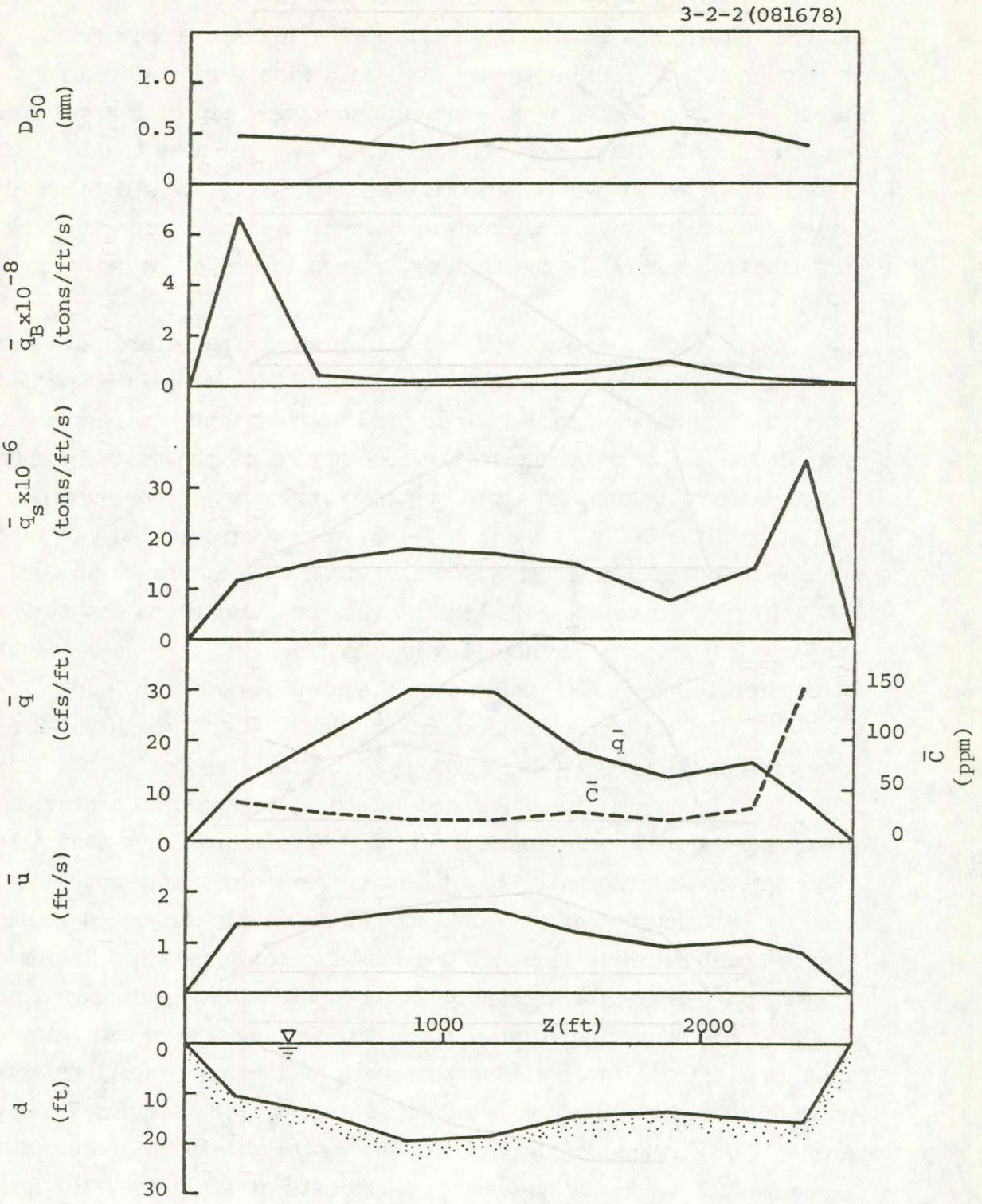

Figure I-C-3.16 Lateral distributions of d, $\bar{u}$, $\bar{q}$, $\bar{C}$, $\bar{q}_s$, $\bar{q}_B$, and D_{50} for section 3-2-2

trip. The decreased flow velocities in the shallow center of the section, which reduced the suspended-sediment transport capacity, and the downstream bifurcation of flow at section 3 caused the low mean concentration observed. At section 3-2-2, the larger unit bed-load discharge measured near the right bank was produced by the unstable upstream tip of Buzzard Island. The source of the high mean concentration observed near the left bank was caused by a flow with more suspended sediment from the side channel behind Taylor Island, or by the increased sediment-transport capacity of the secondary currents formed as the thalweg crossed the river between sections 2-1 and 3-2.

Figures I-C-3.17 and I-C-3.18 present the lateral distributions at sections 4-1-2 and 5-1-2, respectively. The highest mean suspended-sediment concentration at section 4-1-2 occurred at the right bank, as was the case in the first trip, due to the combination of the unstable upstream tip of Buzzard Island and the downstream influence of the suspended-sediment inflow from the DMR. At section 5-1-2, very coarse median particle sizes continued to be found roughly 400 feet from the left bank, as seen in figure I-C-3.18. Close to the left bank at this section, where the flow depth was only 2.9 ft, the surface flow was upstream and thus gave negative values for the mean flow velocity and suspended-sediment load.

The lateral variations at sections 6-1-2 through 9-1-2 are presented in figures I-C-3.19 through I-C-3.22, respectively. This area near the downstream tip of Buzzard Island is regarded as a problem shoaling area that requires occasional dredging. The figures show that although the magnitude of the unit flow discharge remained nearly constant from section 6-1-2 through section 7-1-2, the maximum unit suspended-sediment discharge doubled, while the unit bed-load discharge remained insignificant at section 7-1-2. The increased suspended-sediment load suggests that scouring was occurring between these two sections. Precise interpretation is difficult since the measurements at these two stations were made on different days (section 6-1-2 on 18 August 1978; section 7-1-2 on 21 August 1978). Between these dates, the water discharge increased by an estimated 22 percent. However, measurements at sections 7-1-2 and 8-2-2 were taken on the same day. The figures for these sections reveal that the maximum unit suspended-sediment discharge at section 8-2-2 was roughly one-half of its maximum value at section 7-1-2. The observed reduction in the sediment-transport capacity of the river is attributable to the shoaling problem observed in this area.

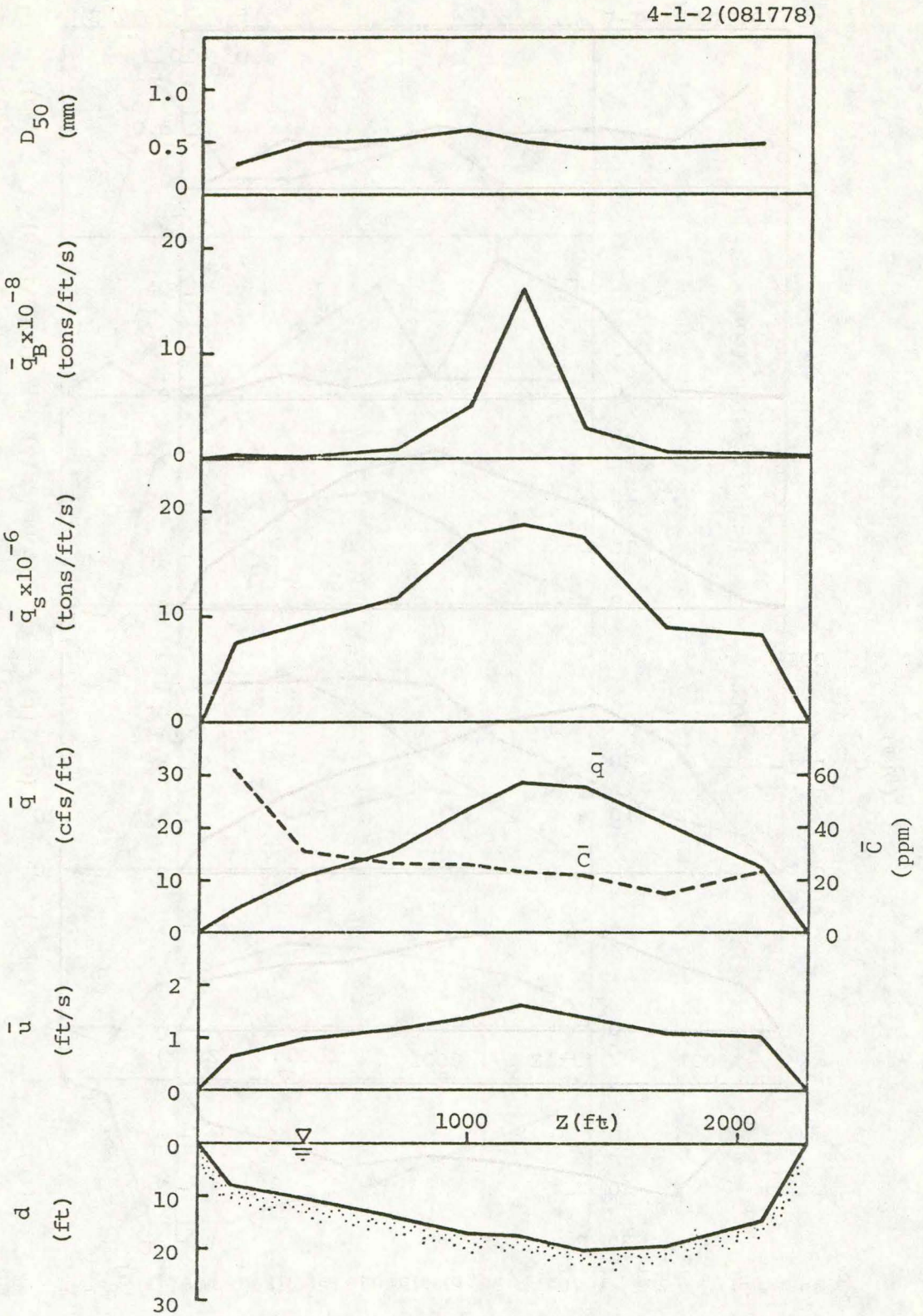

Figure I-C-3.17 Lateral distributions of $\bar{d}$, $\bar{u}$, $\bar{q}$, $\bar{C}$, $\bar{q}_s$, $\bar{q}_B$, and D_{50} for section 4-1-2

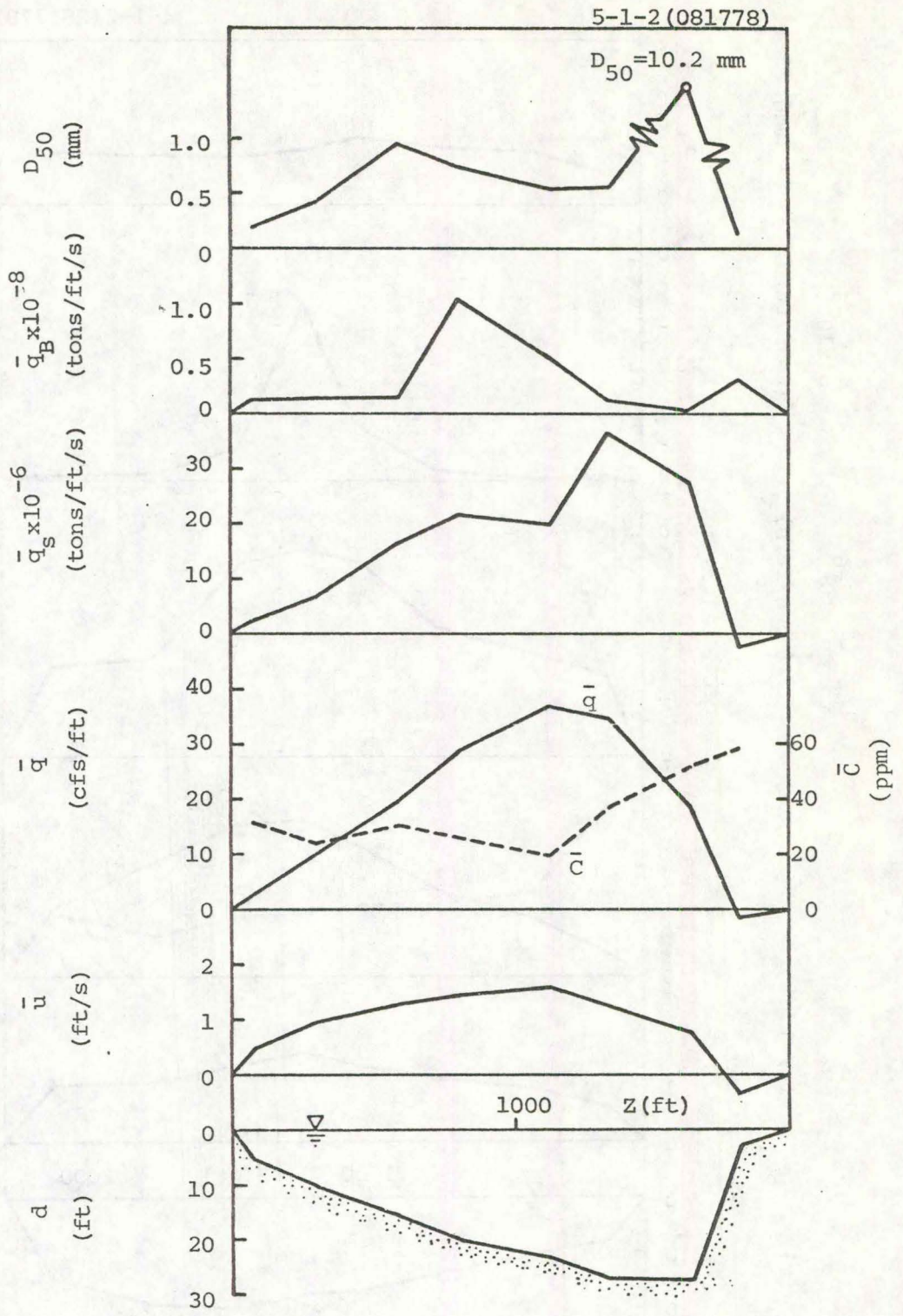

Figure I-C-3.18 Lateral distributions of d, $\bar{u}$, $\bar{q}$, $\bar{C}$, $\bar{q}_s$, $\bar{q}_B$, and D_{50} for section 5-1-2

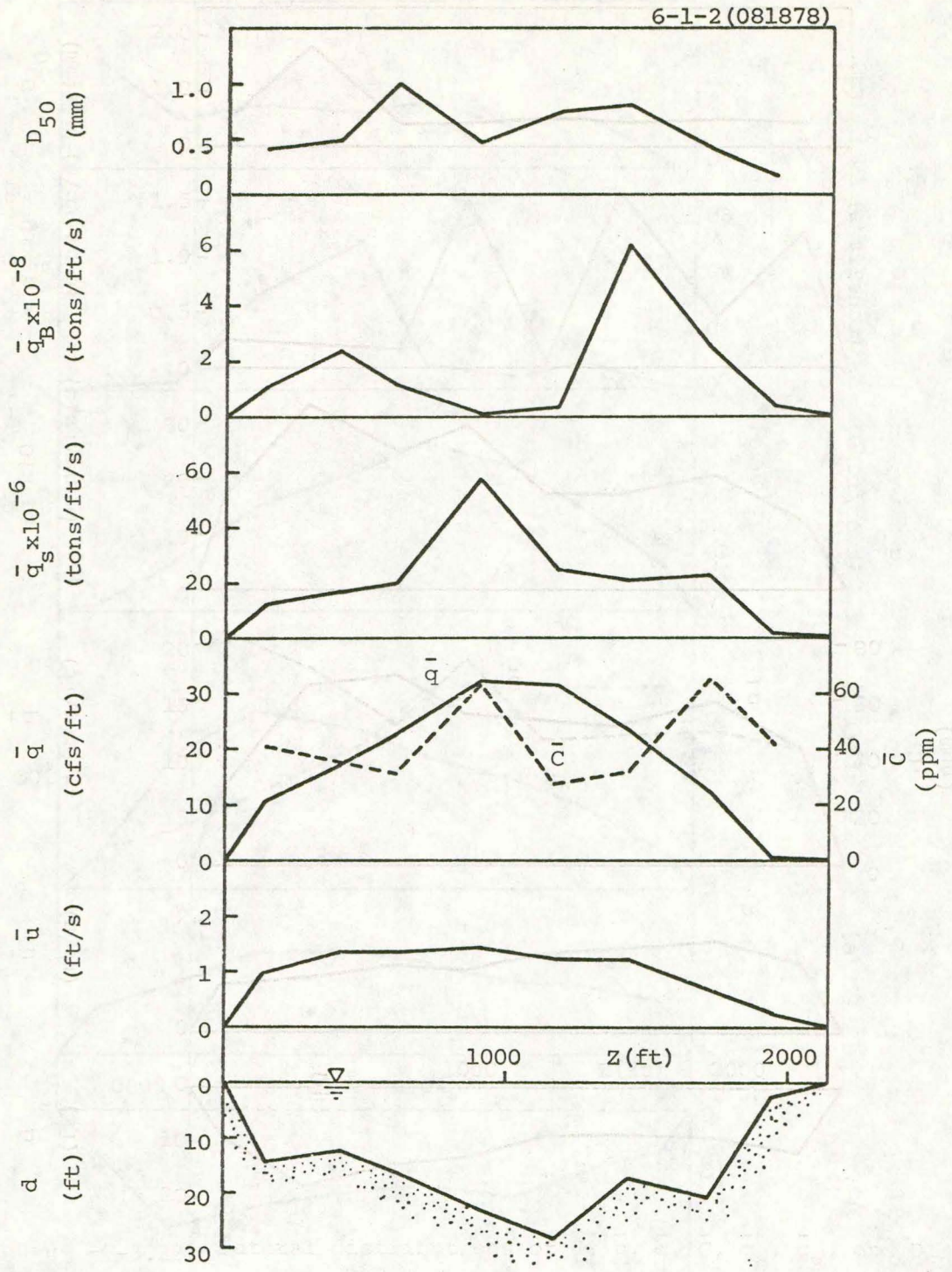

Figure I-C-3.19 Lateral distributions of d, $\bar{u}$, $\bar{q}$, $\bar{C}$, $\bar{q}_s$, $\bar{q}_B$, and D_{50} for section 6-1-2

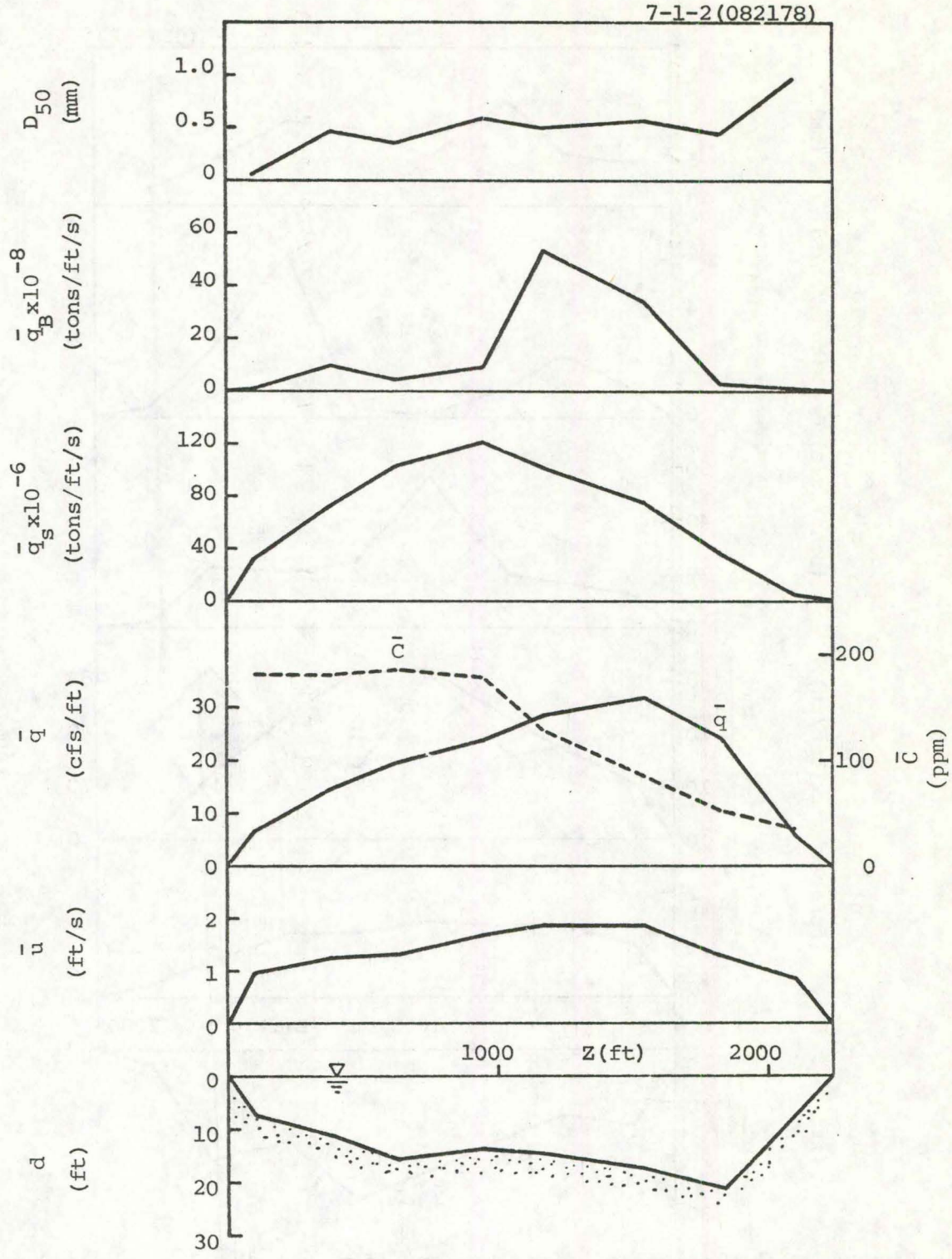

Figure I-C-3.20 Lateral distributions of d, $\bar{u}$, $\bar{q}$, $\bar{C}$, $\bar{q}_s$, $\bar{q}_B$, and D_{50} for section 7-1-2

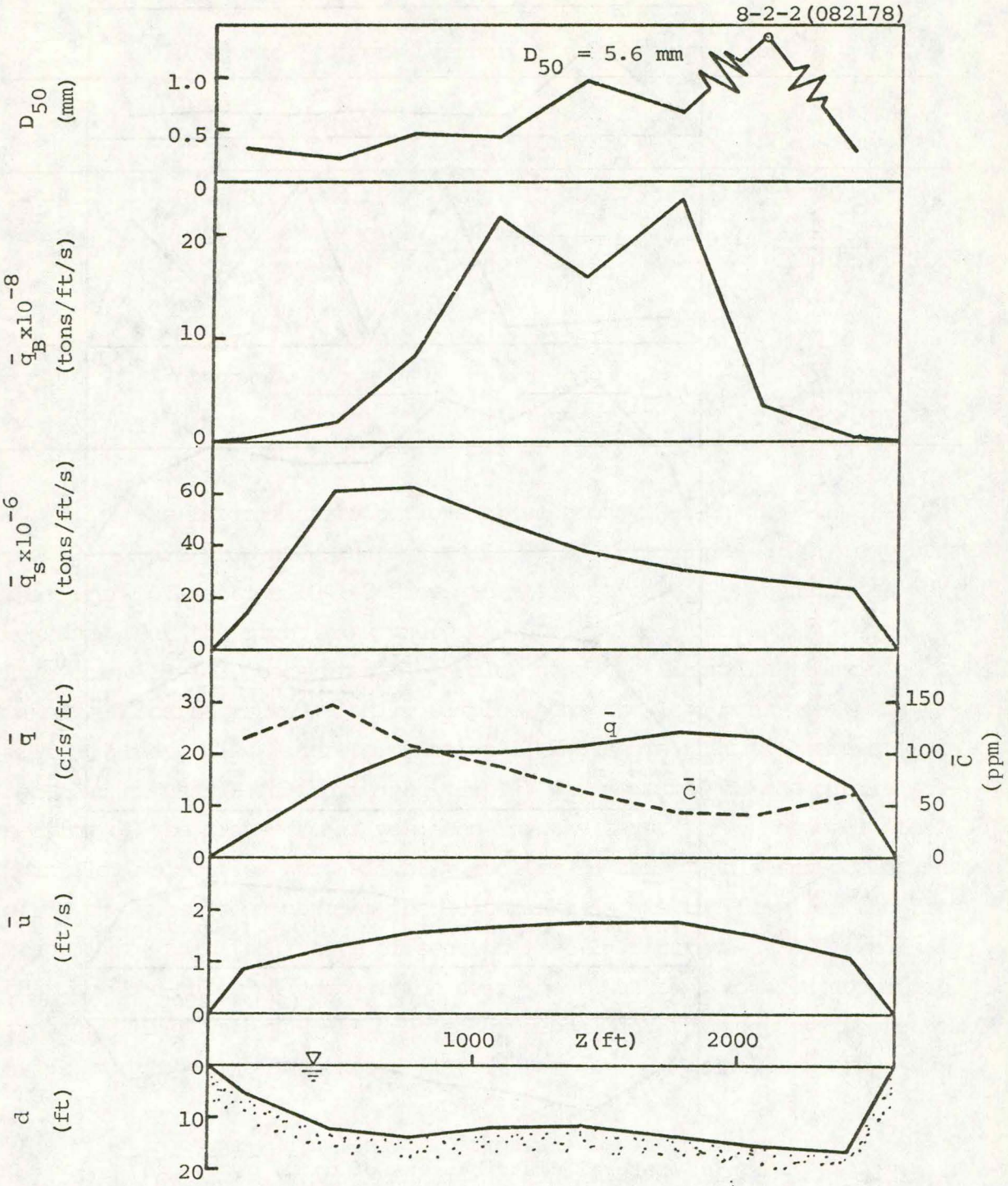

Figure I-C-3.21 Lateral distributions of d, $\bar{u}$, $\bar{q}$, $\bar{C}$, $\bar{q}_s$, $\bar{q}_B$, and D_{50} for section 8-2-2

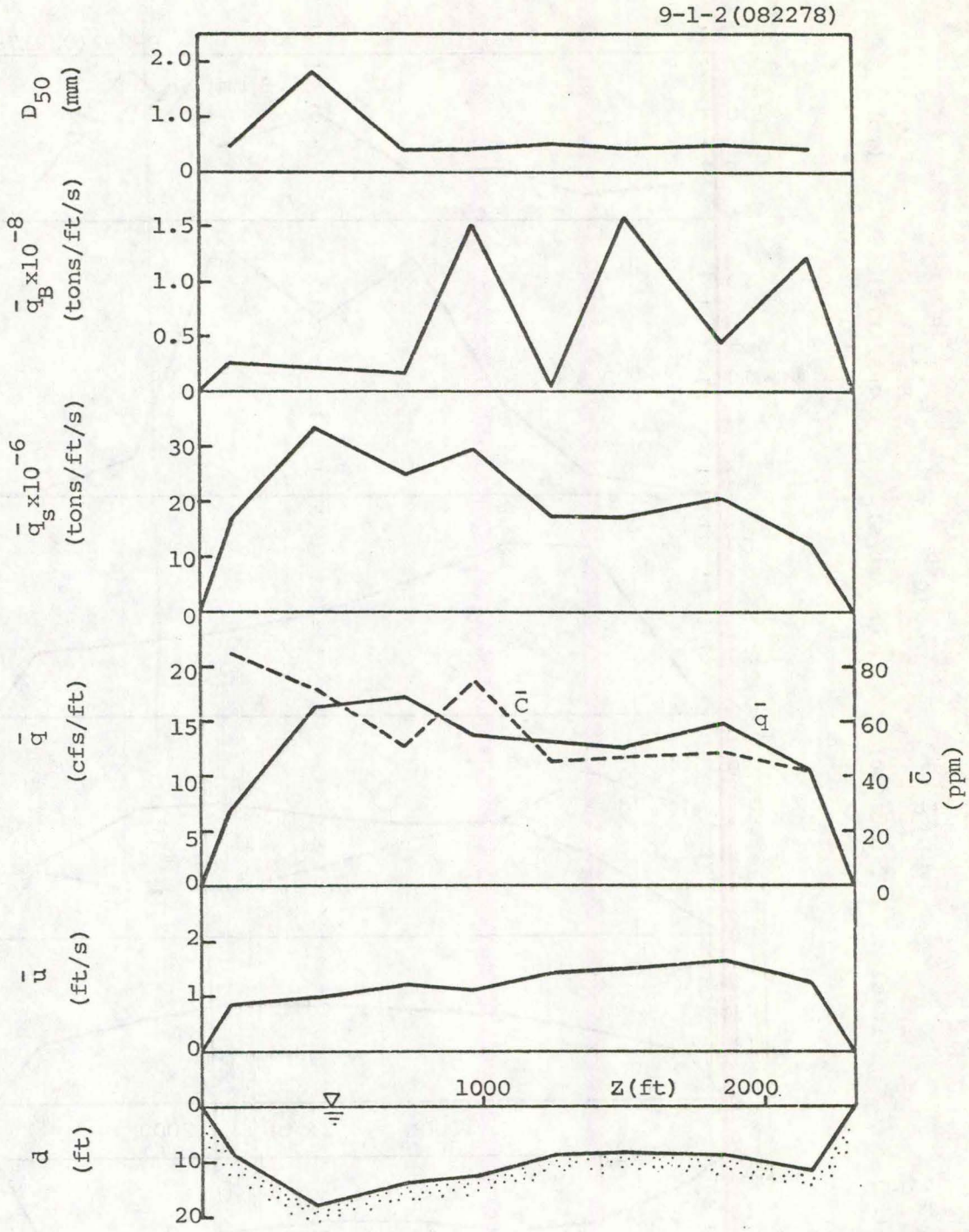

Figure I-C-3.22 Lateral distributions of d, $\bar{u}$, $\bar{q}$, $\bar{C}$, $\bar{q}_s$, $\bar{q}_B$, and D_{50} for section 9-1-2

There are three general features of the MR in this shoaling area that reduce the sediment-transport capacity of the flow. First, the river width increases from section 7-1 to section 8-2, which increases the cross-sectional flow area. For the same discharge, the increased flow area decreases the mean flow velocity, resulting in a decrease in the sediment-transport capacity. Consequently, the excess sediment is deposited until an equilibrium is achieved between the sediment-transport capacity and sediment input. Second, the thalweg crosses the river from the left bank at section 5-1 to the right bank at section 9-1. Near the middle of this crossing an inflection, or so-called "cross-over", results. The cross-over region generally lacks the strong secondary currents produced by bends in the river that significantly increase the sediment-transport capacity of the flow. Finally, the bifurcation of the flow between transects 6 and 9 reduces the main channel flow and therefore diminishes the sediment transport capacity.

Specific features of sections 7-1-2 to 9-1-2 will now be discussed. Figures I-C-3.20 and I-C-3.21 of sections 7-1-2 and 8-2-2 show that the larger depths and unit water discharges occurred near the left bank of Hunt Island, although the larger mean suspended-sediment concentrations and unit suspended-sediment discharges occurred over the navigation channel near the right bank of Buzzard Island. During the first trip, the larger unit suspended-sediment discharges were measured near the left bank at sections 7-1-1 and 8-2-1. It is surmised that the larger flow discharges during the first trip caused a greater extent of lateral dispersion of suspended sediment around Buzzard Island than the smaller discharges during the second trip. The two peaks seen in the unit bed-load-discharge distribution over the shallower central part of section 8-2-2 were due to the effect of the bifurcation downstream at transect 9. The figure for section 9-1-2 shows that the largest depths, unit water, and suspended-sediment discharges occurred along the navigation channel near the right bank. Note, though, that the largest mean velocities were measured near the left bank where the flow bifurcated around the upstream tip of Huff Island. The bed load samples collected at this section were negligible. Table I-C-3.2 summarizes the percentages of water and sediment discharges that flowed into the side-channel sections 7-2-2 and 9-2-2.

Table I-C-3.2

Water and Sediment Discharges at Sections 7 and 9

Section	Date	Q (cfs)	Q_S (tons/day)	Q_B (tons/day)
7-1-2	082178	44,509	13,458	30
7-2-2	082178	4,010 Q_2/Q_1=9%	467 Q_{S2}/Q_{S1}=3%	0.07 Q_{B2}/Q_{B1}=0.2%
9-1-2	082278	30,703	4,281	1.4
9-2-2	082278	7,592 Q_2/Q_1=25%	669 Q_{S2}/Q_{S1}=16%	0.3 Q_{B2}/Q_{B1}=21%

The lateral distributions at sections 10-1-2, 11-1-2, 11-2-2, and 12-1-2 are presented in figures I-C-3.23 through I-C-3.26, respectively. The figure of section 10-1-2 shows that the largest flow quantities were measured near the right bank where the navigation channel was located. At section 11-1-2, bed-material samples near the right bank consisted mainly of coarse gravels, while samples near the left bank were mainly silt and clay. The figure of section 11-2-2 shows that the largest unit bed-load discharge (although negligible) was measured in the middle subsection of the transect, as was seen for the first trip. However, the mean flow velocities were slightly greater in this middle subsection instead of in the subsection nearest the left bank, as was the case for the first trip. Note that the figure of section 12-1-2 (figure I-C-3.26) shows that the bed-material composition near the right bank changed appreciably from the first trip and was due to the deposition that occurred here between trips, which will be discussed later.

4. Longitudinal distributions. Longitudinal distributions of the major flow and sediment quantities are plotted for the main-channel sections in figures I-C-4.1 and I-C.4.2, and for the complete river cross sections in figure I-C-4.3. The longitudinal variations of water discharge, Q; suspended-sediment discharge, Q_S; and bed-load discharge, Q_B; are presented in figures I-C-4.1 and I-C.4.3, while the variations of

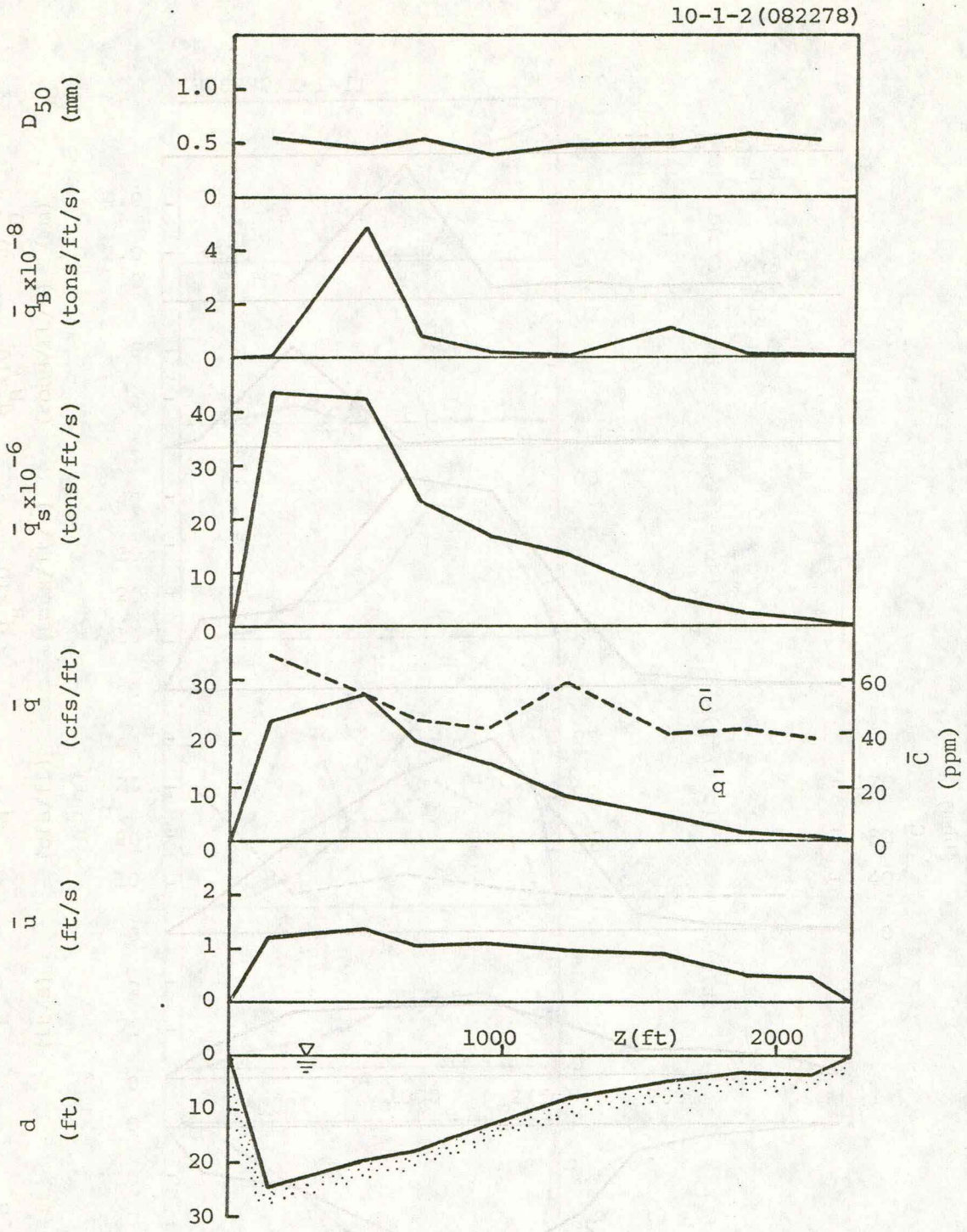

Figure I-C-3.23 Lateral distributions of d, $\bar{u}$, $\bar{q}$, $\bar{C}$, $\bar{q}_s$, $\bar{q}_B$, and D_{50} for section 10-1-2

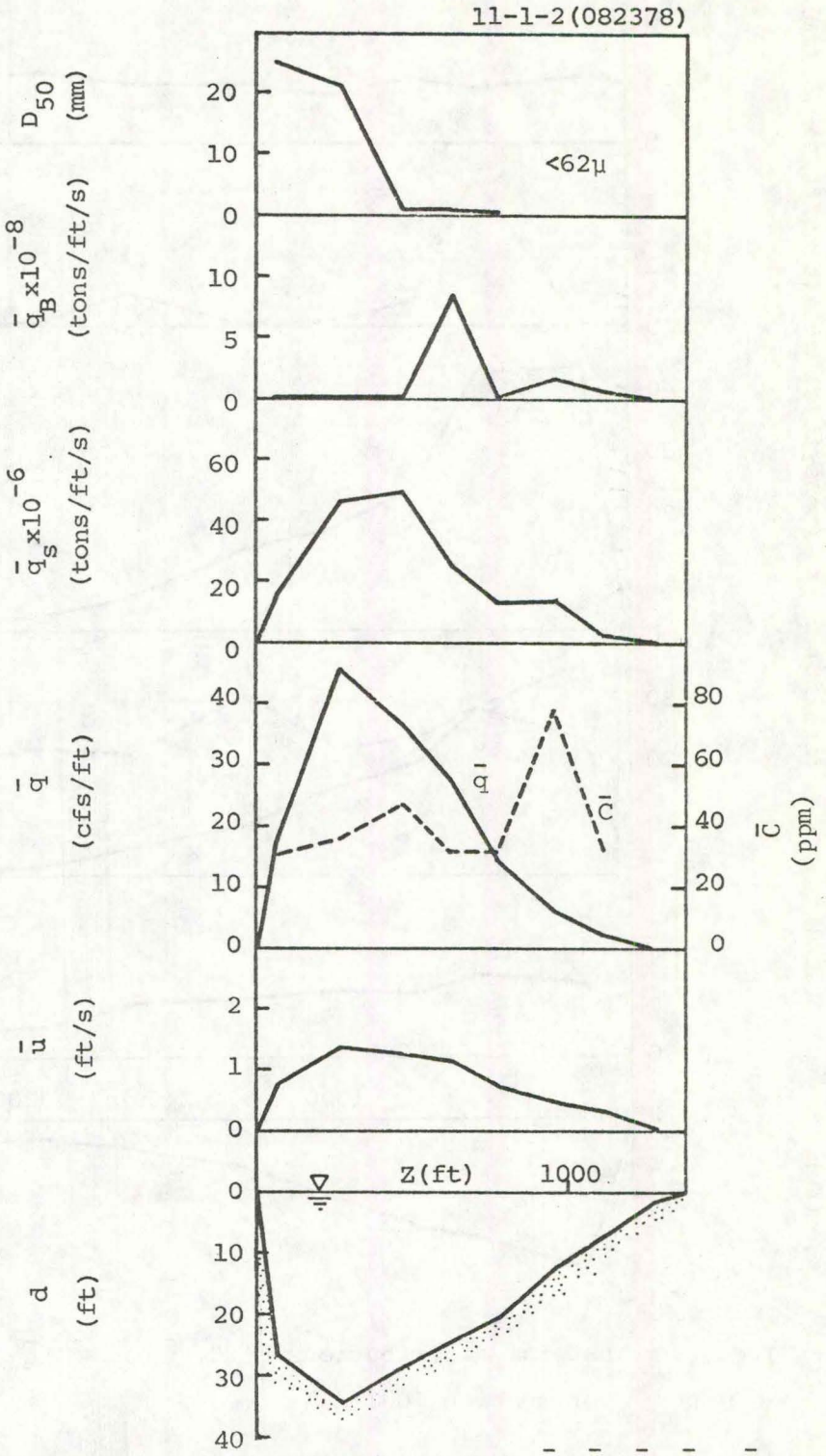

Figure I-C-3.24 Lateral distributions of d, $\bar{u}$, $\bar{q}$, $\bar{C}$, $\bar{q}_s$, $\bar{q}_B$, and D_{50} for section 11-1-2

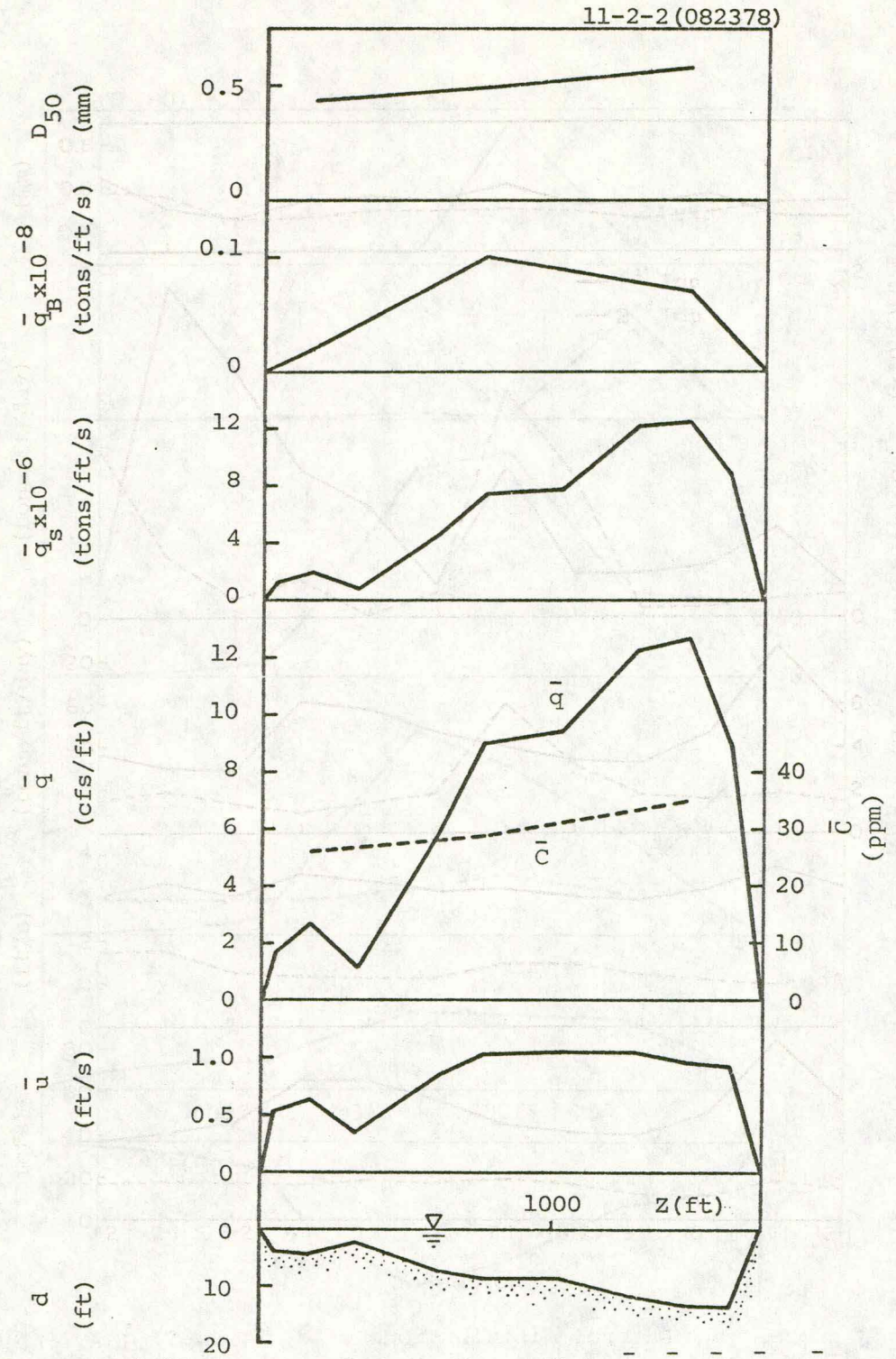

Figure I-C-3.25 Lateral distributions of d, $\bar{u}$, $\bar{q}$, $\bar{C}$, $\bar{q}_s$, $\bar{q}_B$, and D_{50} for section 11-2-2

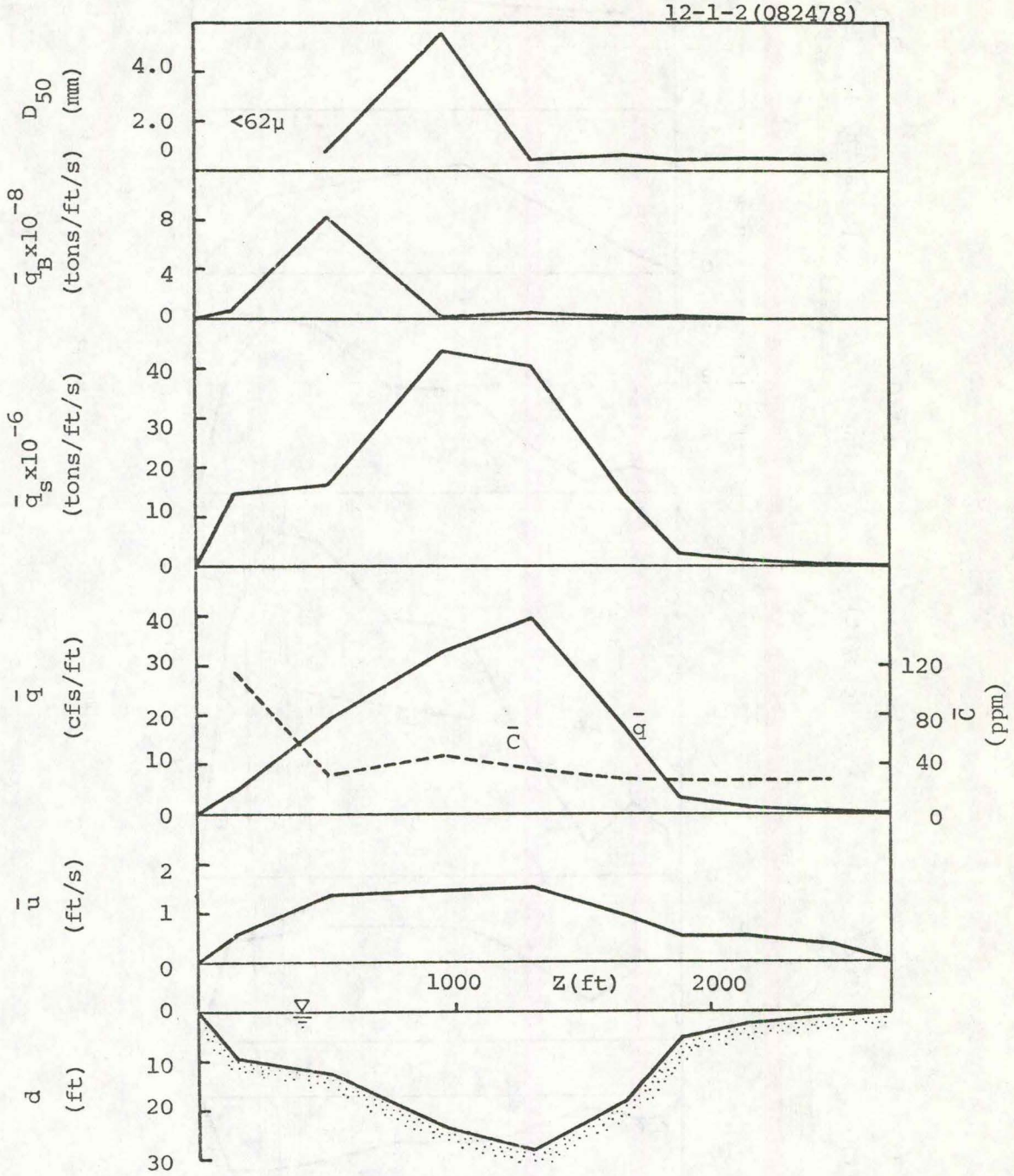

Figure I-C-3.26 Lateral distributions of d, $\bar{u}$, $\bar{q}$, $\bar{C}$, $\bar{q}_s$, $\bar{q}_B$, and D_{50} for section 12-1-2

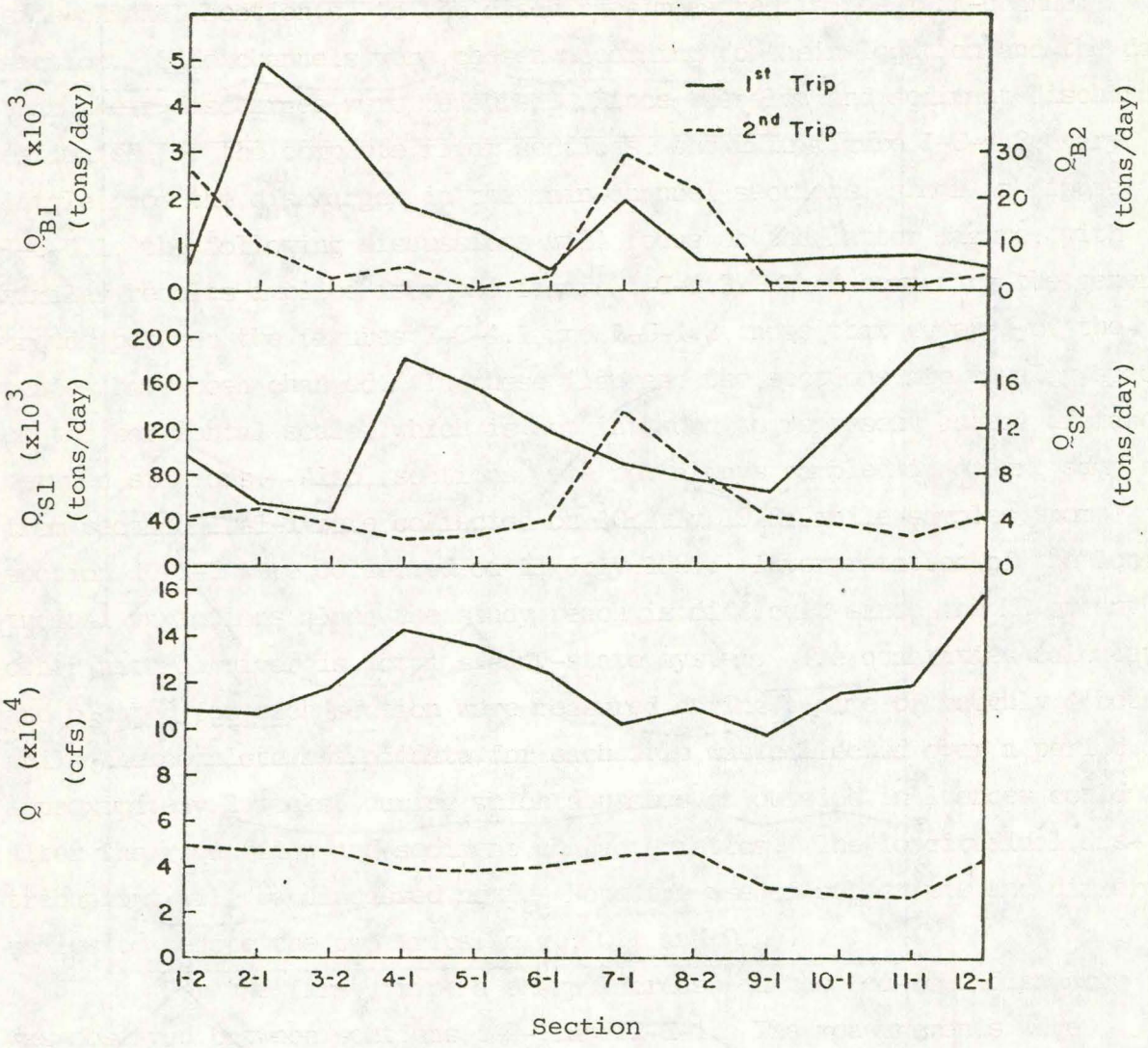

Figure I-C-4.1 Longitudinal variations of Q, Q_s, and Q_B for the main-channel sections

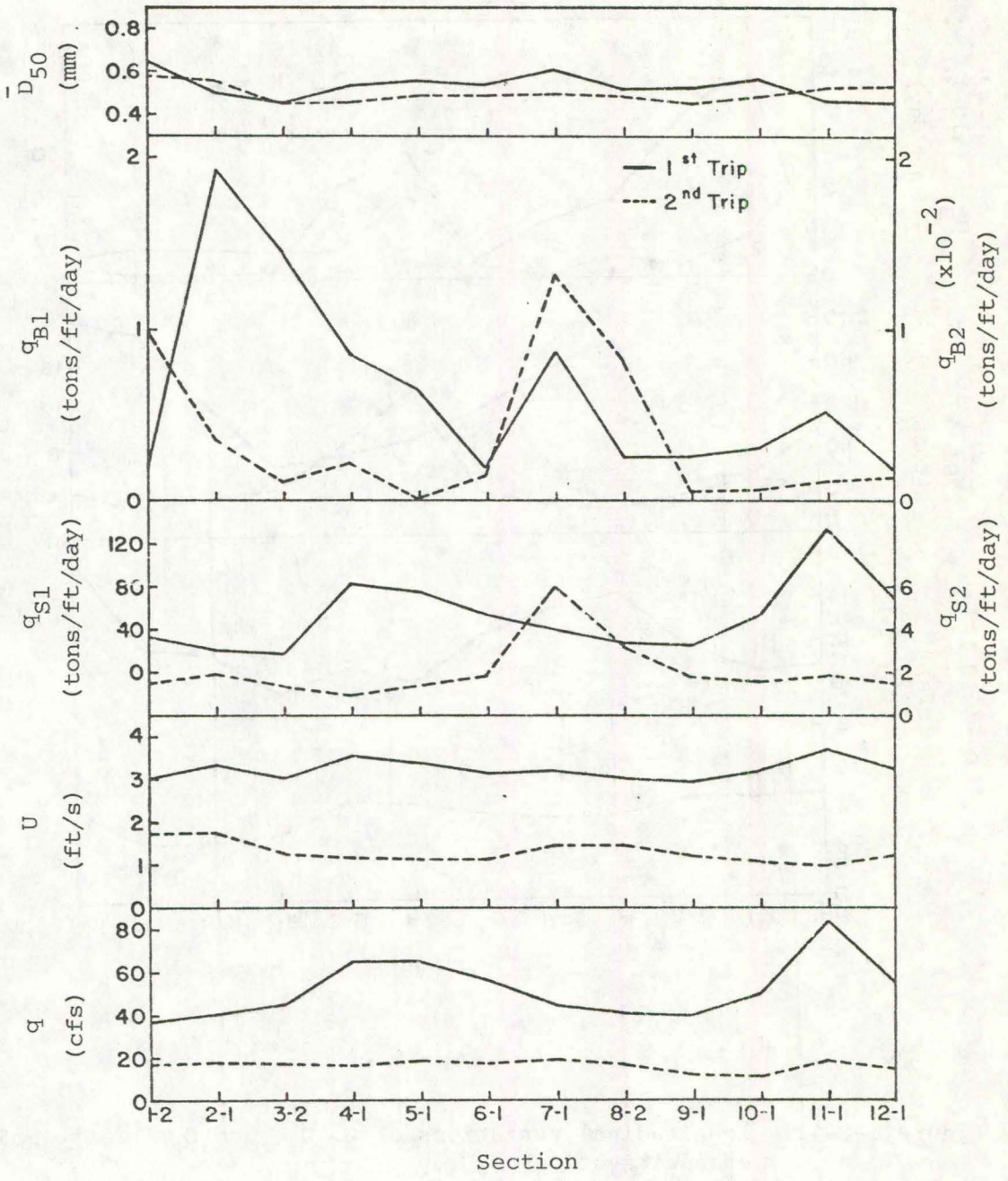

Figure I-C-4.2 Longitudinal variations of q, U, q_s, q_B, and $\bar{D}_{50}$ for the main-channel sections

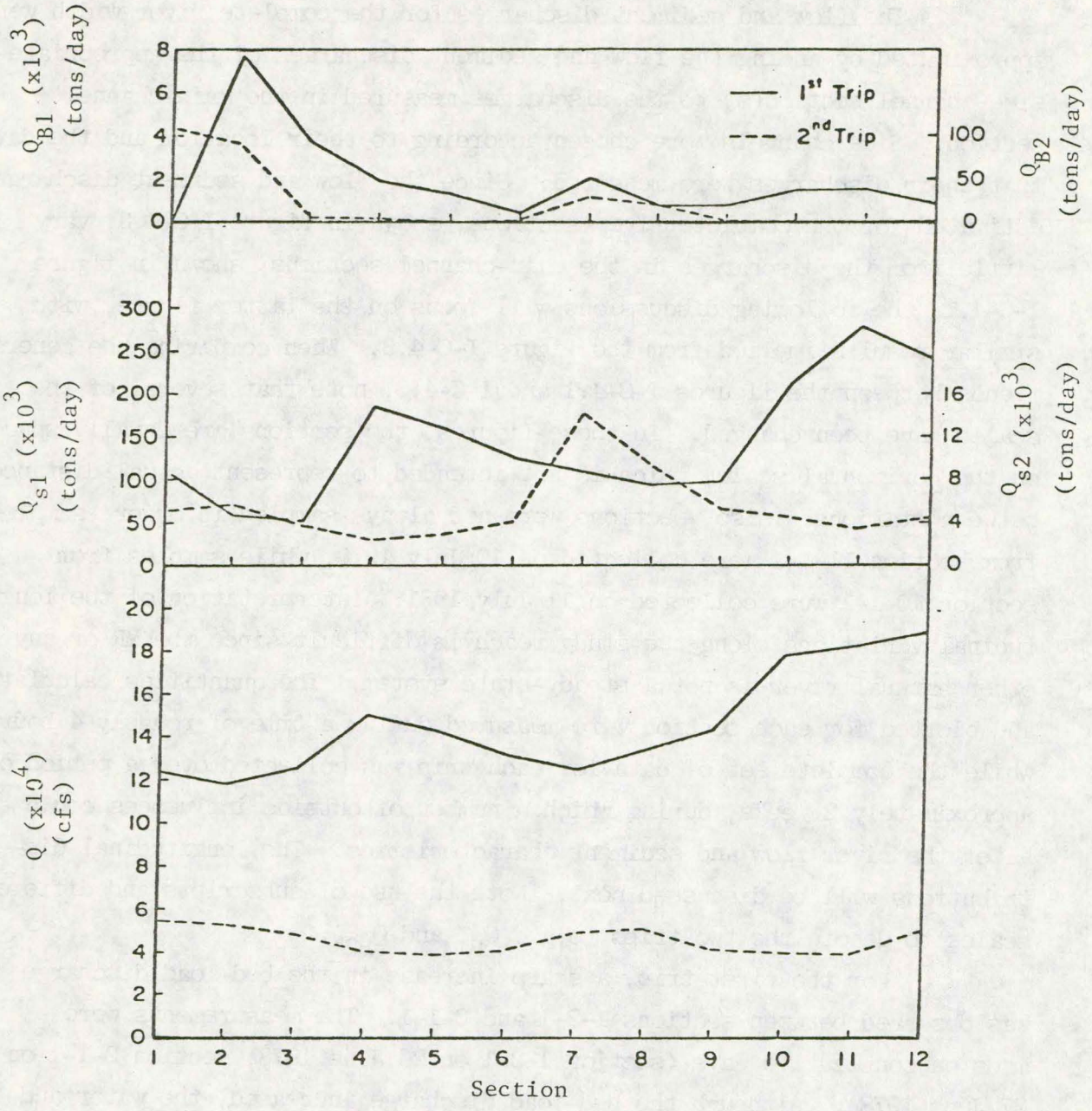

Figure I-C-4.3 Longitudinal variations of Q, Q_s, and Q_B for the complete river cross sections

unit water discharge q (=Q/W), mean flow velocity U (=Q/A), unit suspended-sediment discharge q_s (=Q_s/W), unit bed-load discharge q_B (=Q_B/W), and mean median bed-material size, $\bar{D}_{50}$, are presinted in figure I-C-4.2.

The flow and sediment discharges for the complete river width were approximated by adding the flow and sediment discharges of the appropriate side-channel section(s) to the discharges measured in the main-channel section. Side channels were chosen according to their location and the day that their discharges were measured. Since the flow and sediment discharges estimated for the complete river sections, shown in figure I-C-4.3, vary little from the discharges in the main-channel sections, shown in figure I-C-4.1, the following discussions will focus on the latter figure, with similar results implied from the figure I-C-4.3. When comparing the general trends between the figures I-C-4.1 and I-C-4.3, note that several of the scales have been changed. In these figures, the sections are equally spaced on the horizontal scale, which is not intended to represent actual distances between stations. Also, sections were not always sampled in order; samples from section 11-1-1 were collected on 10 July 1978, while samples from section 10-1-1 were collected on 11 July 1981. Interpretation of the longitudinal variations along the study reach is difficult since the MR or any other natural river is not a steady-state system. The quantities calculated and plotted for each section were measured during a time of roughly 4 hours, while the complete set of data for each trip was collected over a period of approximately 2 weeks, during which a number of outside influences could alter the river flow and sediment characteristics. The longitudinal distributions will be discussed next. Note the use of subscripts and different scales to denote the two trips (e.g., Q_{B1} and Q_{B2}).

For the first trip, a sharp increase in the bed-load discharge was observed between sections 1-2-1 and 2-1-1. The measurements were made on consecutive days (section 1-2-1 on 26 June 1978; section 2-1-1 on 27 June 1978). Although the bed-load discharge increased, the water and suspended-sediment discharges decreased. As seen in figure I-A.1, section 2-1 was located at a river bend, where the main channel width was narrower than at section 1-2. The narrower river width reduced the cross-section area and increased the mean flow velocity, which, to a minor extent,

increased the bed-load-transport capacity. The strong secondary currents occurring in the river bend are the primary cause of the bed-load movement. The entirely different cross-sectional profiles of sections 1-2 and 2-1 shown in figure I-C-2.1 illustrate the effect the secondary currents have had along the right bank of section 2-1. The tributary inflow from the Fox River, which entered the MR approximately 1.5 mi upstream from section 2-1, might have also contributed to the large bed-load movement. No flow measurements were taken in the Fox River, so a comparison was not possible. The bed-load discharge decreased at the next several sections downstream from section 2-1-1.

Heavy rains throughout Iowa during the first trip on 25 and 27 June 1978 caused the increased water and suspended-sediment discharges measured at section 4-1-1 on 29 June 1978. These high discharges gradually diminished over the following week.

Although the water and suspended-sediment discharges continued to decrease at sections 6-1-1 and 7-1-1, the bed-load discharge displayed a significant rise at section 7-1-1 and then decreased at section 8-2-1. Table I-C-4.1 summarizes the flow and sediment discharges measured during the first trip at sections 6, 7, and 8. The bed-load discharge increased by a factor of 5 at transects 6 and 7, which suggests that scouring was taking place along this reach. The cross-sectional profiles of section 7-1 in figure I-C-2.1 indicate that some scouring had occurred here between trips. Although roughly 16 percent of the main channel flow entered the side channel (section 7-2) and the river width increased between sections 6-1 and 7-1, the cross-sectional area decreased from an estimated 39,200 ft^2 at section 6-1-1 to 31,600 ft^2 at section 7-1-1. Estimation of the percentage of water discharge from section 6-1 that would flow through section 7-1, based on the first-trip measurements, gives a 7 percent increase in the mean flow velocity. This increased mean flow velocity would increase the amount of bed load being transported at section 7-1, although not to the extent that was observed during the first trip.

Table I-C-4.1

Water and Sediment Discharges at Sections 6, 7, and 8

Section	Date	Q (cfs)	Q_S (tons/day)	Q_B (tons/day)
6-1-1	070578	123,949	118,541	414
7-1-1	070578	101,830	89,467	1,958
7-2-1	070678	16,155	13,280	102
		117,985	102,747	2,060
8-2-1	070678	108,694	75,436	681

Since measurements for sections 7-1-1 and 8-2-1 were taken on consecutive days, flow discharges should compare favorably. Although the flow discharge increased slightly from 7-1-1 to 8-2-1, the suspended-sediment discharge decreased and the bed-load discharge at 8-2-1 was only one-third of that at 7-1-1. The mean velocity, U, had a slight reduction from 3.22 ft/s to 3.04 ft/s as the cross-sectional area increased from 31,600 ft^2 to 35,700 ft^2. For the same discharge, the mean flow velocity would decrease roughly 10 percent from sections 7-1 to 8-2. This reduced mean velocity would decrease the sediment-transport capacity of the river, thus causing the deposition of sediment in the reach between sections 7-1 and 8-2. This area located near the downstream tip of Buzzard Island, as discussed earlier, is known for its frequent shoaling problems (Nakato and Kennedy,1977).

During 7-9 July 1978, heavy rain and flooding in northwest Iowa caused an increase in flow along the MR. The effect of this rain is seen in the large water and suspended-sediment discharges at sections 10-1, 11-1, and 12-1. Note that part of the large increase observed in the water discharge between sections 11-1 and 12-1 was due to the incoming flow through section 11-2. Table I-C-4.2 summarizes the water and sediment discharges through sections 11 and 12 for the first trip. The numbers in parentheses indicate the percentage of the respective total discharge passing through side channel 11-2.

A water discharge of 115,767 cfs was measured on 11 July 1978 at section 10-1. Since the water discharge measured on the previous day at section 11-1 was approximately 2 percent larger, there was practically no change in the flow conditions from 10 to 11 July 1978, during which transects 11 and 12 were measured. Then from continuity considerations, the water or sediment discharges at section 12-1-1 should closely approximate

Table I-C-4.2 Water and Sediment Discharges at Stations 11 and 12

Section	Date	Q (cfs)	Q_s (tons/day)	Q_B (tons/day)
11-1-1	071078	Q_1 = 118,558	Q_{s1} = 188,646	Q_{B1} = 733
11-2-1	071078	Q_2 = 64,772 (35%)	Q_{s2} = 91,454 (33%)	Q_{B2} = 864 (54%)
		$Q_1 + Q_2$ = 183,330	$Q_{s1} + Q_{s2}$ = 280,100	$Q_{B1} + Q_{B2}$ = 1,597
12-1-1	071178	159,183	202,245	516

the discharge measured at section 11-1-1 plus part of the incoming discharge from section 11-2-1. Approximately 54 percent of the water, suspended-sediment, and bed-load discharges measured at section 11-2-1 entered the main channel upstream from section 12-1-1. Using this 54 percent approximation, the main-channel water discharge at section 12-1, estimated from section 11, differed by less than 4 percent from the water discharge measured at section 12-1. However, the bed-load discharge measured at section 12-1-1 was less than that measured at section 11-1-1, without considering the extra bed-load discharge passed through section 11-2-1 into the main channel. In addition, an estimated 49,800 tons/day of the suspended-sediment discharge at section 11-2-1 entered the main channel upstream from section 12-1 through the two subsections nearer the right bank of section 11-2-1. When added to the suspended-sediment discharge through section 11-1-1, the total exceeds the suspended-sediment discharge measured at section 12-1-1 by nearly 20 percent. The reduction in bed-load discharge resulted from the smaller flow velocity at section 12-1, compared to those at sections 11-1 and 11-2. The mean velocity, U, shown in figure I-C-4.2, decreased from 3.71 ft/s at section 11-1-1 to 3.25 ft/s at section 12-1-1 due to the increased river width. The lateral distributions at sections 11-1-1, 11-2-1, and 12-1-1 in figures I-C-3.11, I-C-3.12, and I-C-3.13, respectively, show this velocity decrease in greater detail across the transects. The lower flow velocities across section 12-1-1 diminished the sediment-transport capacity of the river, which, therefore, reduced the suspended-sediment and bed-load discharges. The cross-section profiles of section 12-1 in figure I-C-2.1 show that deposition occurred over most of the bed, with up to 7-ft rises in the bed elevation. This reach of the MR is sufficiently wide and deep that large amounts of sediment deposition presently do not critically affect the navigation channel. According to COE (RI), depths of over 60 ft have been measured in the main channel two miles downstream, at RM 345.

The water discharge during the second trip showed only minor fluctuations, as seen in figures I-C-4.1 and I-C-4.2. Note that part of the drop in water discharge downstream from section 8-2-2 was due to the flow bifurcation at transect 9. Most of the flow through the side channel, section 8-2-2, reentered the main channel through section 11-2-2 and caused some of the subsequent rise in water discharge at section 12-1-2.

Distinct peaks occurred in the suspended-sediment and bed-load discharges at section 7-1-2. This coincidence of peaks is interesting, since these sediment quantities were calculated independently of each other. This peaking occurred in the same shoaling area that was discussed for the first trip except now the sediment discharges decreased toward transect 9, instead of transect 8. Table I-C-4.3 summarizes the measured flow quantities and sampling dates for sections 6 through 9.

Table I-C-4.3

Water and Sediment Discharges at Sections 6 through 9

Section	Date	Q (cfs)	Q_S (tons/day)	Q_B (tons/day)
6-1-2	081878	39,790	4,046	3.2
7-1-2	082178	44,509	13,458	30.0
7-2-2	082178	4,010	467	0.07
		48,519	13,925	30.07
8-1-2	082278	1,363	243	0.3
8-2-2	082178	46,400	8,523	21.0
		47,763	8,766	21.3
9-1-2	082278	30,703	4,281	1.4
9-2-2	082278	7,592	669	0.3
		38,295	4,950	1.7

Due to the changes in flow conditions between the days when sections 6 and 7 were measured, the primary cause of the increased sediment discharge observed at section 7 cannot be resolved. Since measurements at sections 7-1-2 and 8-2-2 were completed on the same day, the water and sediment discharges should compare closely. The 4 percent difference seen in the water discharge was due to inaccuracies of the measurements and any minor flow fluctuations that occurred during the 8-hr sampling period. The significant reduction in the suspended-sediment discharge illustrates the decreased sediment-transport capacity of the flow at section 8-2-2. The overnight decrease in flow conditions from 21 to 22 August 1978 is believed to have caused the diminished sediment discharges that were measured at transect 9.

The longitudinal profile of the composite median diameter, $\bar{D}_{50}$, shows that the particle sizes were generally finer during the second trip. This decrease in $\bar{D}_{50}$ was likely due to the frequent rains throughout the Midwest during June and July, which produced high water discharges and flow velocities in the MR that transported large amounts of fine sediment. These high flow conditions were evident during the first trip. The second trip in August, however, found water discharges and flow velocities roughly one-third and one-half, respectively, of those measured during the first trip. This reduction in flow significantly decreased the river's sediment-transport capacity so that the suspended-sediment discharges during the second trip were only approximately 4 percent of those during the first trip. Consequently, part of the sediment that was in suspension during the first trip settled out of the flow and became bed material. The sediment deposited from the lower flows was finer than the median particle size in the existing bed, which resulted in a higher proportion of fine sediment, and therefore a finer median bed-material size.

One final observation was that the composite median diameter, $\bar{D}_{50}$, at section 12-1 was larger during the second trip than the first trip. This observation is in agreement with the previous discussion, since the bed load deposited at section 12-1 came from upstream reaches where the mean particle size was larger.

5. Velocity and suspended-sediment-concentration profiles. Velocity and concentration profiles were constructed for the DMR and the main-channel sections of the MR where detailed flow velocity and suspended-sediment-concentration measurements were taken. The method of least squares was used to calculate the equation of the line representing each velocity and suspended-sediment-concentration profile. Representative profiles are shown in figure I-C-5.1 for the vertical 141 m from the right bank of section 9-1-1.

The velocity profiles were represented by the well-known logarithmic relation:

$$u = \frac{2.30u_*}{\kappa} \log (y/d) + \text{const.} \qquad (1.1)$$

where $u_* = \sqrt{gdS}$; g is the gravitational constant; S is the energy slope;

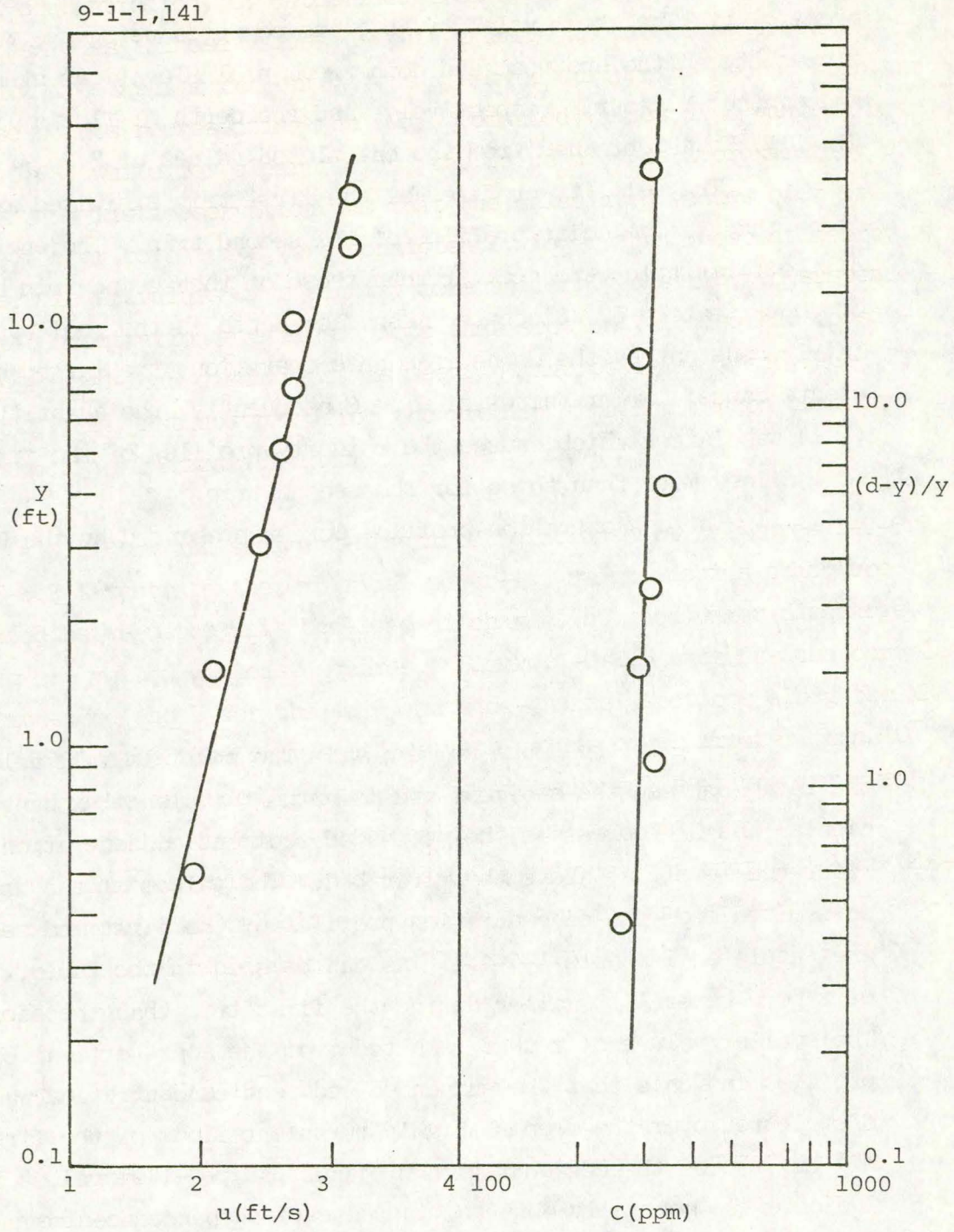

Figure I-C-5.1 Representative velocity and concentration profiles at section 9-1-1

and κ is the Karman constant. The quantity $2.3\ u_*/\kappa$ was determined for each velocity profile as the increment in velocity over a logarithmic cycle of y. The shear velocity, u_*, was computed using the water-surface slope between the upstream and downstream pool elevations at Keokuk, Iowa, and Canton, Missouri, respectively, and the depth of flow at the vertical. Finally, κ was obtained from the calculated values of $2.3u_*/\kappa$ and u_*.

The velocity profiles of the first trip exhibited a steeper slope than the velocity profiles of the second trip. The energy gradients of the first trip were greater than those of the second trip by a factor of approximately 5. Since the mean flow depth in the pool was maintained fairly constant by the downstream gate operation, the larger energy gradients caused larger values of u_*. Consequently, the quantity $2.3u_*/\kappa$ in (1.1) was larger which caused the velocity profiles of the first trip to be inclined more than those for the second trip.

The concentration profiles were represented by the Rouse equation:

$$\frac{C}{C_a} = \left(\frac{d-y}{y}\ \frac{a}{d-a}\right)^z \qquad (1.2)$$

where $z = \frac{w}{\beta\kappa u_*}$ is the Rouse number; w is the particle fall velocity; β is the ratio between the sediment and momentum turbulence exchange coefficients; and C_a represents the suspended-sediment concentration at some reference level, a, above the river bed. The values of the Rouse number determined from the concentration profiles of the first and second trips are tabulated in table I-C-4.4. As can be seen in the table, the values of z were generally smaller during the first trip than the second trip. The smaller values of z that resulted from the near-vertical concentration profiles indicate that the suspended-sediment concentration was uniformly distributed over the deeper, highly turbulent flows of the first trip. All but two of the concentration profiles had positive values for z, which indicate the generally observed increase of suspended-sediment concentration from the water surface to the river bed (increasing (d-y)/y). The two negative values calculated for z resulted from the least-squares analysis of inexact suspended-sediment concentration measurements, which were less than 50 ppm at both sections and varied less than 7 ppm over the flow depth. The table also lists the values of the Karman constant, κ,

Table I-C-4.4

Calculated Values of u_*, κ, $\bar{C}$, and z for the Major Verticals

Section and Trip No.	Distance from R.B. (m)	u_* (ft/s)	κ	$\bar{C}$ (ppm)	z
13-1-1	99	0.241	0.30	1791	0.0076
1-2-1	162	0.170	0.26	621	0.032
2-1-1	174	0.168	0.31	218	0.037
3-2-1	353	0.187	0.42	142	0.161
4-1-1	183	0.211	0.44	1193	0.018
5-1-1	260	0.210	0.52	690	0.015
6-1-1	206	0.206	0.26	428	0.016
7-1-1	111	0.181	0.46	431	0.0081
8-2-1	151	0.179	0.53	258	0.051
9-1-1	141	0.186	0.55	292	0.030
10-1-1	36	0.191	0.32	422	0.015
11-1-1	30	0.230	0.29	679	0.0094
12-1-1	294	0.199	0.40	465	0.0018
13-1-1	80	0.235	0.98	358	0.024
13-1-2	86	0.145	0.82	101	0.175
1-2-2	170	0.075	0.25	35	0.036
2-1-2	56	0.072	0.32	84	0.163
3-2-2	262	0.089	0.21	21	0.126
4-1-2	305	0.073	0.46	26	0.081
5-1-2	246	0.078	0.66	26	0.063
6-1-2	188	0.078	0.60	31	0.038
7-1-2	119	0.080	0.40	182	0.013
8-2-2	141	0.075	0.46	147	0.073
9-1-2	124	0.077	0.35	72	0.041
10-1-2	44	0.078	0.25	69	0.168
11-1-2	19	0.092	0.65	31	-0.012
12-1-2	291	0.075	0.35	47	-0.0026

calculated from the logarithmic velocity profiles, and the mean suspended-sediment concentration, $\bar{C}$, determined from depth-integrated suspended-sediment samples. These values exhibit a large amount of scatter, especially for the smaller concentrations observed during the second trip and for those points representing the DMR. Computed values of κ ranged from 0.21 to 0.98, while for clear fluids, the value of κ is approximately 0.4.

One last observation was that the calculated values of z at section 7-1 for both trips were consistently lower than those at nearby sections. Lower values of z signify more uniformly distributed suspended-sediment-concentration profiles. Note that section 7-1 also had consistently high bed-load discharges, as seen in figures I-C-4.1 and I-C-4.2. This section is just upstream from the problem shoaling region near the downstream tip of Buzzard Island.

6. Flow and sediment-discharge relationships. Figures I-C-6.1 and I-C-6.2 illustrate the empirical power-law relationships that were formulated between the unit bed-load discharge, q_B, and water discharge, Q, using the method of least squares. Figure I-C-6.1 presents the correlation between q_B and U for the main-and side-channel sections along the MR study reach. Note that only sections with values of q_B greater than 10^{-3} tons/ft/day were included. Although the side-channel sections were generally much smaller in cross-sectional area and had smaller water and sediment discharges than the main-channel sections, the unit bed-load discharges and mean flow velocities for both the main- and side-channel sections were of comparable magnitude. The result for the least-squares analysis yielded

$$q_B = 6.36 \times 10^{-4} U^{5.5} \qquad (1.3)$$

Figure I-C-6.2 illustrates the relationship between q_B and U for the main-channel sections (including section 11-2-1), which is represented by

$$q_B = 5.66 \times 10^{-4} U^{5.7} \qquad (1.4)$$

This equation shows that q_B is very sensitive to changes in U, and that a 1-percent increase in the mean flow velocity would be expected to produce

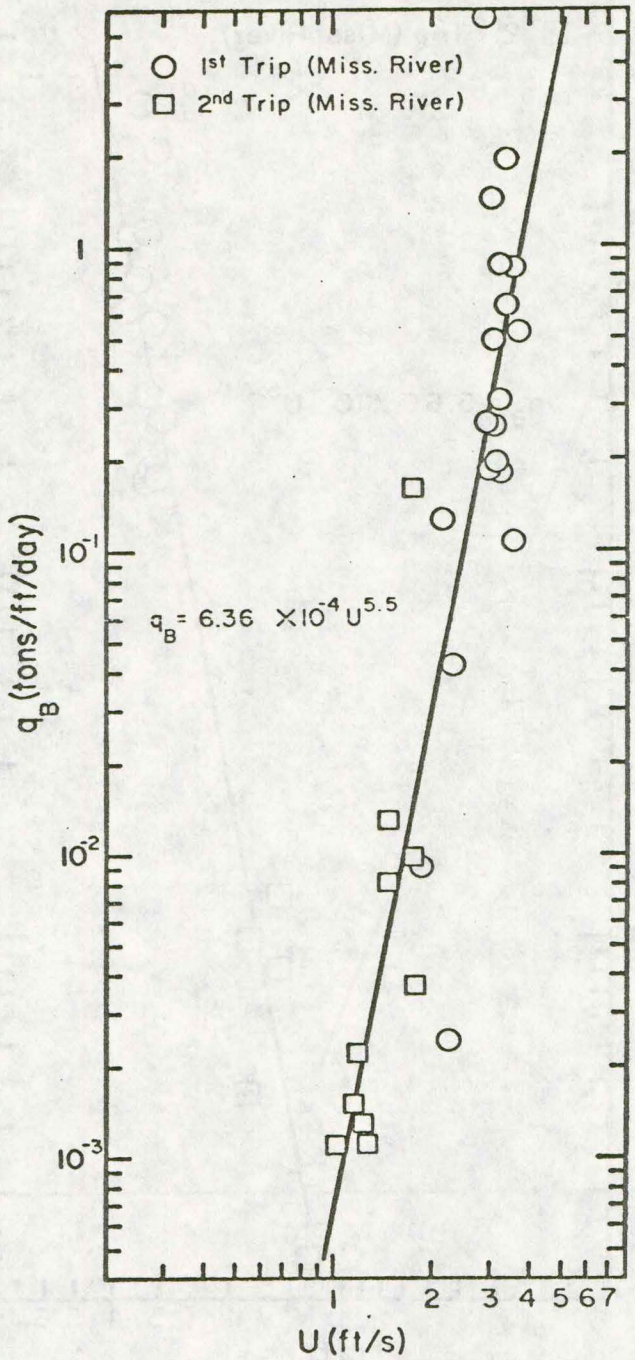

Figure I-C-6.1 Relationship between U and q_B for the main- and side-channel sections

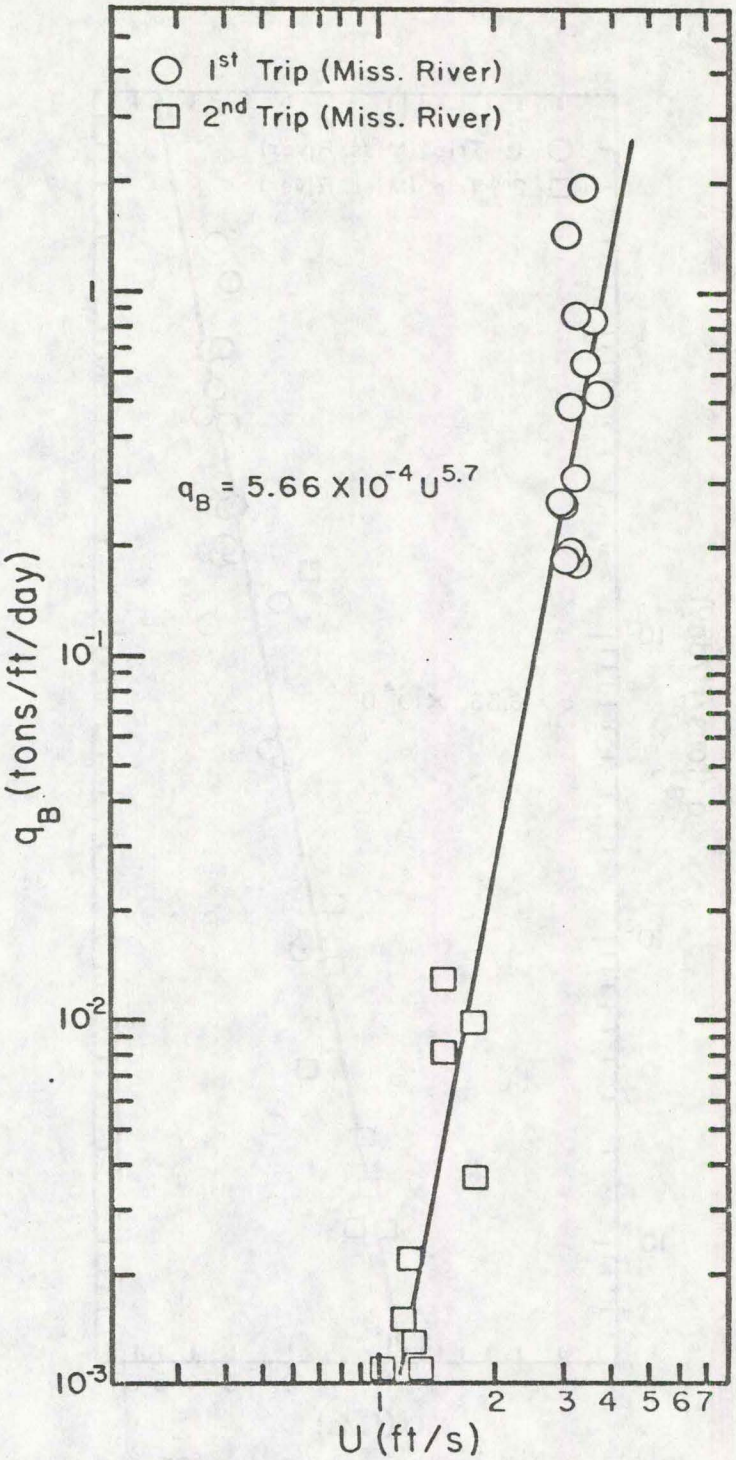

Figure I-C-6.2 Relationship between U and q_B for the main-channel sections

approximately a 6-percent increase in the unit bed-load discharge. The expected increase in the unit bed-load discharge for an increase in the mean flow velocity can be estimated from (1.4). For example, closing side channel 9-2 would increase the mean flow velocity through section 9-1 by an estimated 28 percent (the average of the values of 31 percent during the first trip and 25 percent during the second trip, as listed in tables I-C-3.1 and I-C-3.2, respectively), assuming the cross-sectional area remained constant. From (1.4), this increased flow velocity would be expected to increase the unit bed-load discharge in section 9-1 by a factor of approximately 2.6. Similarly, the closure of section 7-2 would increase U in section 7-1 by an estimated 12 percent (the average of the values of 16 percent during the first trip and 9 percent during the second trip, as shown in tables I-C-3.1 and I-C-3.2, respectively), assuming a constant cross-sectional area. This increased U would be expected to increase the bed-load discharge through section 7-1 by approximately 68 percent.

Figure I-C-6.3 shows the correlation between the suspended-sediment discharge, Q_s, and the water discharge, Q, for the MR main-channel sections (note that section 11-2 was included due to its large flow discharge). The power-law relation is

$$Q_s = 1.44 \times 10^{-8} Q^{2.5} \qquad (1.5)$$

The suspended-sediment discharge is not as sensitive to changes in the water discharge as the unit bed-load discharge is to changes in the mean flow velocity. It is shown by (1.5) that for the 28 percent average increase in Q expected if section 9-2 were closed, the suspended-sediment discharge through section 9-1 would increase by 70 percent. The 12 percent average increase in Q through section 7-1 expected if section 7-2 were closed would increase the suspended-sediment discharge through section 7-1 by approximately 30 percent. Therefore, the closure of section 7-2 or 9-2 would significantly increase both the bed-load and suspended-sediment discharges through the main channel. Accordingly, it can be concluded that the closure of either side section would help alleviate the shoaling problem near the downstream tip of Buzzard Island.

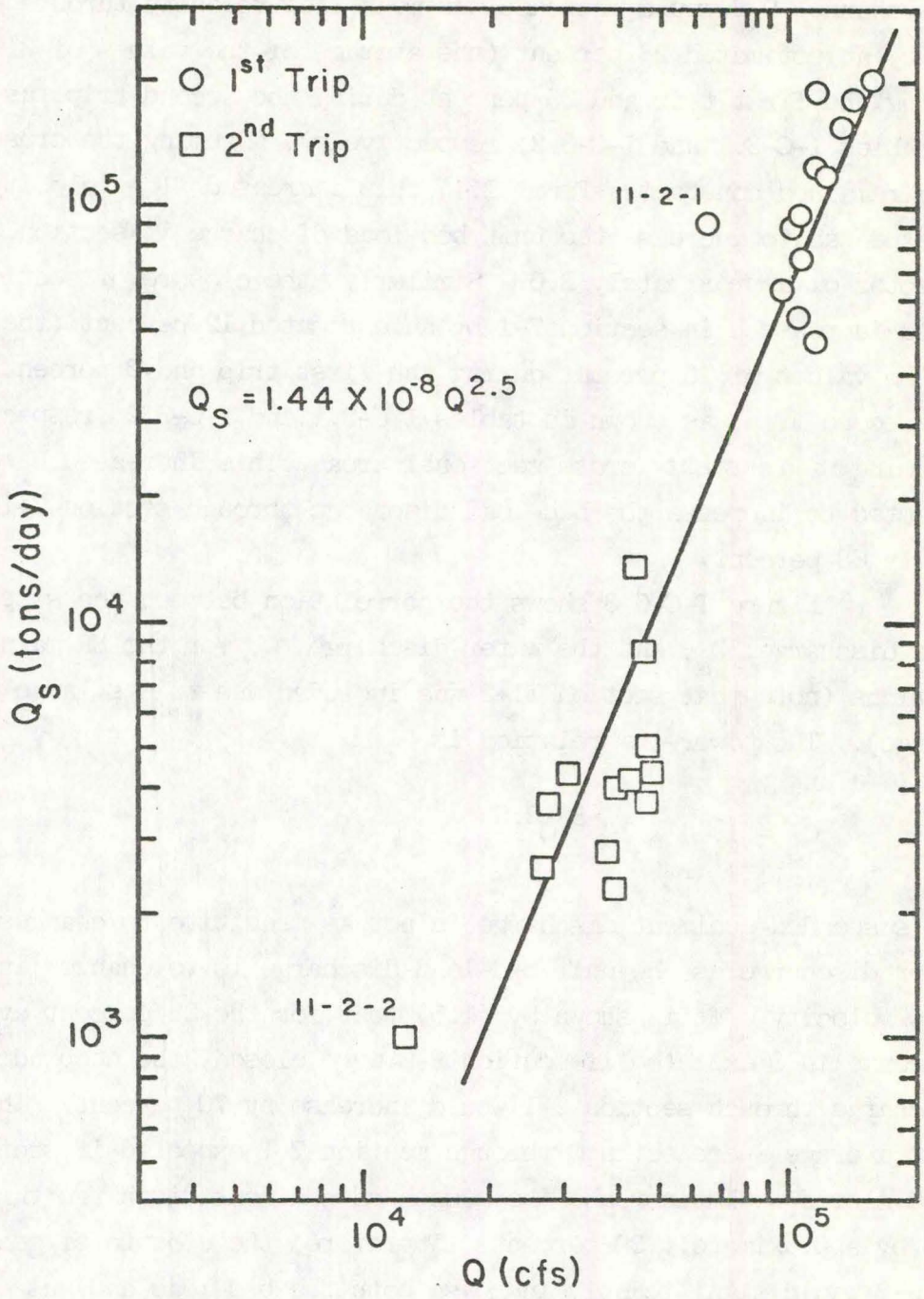

Figure I-C-6.3 Relationship between Q and Q_s for the main-channel sections

One final point worth mentioning is the portion that the bed-load discharge contributed to the measured total-load discharge, $Q_T = Q_B + Q_S$. From the data collected during this study, it appeared that in all but a few sections the bed-load discharge constituted less than 1 percent of the total measured sediment discharge, especially for the low discharges during the second trip. Note that the suspended-sediment load was considered to be primarily wash load.

D. Conclusions. The principal conclusions derived from the present study are summarized as follows:

1. There are three general features of the MR near the shoaling reach at Buzzard Island to which the shoaling problem is attributed. First, the main-channel flow bifurcates at two locations in this reach. Second, the river widens and reduces the sediment-transport capacity since the increased cross-sectional flow area decreases the mean flow velocity. Finally, located near the downstream tip of Buzzard Island is a cross-over reach which generally lacks the strong secondary currents that are produced by bends in the river and significantly increase the sediment-transport capacity of the flow there.

2. The sediment causing the shoaling problem originates primarily from the DMR. The smaller energy slope and velocity of the MR, in comparison with those of the DMR, are unable to transport the coarse sediment inflow from the DMR, and deposition results.

3. During the high discharges typical of the first trip, the large flow velocities in the MR swept the sediment inflow from the DMR abruptly downstream from the confluence. Since the river exhibits little curvature downstream from the confluence, the cross-stream mixing was gradual. Consequently, the mean suspended-sediment concentrations measured at the downstream sections were considerably higher near the right bank, and continued so for roughly 12 mi. In addition, the first-trip measurements revealed that the right bank suspended-sediment concentrations 6 to 10 mi downstream from the confluence were roughly one-third of the concentrations measured in the DMR.

4. The velocity profiles of the major verticals along the study reach were described well by the logarithmic relation, given by (1.1). The Karman constant, κ, was found to vary widely for concentrations less than 1,800 ppm, when plotted against the mean suspended-sediment concentrations measured at the respective verticals. This variation was especially true for the DMR and the small concentrations found in the MR during the second trip. The suspended-sediment-concentration profiles for the major verticals were generally well-described by the Rouse distribution, given by (1.2).

5. Measurements revealed a significant increase in the bed-load discharge at section 7-1, upstream from the shoaling area, with a subsequent decrease in the bed-load discharge at section 8-2 immediately downstream from the shoaling area. It was also found that the river bed had been scoured at section 7-1 between the time that the two trips were conducted.

6. Power-law relations formulated for the main-channel sections, given by (1.4) and (1.5), show that the unit bed-load discharge, q_B, varies as the 5.7-power of the mean flow velocity, U, while the suspended-sediment discharge, Q_S, varies as the 2.5-power of the water discharge, Q.

7. Flow measurements showed that approximately 12 percent of the main-channel flow entered the side channel, section 7-2, while more than 25 percent of the main-channel flow entered the side channel, section 9-2. This flow bifurcation reduces the main-channel mean velocity, which in turn diminishes the sediment-transport capacity and causes sediment deposition. Application of the power-law relation leads to estimates that closure of section 7-2 would increase the bed-load discharge and suspended-sediment discharge through section 7-1 by approximately 70 percent and 30 percent, respectively. Similarly, the closure of section 9-2 would increase the bed-load discharge by a factor of 2.6, and increase the suspended-sediment discharge by roughly 70 percent. Hence, it would appear that closure of either section 7-2 or 9-2 would significantly help in alleviating the shoaling problem. Note that the estimates for both sections were obtained by assuming that the cross-sectional flow areas for sections 7-1 and 9-2 would remain relatively constant after closure.

8. The effect that the increased sediment discharge would have on the reach downstream from the shoaling area after the closure of the side channels appears minor. In spite of the low flow regime during the second trip, depths measured along the navigation channel at section 12-1 were well over 25 ft, and thus posed no problem to navigation. Moreover, flow depths of over 60 ft have been recorded in the main channel by COE (RI) 2 mi farther downstream, at RM 345. Thus, it would appear that the extra sediment being transported and possibly deposited through this downstream reach as a result of the closure of sections 7-2 or 9-2 would not critically affect the navigation channel.

II. AN EVALUATION OF FOUR NUMERICAL MODELS

Pool 20 of the MR, extending upstream from L&D 20 at Canton, Missouri, to L&D 19 at Keokuk, Iowa, was the site of two recent field studies conducted by the IIHR (Nakato and Kennedy, 1977; Vadnal, 1979). Localized areas of shoaling near Fox Island, RM 355-56, and Buzzard Island, RM 349-50, presented troublesome conditions for barge navigation due to the shallow water depths that resulted. A mathematical, computer-based model able to simulate the flow conditions in this reach would be extremely useful for the prediction of future deposition and scour trends, as well as for a comparison of the predicted consequences resulting from the implementation of various proposed corrective measures. Numerous mathematical models representing the state of the art are currently available. This section of the report evaluates the performance of four numerical models that were applied to the Pool 20 reach of the MR (RM 343.2 - 364.2). These models include: the HEC-6 model developed by the Hydrologic Engineering Center, U.S. Army Corps of Engineers; the UUWSR and SUSR models developed at Colorado State University; and the CHAR2 model developed by Sogreah, a consulting firm in Grenoble, France.

A. The HEC-6 Mathematical Model.

1. General model description. The HEC-6 mathematical model was supplied by the Hydrologic Engineering Center (HEC), U.S. Army Corps of Engineers. The model is a one-dimensional steady-flow simulation program designed to analyze scour and deposition in rivers and reservoirs. Cross sections are each subdivided into a part which has a movable bed, and a part with a fixed bed. The entire movable-bed portion moves vertically, due to degradation and aggradation, while the other part remains fixed throughout the simulation. The model cannot simulate the development of meanders, the lateral distribution of sediment load across a cross section, or density and secondary currents. Bed forms are considered only indirectly by varying Manning's roughness coefficient (n) with water discharge or stage elevation. Additional features of the model include its ability to account for sediment particle armoring and dredging operations.

The initial IIHR field study took place from May through September 1976, while the complementary study occurred from June through August 1978. Consequently, the data from the 1978 study provided the basis for evaluating the results sought from a mathematical program that utilized the 1976 data for its initial conditions. Thus, the model-study procedure first required the conversion of the information gathered from the 1976 field study into data that were used for the initial conditions of the model. The HEC-6 simulation model program was then run using monthly-, weekly-, and daily-averaged flow quantities for the 28-month period from May 1976 through August 1978. The results of the three runs are discussed and, where possible, compared to the information gathered during the 1978 field study. Finally, an evaluation of the applicability of the HEC-6 mathematical model for predicting deposition and scour trends is made.

Figure II-A-1.1 shows a detailed index map of the study reach along the MR. Figure II-A-1.2 presents a schematic model outline of the reach. Twenty-seven cross sections were included over the 21-mile reach between the upstream boundary at Keokuk, Iowa (L&D 19) and the downstream boundary at Canton, Missouri (L&D 20). Note that the tributary entry point for the DMR is at RM 361.4.

The description of the data required for the model is presented in section 2, while section 3 describes the model calibration. Section 4 explains several sensitivity tests that were made, and section 5 presents the results of the simulation runs.

2. Data availability.

a. Geometric data. Cross sections within the problem-shoaling areas near Fox and Buzzard Islands were obtained from the 1976 field study. Other cross sections were obtained from topographic maps of the area that were compiled in a 1945 survey by the COE(RI). The cross sections taken directly from the 1976 field-study report were more detailed and included the cross-sectional areas of adjacent side channels. Reach lengths between cross sections vary from 0.16 mi in one of the shoaling areas to 1.2 mi at the upstream model boundary, with a typical reach length of 1.0 mi. The movable-bed portion of each of the field-study cross sections was chosen to correspond to that portion of the bed with a bed-material particle-size distribution primarily in the sand range. For other cross sections, the movable-bed portion was chosen on the basis of engineering judgment and experience.

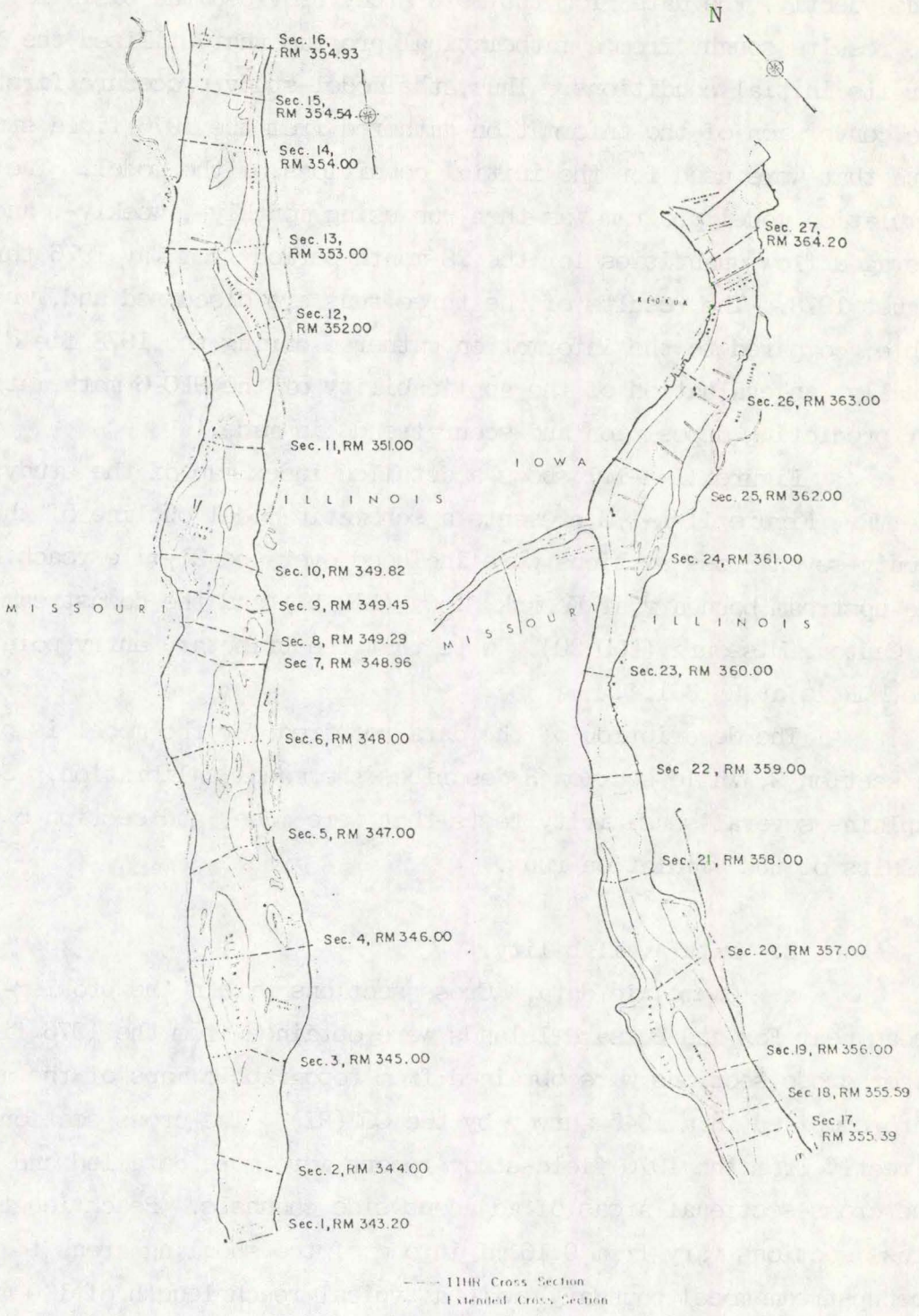

Figure II-A-1.1 Index map showing the locations of computational cross sections for mathematical modeling of Pool 20 (HEC-6 and CSU models)

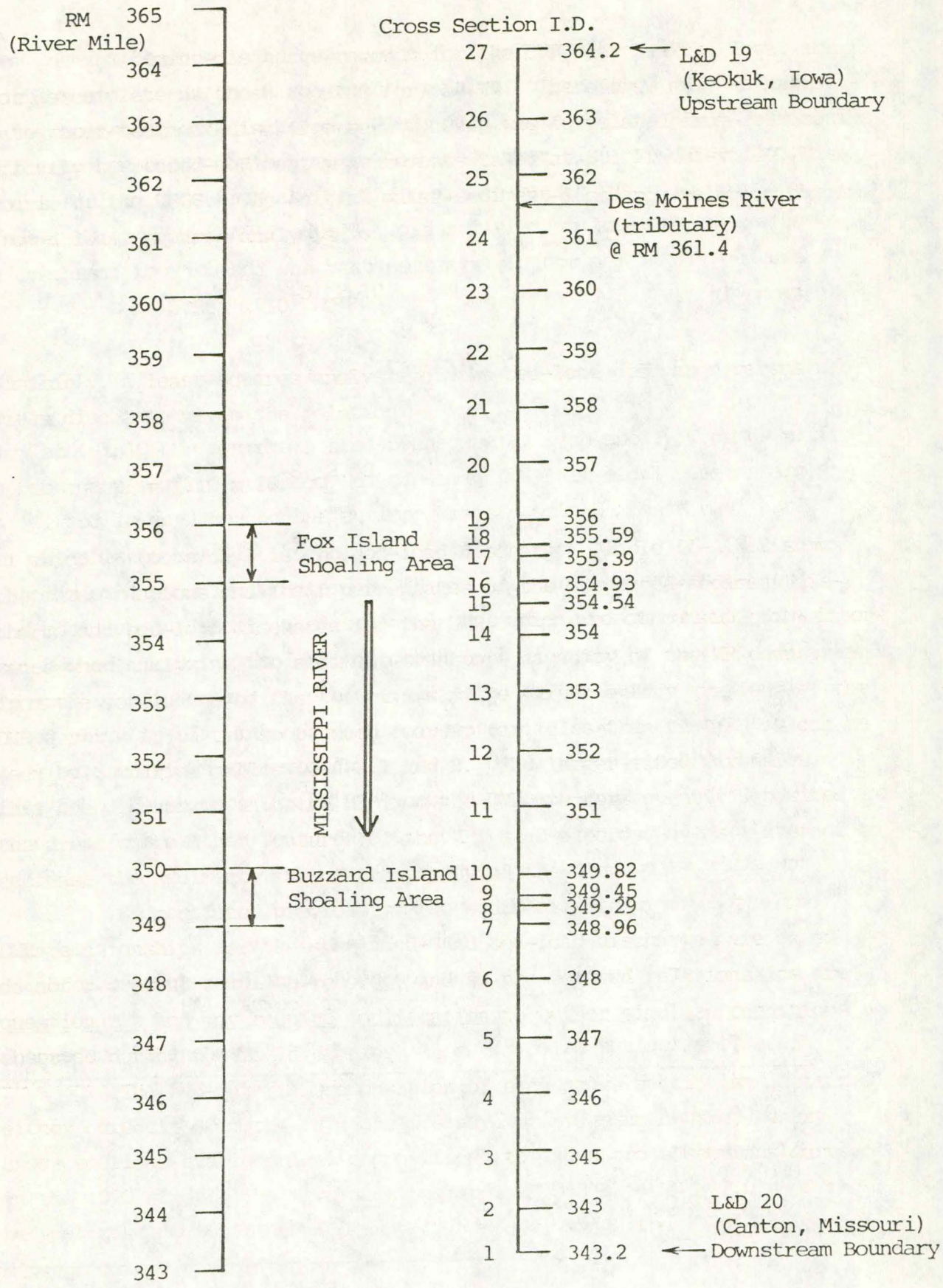

Figure II-A-1.2 HEC-6 schematic outline of Pool 20 model

b. Sediment data. The sediment data required for the model consist of the boundary inflowing sediment loads and their size gradations for the DMR and MR, along with the bed-material size gradation for each cross section. A 10-year record of water and suspended-sediment discharges measured directly downstream from L&D 19 was used to formulate a logarithmic water-sediment-inflow relationship. Figure II-A-2.1 shows the least-squares fit of the monthly-averaged data and the derived transport relationship:

$$Q_S = 2.39 \times 10^{-8} Q^{2.44} \qquad (2.1)$$

in which Q_S (tons/day) is suspended-load discharge and Q(cfs) is water discharge. Table II-A-2.1 presents the breakdown of the suspended-sediment load into standard size classifications and percentages of total load for the MR. Note that only one size fraction of silt was considered, although four sizes are available in the HEC-6 program. Transport relationships were then formulated for each size fraction. Since the upstream boundary of the model is directly downstream from a lock and dam, the bed-load discharge was assumed to be negligible due to the settling effect of particles in the backwater area approaching the dam. In general, the suspended load of the MR in the study reach consists almost entirely of wash load. The sediment-discharge records used are considered to be reliable, and thus, the equation from the least-squares fit was applied throughout the study without modification.

Table II-A-2.1

Particle-Size Distribution as Percent of Suspended Load
(Mississippi River at Keokuk, IA)

Classification and Size	Percent of Suspended Load
Clay (< 0.004 mm)	25.6
Silt (medium) (0.016-0.031 mm)	73.8
Very Fine Sand (0.0625-0.125 mm)	0.6

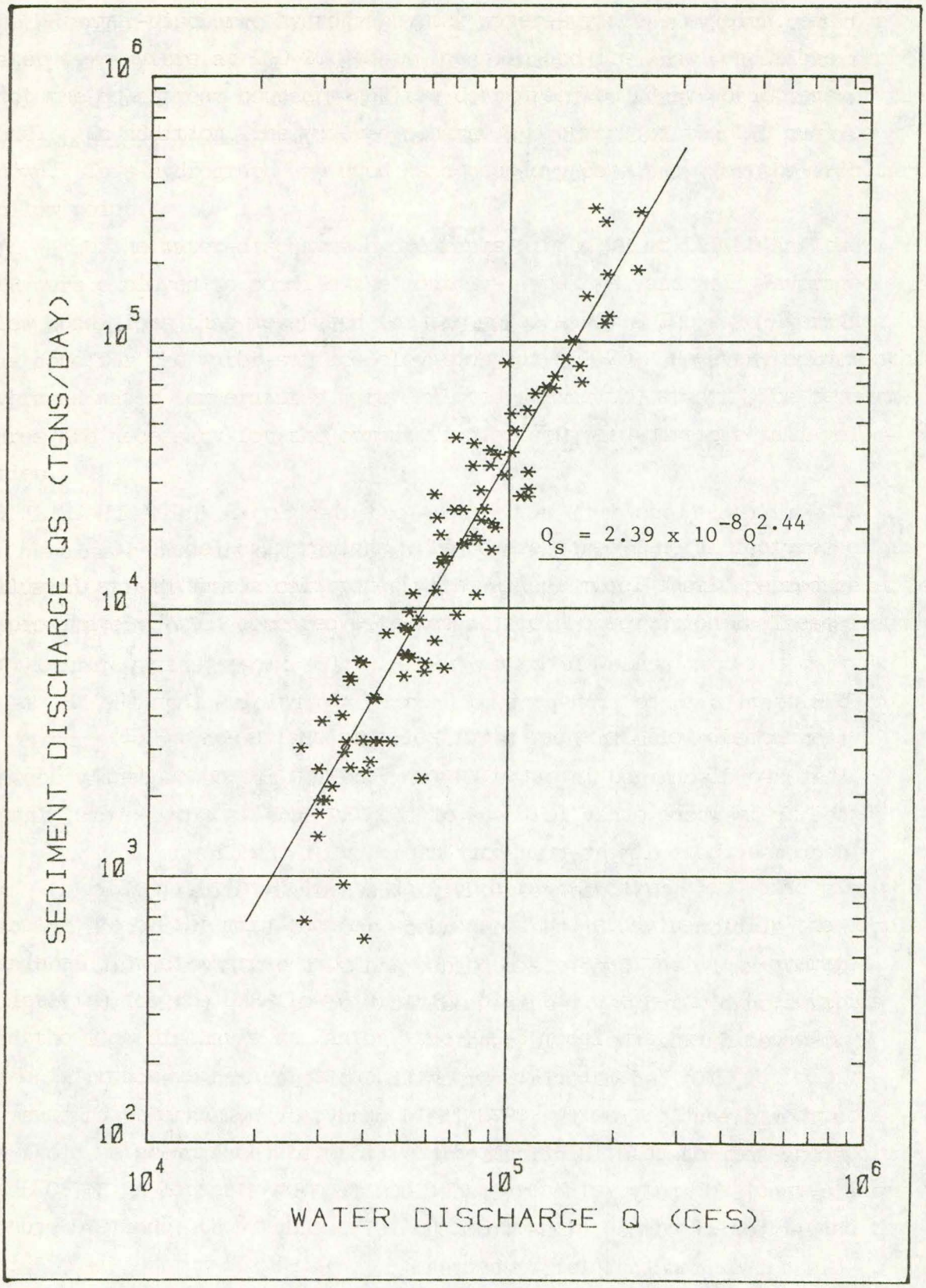

Figure II-A-2.1 Relationship between Q and Q_s for the Mississippi River at Keokuk, Iowa

Sediment-discharge records for the DMR near Keokuk, Iowa, are not as complete as those records for the MR. Therefore, only an approximate water-sediment-discharge relationship was formulated from four months of daily suspended-sediment measurements taken at St. Francisville, Missouri, by the USGS. The initial water-sediment-discharge relation obtained from a least-squares analysis is

$$Q_S = 5.284 \times 10^{-5} Q^{2.10} \qquad (2.2)$$

Similarly, a least-squares analysis of the bed-load discharge versus the water discharge gives the relation:

$$Q_B = 1.19 \times 10^{-8} Q^{2.59} \qquad (2.3)$$

in which Q_B (tons/day) is the bed-load discharge. Table II-A.2.2 shows the size fractions and their percentages of the suspended-sediment discharge and bed-load discharge for the DMR, which are of considerable importance when analyzing the sediment-transport capacity of the MR downstream from the confluence of the two rivers. The larger energy gradient of the DMR permits it to transport much coarser particles than the MR, as can be seen by comparing tables II-A-2.1 and 2. The larger-sized particles that are discharged into the MR from the DMR are consequently deposited in the areas where other features of the MR, such as cross-overs, interact to decrease the sediment-transport capacity of the flow.

As mentioned previously, the sediment data on which the two DMR relationships for the suspended- and bed-load discharges are based do not represent complete records, and so the derived relationships are questionable and may require modification to better simulate conditions observed during the field studies.

The bed-material composition of each cross section was obtained either directly from the 1976 field study, or by assuming that nearby cross sections had identical compositions to those cross sections surveyed in the 1976 study. The five sections from RM 343.2 to RM 347.0 used the bed-material compositions from the 1978 study, since the 1976 study reach did not extend that far downstream.

Table II-A-2.2

Particle-Size Distribution as Percent of Suspended and Bed Loads
(Des Moines River)

Classification and Size	Percent of Suspended Load
Clay (< 0.004 mm)	15.0
Silt (medium) (0.016-0.031 mm)	60.0
Very Fine Sand (0.0625-0.125 mm)	25.0
	Percent of Bed Load
Fine Sand (0.125-0.250 mm)	1.6
Medium Sand (0.25-0.50 mm)	8.0
Coarse Sand (0.5-1.0 mm)	50.0
Very Coarse Sand (1.0-2.0 mm)	25.6
Very Fine Gravel (2.0-4.0 mm)	10.2
Fine Gravel (4.0-8.0 mm)	4.6

c. Hydrologic data. The required hydrologic data consist of the MR water-discharge hydrograph, the water-surface elevation, and the water temperature at L&D 20. This location and its flow conditions represent the downstream boundary and the downstream boundary conditions of the model. In addition, the water-discharge hydrograph of the DMR must be known. This hydrograph was used as a boundary condition for the tributary inflow point.

The water-discharge hydrographs of the MR at L&D 20 and the DMR were employed to compile the monthly-, weekly-, and daily-averaged flow conditions that were used for the model study. The same averaging was done for the water-surface elevations at L&D 20. However, only monthly-averaged water temperatures were employed during the study. The temperatures are necessary for the computation of sediment particle fall velocities.

3. Model calibrations. There are three general features of an alluvial stream that a calibrated mathematical model should reproduce at least approximately, when compared with actual field observations. These features are:

(1) Water-surface profiles for a range of flow discharges,
(2) Sediment-transport quantities, and
(3) General bed-profile trends.

The first step was to develop a rating curve that would give Manning's n of the main-channel sections in the study reach for the complete range of flow discharges expected in the MR. Using the daily-averaged quantities for the DMR flow discharge, plus the water-surface elevation and the flow discharge at Canton, the HEC-6 model was run for one-day time intervals using a wide range of flow discharges. For each daily-averaged discharge used, a value of n was selected so that the computed upstream water-surface elevation would correctly match the measured value at L&D 19. A linear interpolation of the results using the least-squares method was made, the result of which is shown in figure II-A-3.1, and the relation is expressed by

$$n = 9.50 \times 10^{-8} Q + 0.0101 \quad \text{for } Q \leq 118{,}000 \text{ cfs} \qquad (2.4)$$

$$n = 0.0213 \quad \text{for } Q \geq 118{,}000 \text{ cfs} \qquad (2.5)$$

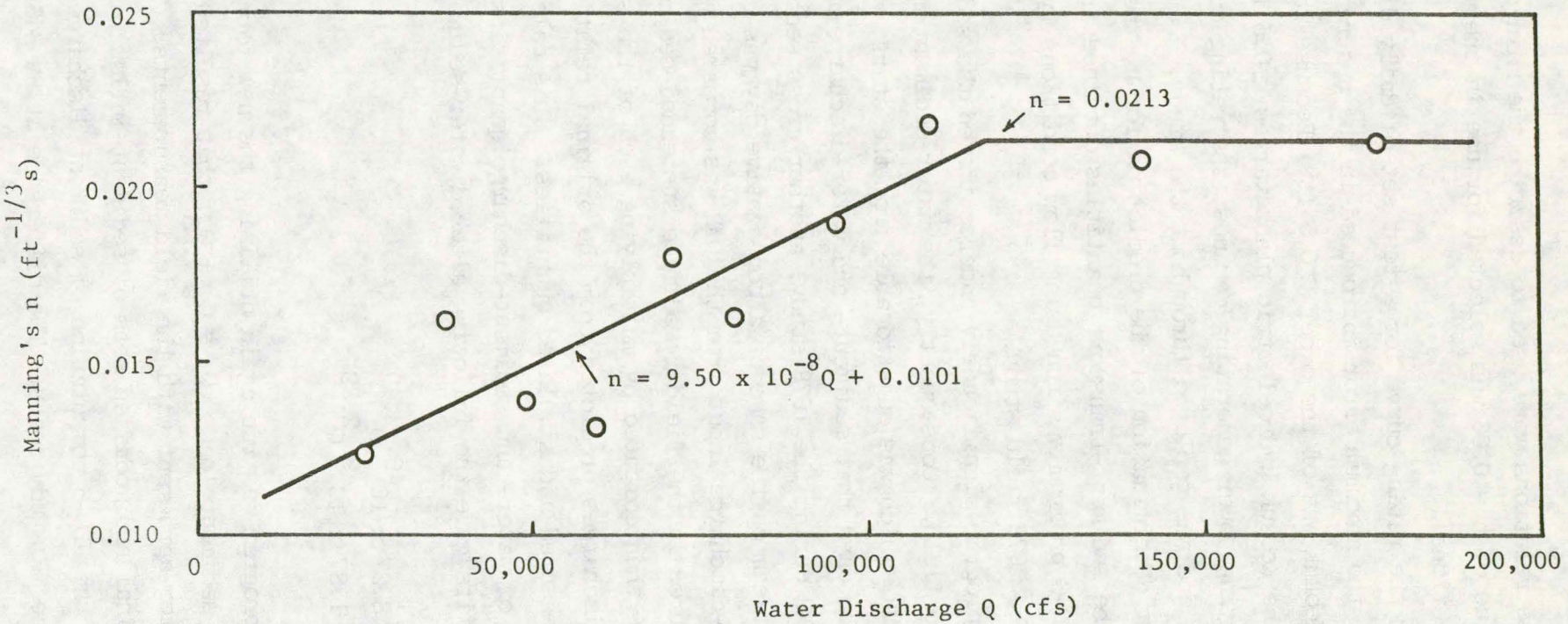

Figure II-A-3.1 Relationship between Manning's n and flow discharge

Note that these relations were used to describe the main channel only. A constant value of n = 0.06 was selected for use in the model for all overbank subsections.

From the rating curve for a test set of daily discharges, it was found that the maximum error introduced in the upstream water-surface elevation at Keokuk was of the order ±0.5 ft. Because the water-surface elevation at the Keokuk hydroelectric plant varies ±0.5 ft during the day due to varying power generating demands, the rating curve was judged to be adequate and was employed throughout the study.

After determination of the prediction for n, the next step was to reproduce the sediment-transport quantities obtained from field measurements. The HEC-6 program was run using flow conditions typical of those found during the 1978 field study.

The program significantly underestimated the sediment discharges measured in the field. Consequently, the water-sediment-inflow relationship for the DMR, which was questionable from the start, was modified as follows. On the days that sediment- and water-discharge measurements were taken on the DMR during the 1978 study, another cross section that was measured downstream on the same or a consecutive day was chosen. The simulated sediment-discharge input from the DMR was compared with the sediment discharge measured in the field. Modified suspended-sediment and bed-load discharges were then computed by multiplying each of the suspended-sediment and bed-load discharges predicted from the original relationship by the ratio of the field-measured and simulated quantities. This calculation yielded a modified set of water- and sediment-discharge quantities, through which least-squares fits gave the following altered water-sediment-inflow formulas:

$$Q_S = 8.27 \times 10^{-6} Q^{2.40} \qquad (2.6)$$

$$Q_B = 1.87 \times 10^{-9} Q^{2.89} \qquad (2.7)$$

The program was run again utilizing the new formulas, and the computed total sediment loads, $Q_T = Q_S + Q_B$, that resulted were found to be in much better agreement with the field measurements. Table II-A-3.1 shows the original and modified sets of sediment-inflow relations used for the DMR in the HEC-6 computation of sediment discharge at specific locations in the MR study reach. The difference at RM 346.97 was expected

because the model cannot adequately simulate the significant sediment contribution from a side channel upstream from this section. In other words, the model cannot account for effects due to channel bifurcation. In addition, the model underestimated the sediment discharges during the two low-flow periods. However, the MR is in a comparatively static or stable condition during low flows, so the discrepancies occuring during similar periods of low flow are not considered critical to the model performance.

Table II-A-3.1

Comparison of Total Sediment Discharges Using Original and Modified Des Moines River Rating Curves

River Mile	Water Discharge Q(cfs)	Field Measured Q_T (tons/day)	Original Q_T (tons/day)	Modified Q_T (tons/day)
346.97	159,183	223,544	126,997	157,872
350.83	142,010	200,534	124,916	210,273
354.89	107,869	106,509	61,125	103,335
351.87	47,257	5,538	1,783	1,816
346.97	42,727	4,621	563	565

Finally, the calibrated model should reproduce general bed-profile trends. A 4-month run from May through August 1978 was compiled to acquire a rough idea of how well the model results would approximate the 1978 field study results. Figure II-A-3.2 shows the simulated-bed fluctuation of the monthly-averaged flows of June and August 1978 compared to the results from the two different sampling periods during the 1978 field study. This run employed general cross sections obtained from the topographic maps. The detailed cross sections from the 1976 field study were included in the model during later runs. The model shows fairly good agreement with field measurements. The bed elevation from field measurements was approximated by subtracting the mean depth (i.e., cross-sectional area divided by river width) from the water-surface elevation. The bed elevation of the second trip (14-24 August 1978) was then subtracted from the bed elevation of the first trip (26 June-11 July 1978) at the respective study sections to obtain the points plotted in the figure. The figure displays the fairly

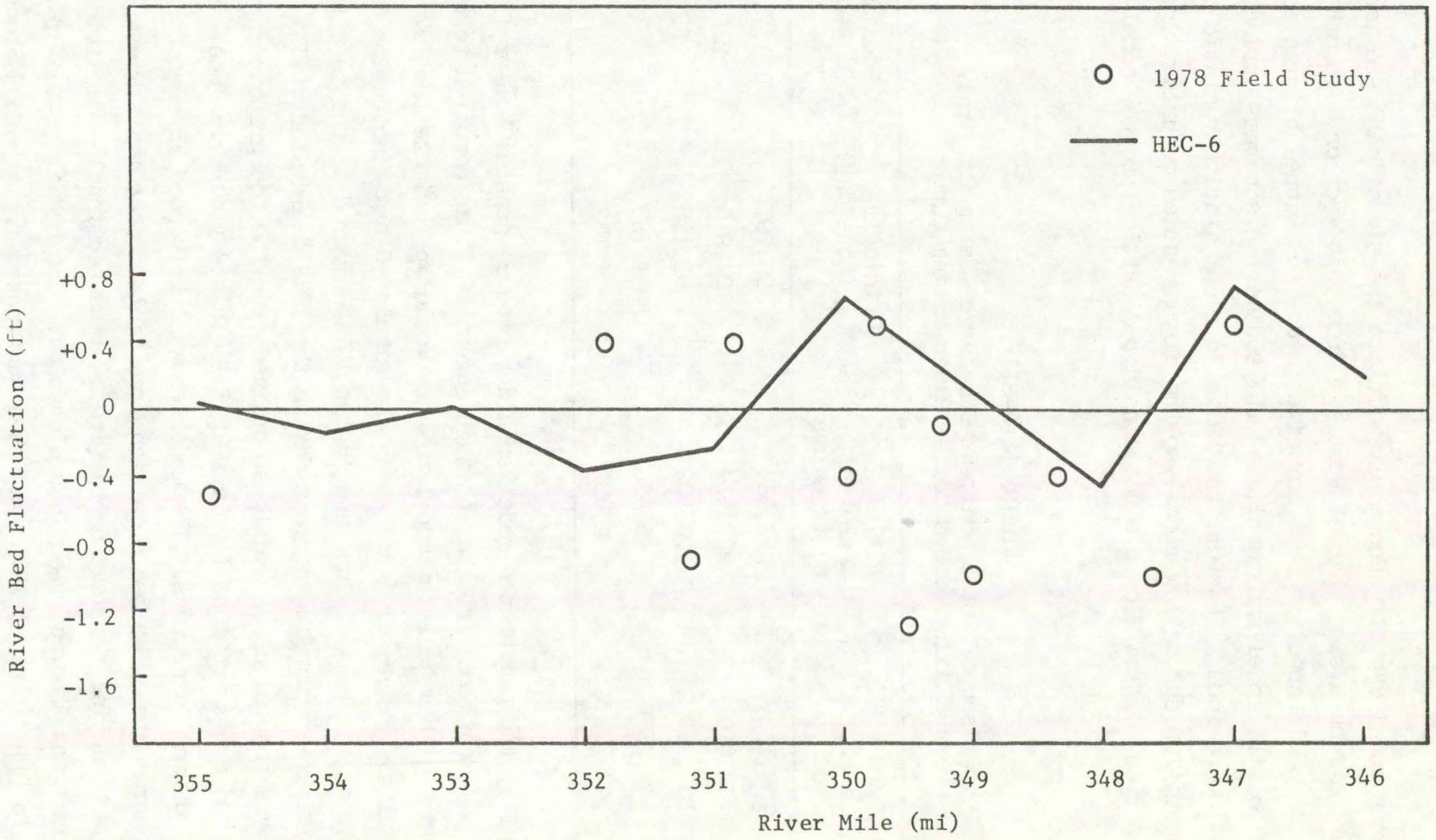

Figure II-A-3.2 Comparison of computed and measured bed-elevation changes

erratic changes that were found over short distances during the field study. The differences clearly demonstrate the problem that is encountered when trying to compare three-dimensional phenomena and measurements acquired from field studies to simulated results that are obtained from one-dimensional mathematical models. Note that after the model calibration, additional cross sections were compiled from the 1976 field study to include more detail with respect to side channels and cross-section geometry in the model.

In summary, the calibration procedure entailed first formulating a rating curve that would give an indication of the main-channel roughness through a value of Manning's n for a given flow discharge. The resulting relation produced a maximum error between the computed and daily-averaged upstream boundary water-surface elevation of not more than ± 0.5 ft. This error was felt to be insignificant since varying power demands throughout the day at the hydro-electric plant produced fluctuations of ± 0.5 ft in the water-surface elevation.

Next, sediment discharges computed from simulation runs were found to be much less than the sediment discharges measured in the field. Consequently the water-sediment-inflow formula for the DMR, which was initially questionable, was revised to better approximate the field measurements, while the MR water-sediment-inflow relation at L&D 19 was left unchanged since it was based on a 10-year record and was considered to be accurate. Sediment discharges computed from simulation runs with the new DMR relations better approximated sediment discharges measured in the MR, although the discharges were still underestimated during low-flow periods. Because the higher flow regimes seemed to be adequately modeled and are considered more important when trying to represent a dynamic river system, while lower flow regimes were relatively stable with little change in river conditions, no further revisions were made.

The final check was to observe the general trends of the bed-profile variation with time. Results from a simulation run showed scour and deposition trends similar to the 1978 field-study observations. The final revisions of the calibrated model were inclusion of additional and more detailed cross sections at locations identical to those studied during the 1976 study, and incorporation of a dredging operation that the COE (RI) performed on 4 September 1978 near the tip of Buzzard Island between RM 349 and 350.

It should be mentioned that more research into the effects of varying the bed-material compositions, the percentages of the various size fractions composing the total transported sediment load, and water-sediment-inflow formulas could produce a better-calibrated model.

4. Sensitivity analysis.

a. Values of Manning's n. The effect of values of Manning's n on the water-surface profile can be seen in figure II-A-4.1. Varying n from 0.0164 to 0.0210 changes the upstream water-surface elevation by only 1.4 ft for a flow discharge of 80,600 cfs in a 21-mi reach. However, the importance of the water-surface elevation is in its involvement in the calculation of the capacity of the flow to transport the sand-sized particles. Figure II-A-4.2 shows, for identical water discharge, how much the sand-sized-sediment discharge may vary depending on the value of n used in calculating the sediment-transport rate. The silt- and clay-sized sediment discharges depend almost entirely on the water discharge, and so are not affected by n. The amount of sand being transported, deposited, and scoured determines the consequent thalweg-elevation shift, which in turn affects the sand-transport capacity of the flow. Hence, because of the intricate dependence among the variables described here, the relationship involving n should be formulated from reliable field data.

b. Water temperatures. Water temperatures are used by the computer program in the calculation of fall velocities. The emphasis is placed on the sand-sized sediment particles, which determine the resulting bed profile. Figure II-A-4.3 exhibits the difference in the transported sand discharges for two fairly extreme temperatures. However, the water temperature seldom undergoes large fluctuations within a week, so rough estimates of temperatures may be used with reasonable confidence.

c. Bed-material profiles. Several short simulation runs were made using different bed-material compositions to examine the effects of the bed-material size distribution on the computational results. Four significantly different bed-material profiles were produced with the median size, D_{50}, ranging from 0.35 mm to 1.12 mm. One profile was

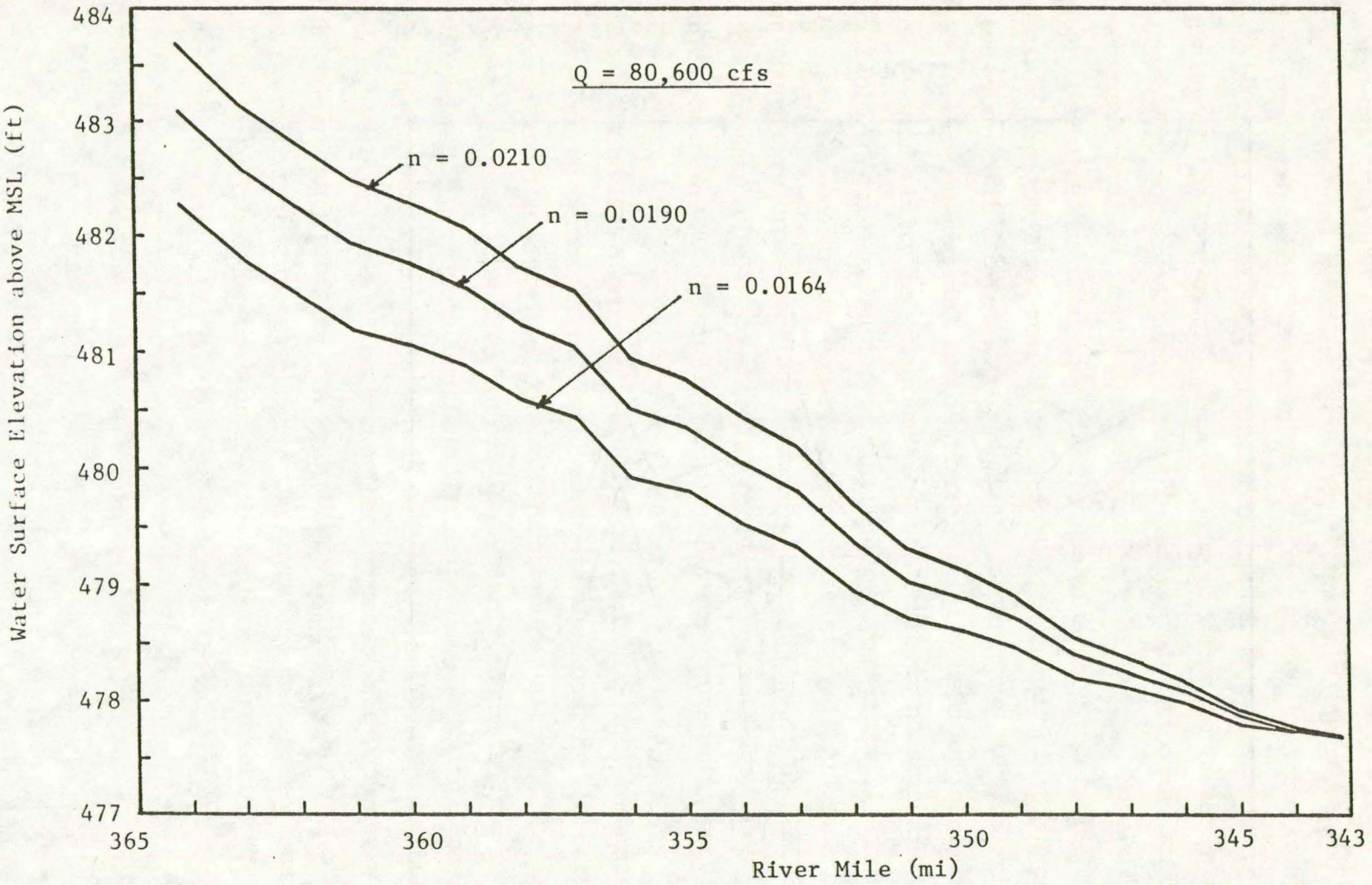

Figure II-A-4.1 Effect of Manning's n on water-surface profiles

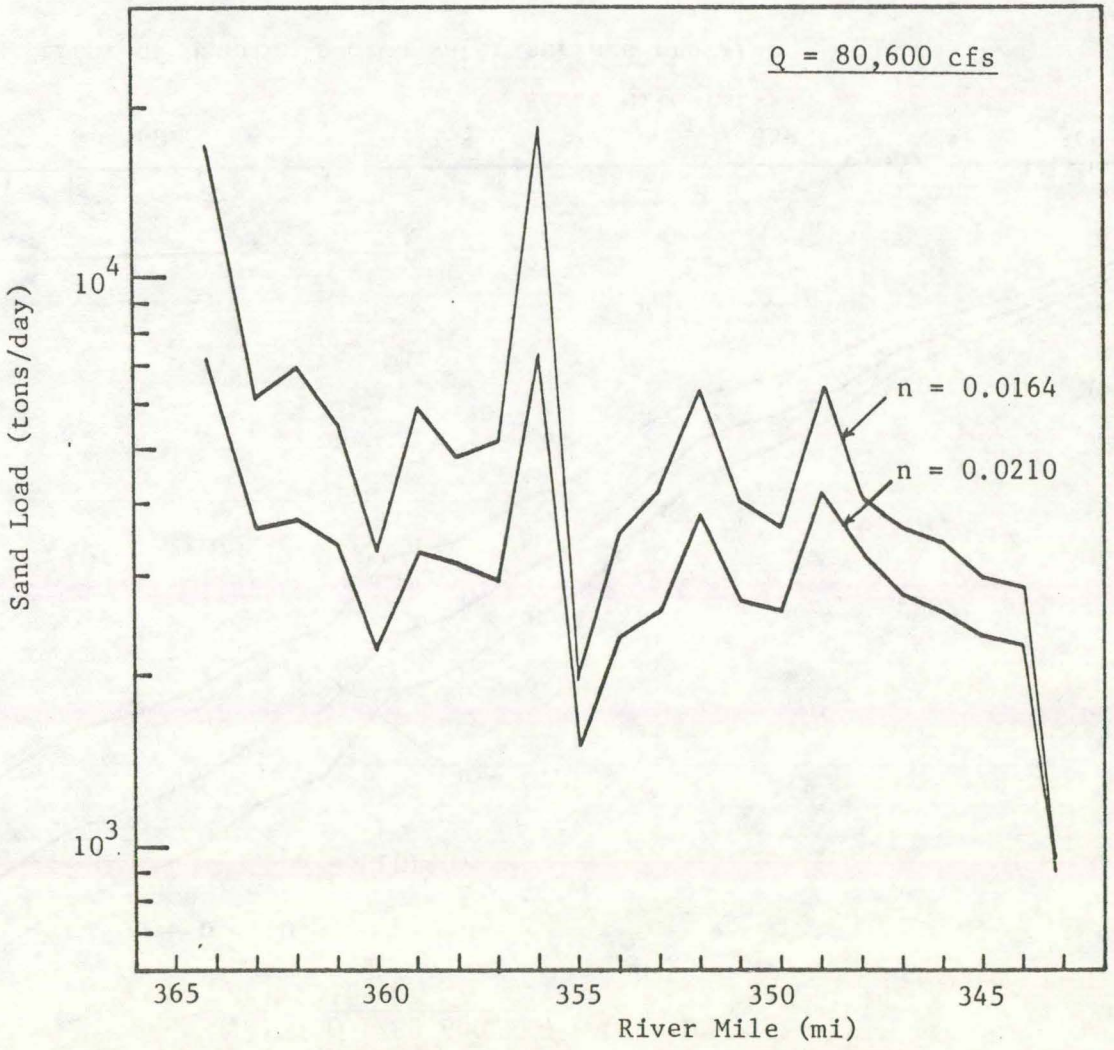

Figure II-A-4.2 Effect of Manning's n on sand load

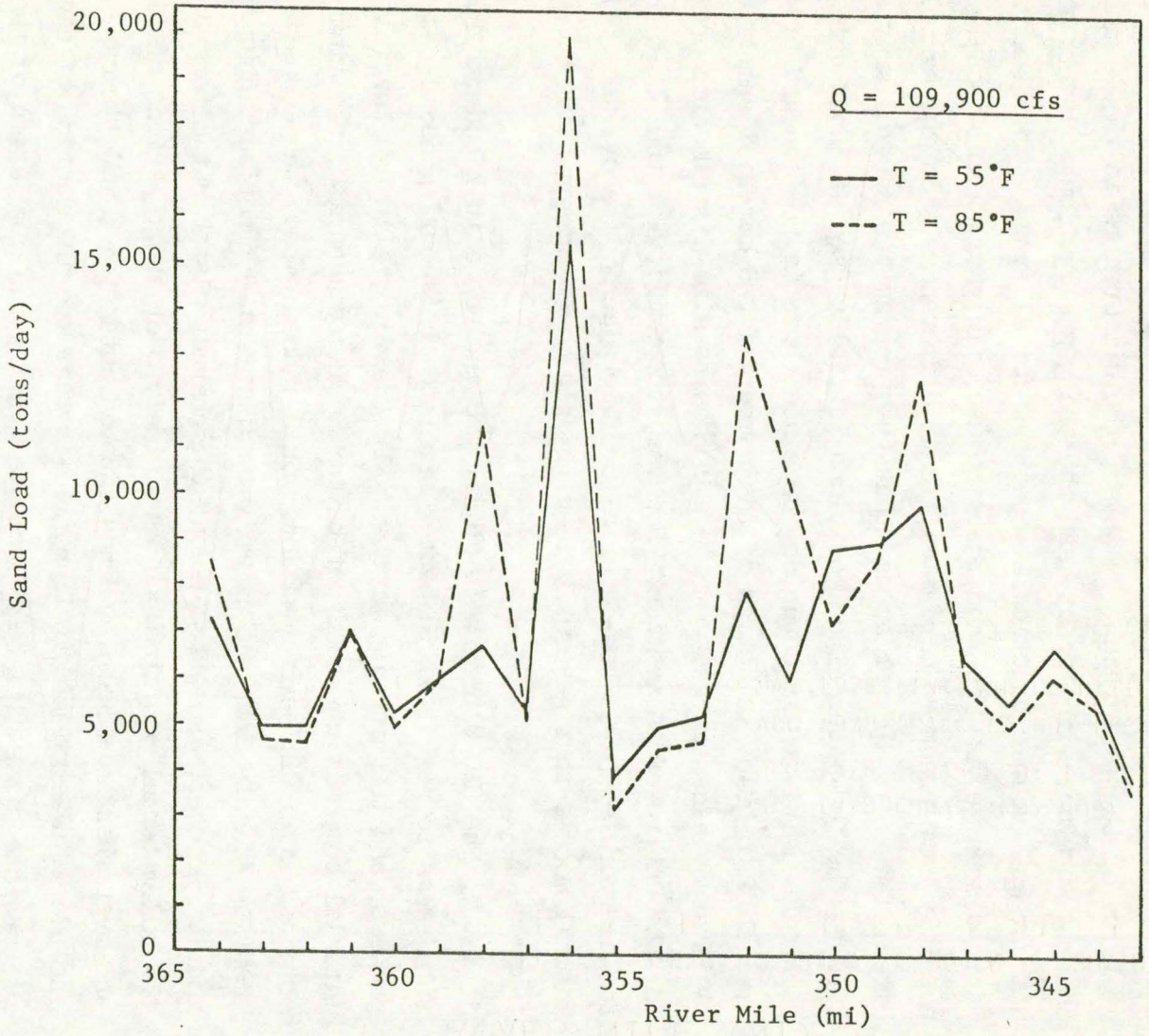

Figure II-A-4.3 Effect of temperature on sand load

inserted into five cross sections covering a four-mile reach and run for a seven-day trial period using a flow discharge of 42,727 cfs. The other three bed-material profiles were then alternately inserted, and similar trial runs were made. The results obtained showed that the coarser bed-material profile (larger D_{50}) produced greater sand discharges, in the vicinity of the test reach. However, the differences in these sand discharges were not significant, and the thalweg elevation and silt and clay discharges remained practically constant for all runs. Note that a low water discharge was used and that the use of higher water discharges would possibly have produced more significant differences. In the example cited above, it did not appear that the program was particularly sensitive to the bed-material compositions initially used as input data. This lack of sensitivity is advantageous since there is no standard procedure available to guide selection of the number of bed-material samples from a field study necessary to compile a composite size-distribution profile for the entire cross section. However, the ability of the HEC-6 program to incorporate a full bed-material profile places it above most other mathematical models that generally require only one representative size, commonly taken as D_{50}.

The HEC-6 program's ability to include a full bed-material profile seems to permit it to better simulate the scouring and deposition process, and the armoring process. Furthermore, although the initial bed-material compositions need not be particularly accurate, the final profiles obtained after long-run durations would indeed embody the deposition and scouring effects from the numerous sediment-size fractions input to the model. However, as will be seen, the characteristic parameters describing the bed-material profiles can vary widely over short periods of time and over short distances. Hence, the advantage of a model's capability to include a full bed-material profile is that the interaction of a wide range of particle sizes will be represented during the simulation of the deposition and scouring processes. Therefore, the model would be able to reflect actual river phenomena to a more realistic extent.

5. Discussion of results from the simulation runs.

a. Bed profiles. Figure II-A-5.1 shows the final thalweg elevations obtained from the runs using the monthly-, weekly-, and daily-

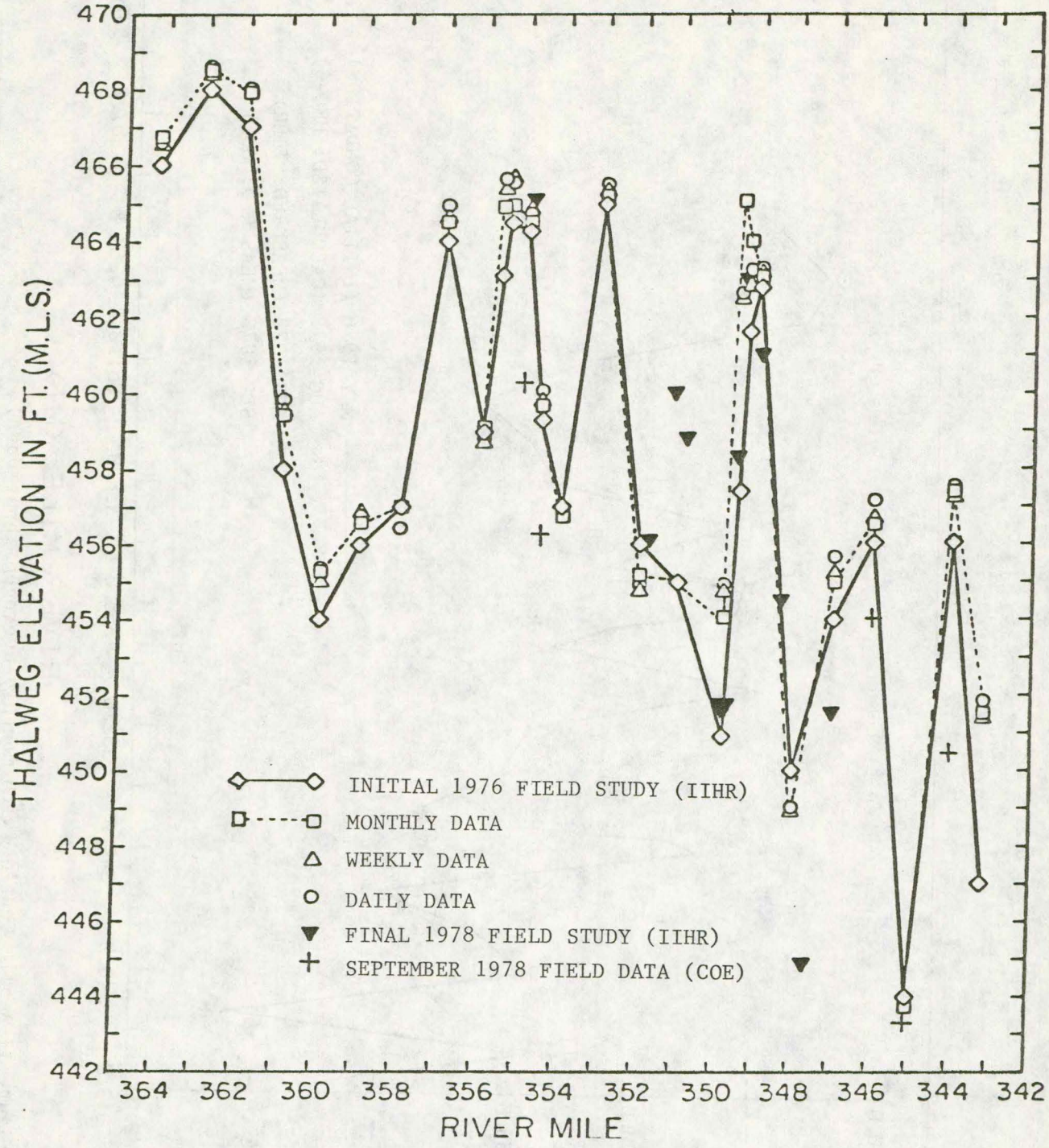

Figure II-A-5.1 Comparison of computed thalweg elevations with field data (HEC-6 model)

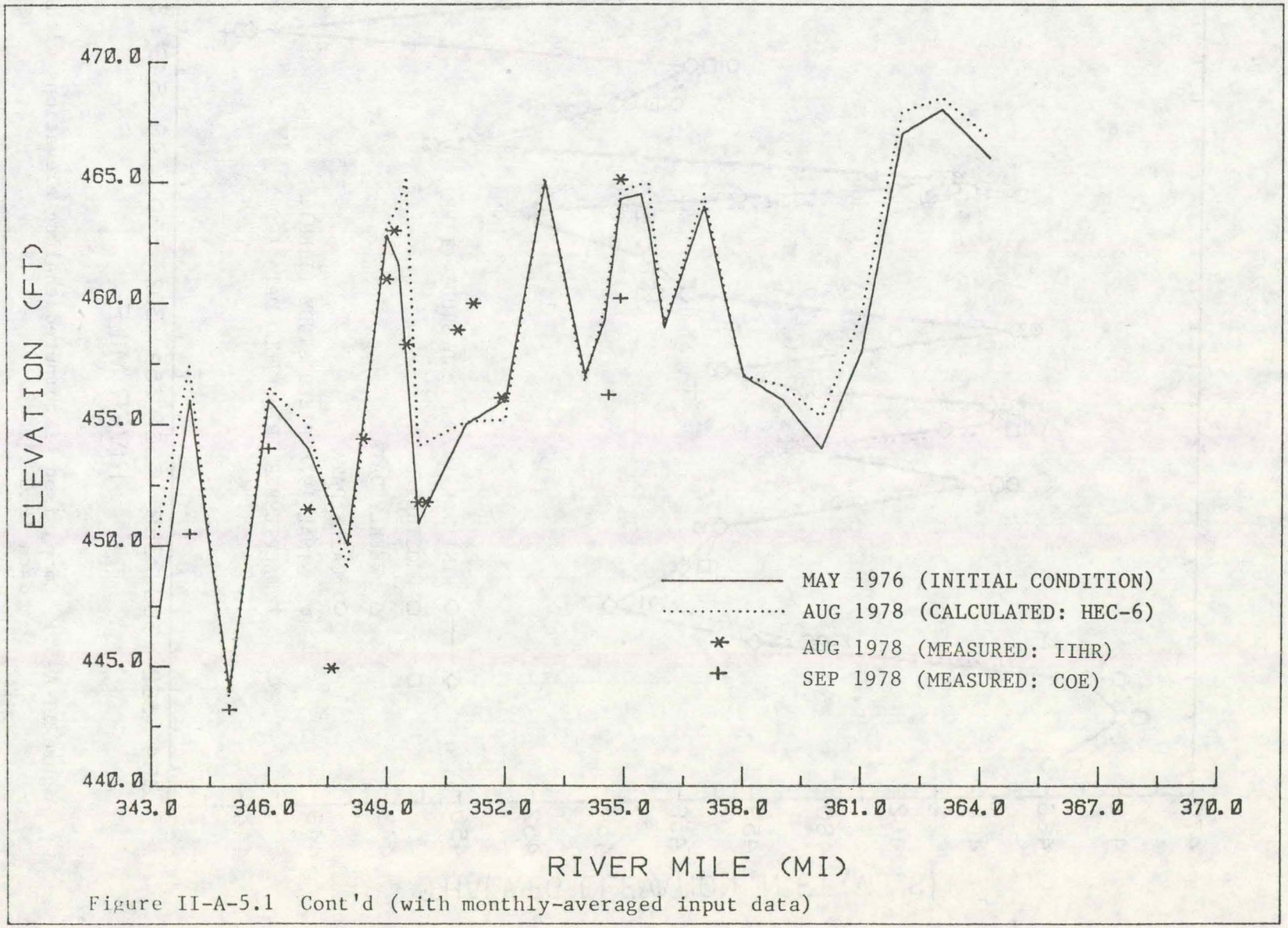

Figure II-A-5.1 Cont'd (with monthly-averaged input data)

averaged flow quantities for the period May 1976 through August 1978. The thalweg is defined as the deepest point in a channel cross section. In general, there are only small differences among the results of the three simulation runs. The similarity is valuable since the cost of running the program using the weekly- and daily-averaged quantities was roughly two and eight times the cost of the monthly-averaged run, respectively. The agreement between the model results and the 1978 field-study results is good in those areas where the model was constructed from the cross sections surveyed during the 1976 field study, but poor in the other areas where the cross sections were established from the old topographic maps. This outcome stresses the importance of having accurate cross-section geometries obtained from field surveys, from which the initial conditions of a mathematical model can be determined.

Figure II-A-5.2 shows the net change between the final and initial bed profiles for each of the three runs. A positive change denotes deposition, while a negative change denotes scouring. The model's overall trends agree well with the observations from the 1976 and 1978 field studies. The areas near Fox Island (Rm 355) and Buzzard Island (RM 349.5) are known for their recurring shoaling problems, which are indicated by the model results, although the 7.6 ft of deposition computed using the monthly-averaged quantities is unreasonable. Deposition was also particularly dominant at RM 347 during the 1978 field study, and it is also exhibited by the model results. Finally, deposition would be expected to occur at the downstream boundary of the model at L&D 20, due to the particle settling effect of the backwater pool. For a supplementary comparison, the differences in the thalweg elevations and the mean bed elevations (i.e., water-surface elevation minus the mean flow depth, $\bar{d} = A/W$) between the 1976 and 1978 field studies are shown in figure II-A-5.3.

b. Water-surface profiles. Figure II-A-5.4 shows the variation in the recorded and computed upstream water-surface elevations at L&D 19 obtained from the simulation run using the daily-averaged flow quantities. Note that only one point per week has been plotted. The agreement is good except near days 580 to 700, representing 1 December 1977 to 1 April 1978. This disagreement is believed to be due to the effect of the ice cover in Pool 20, which prevented the water surface from rising to

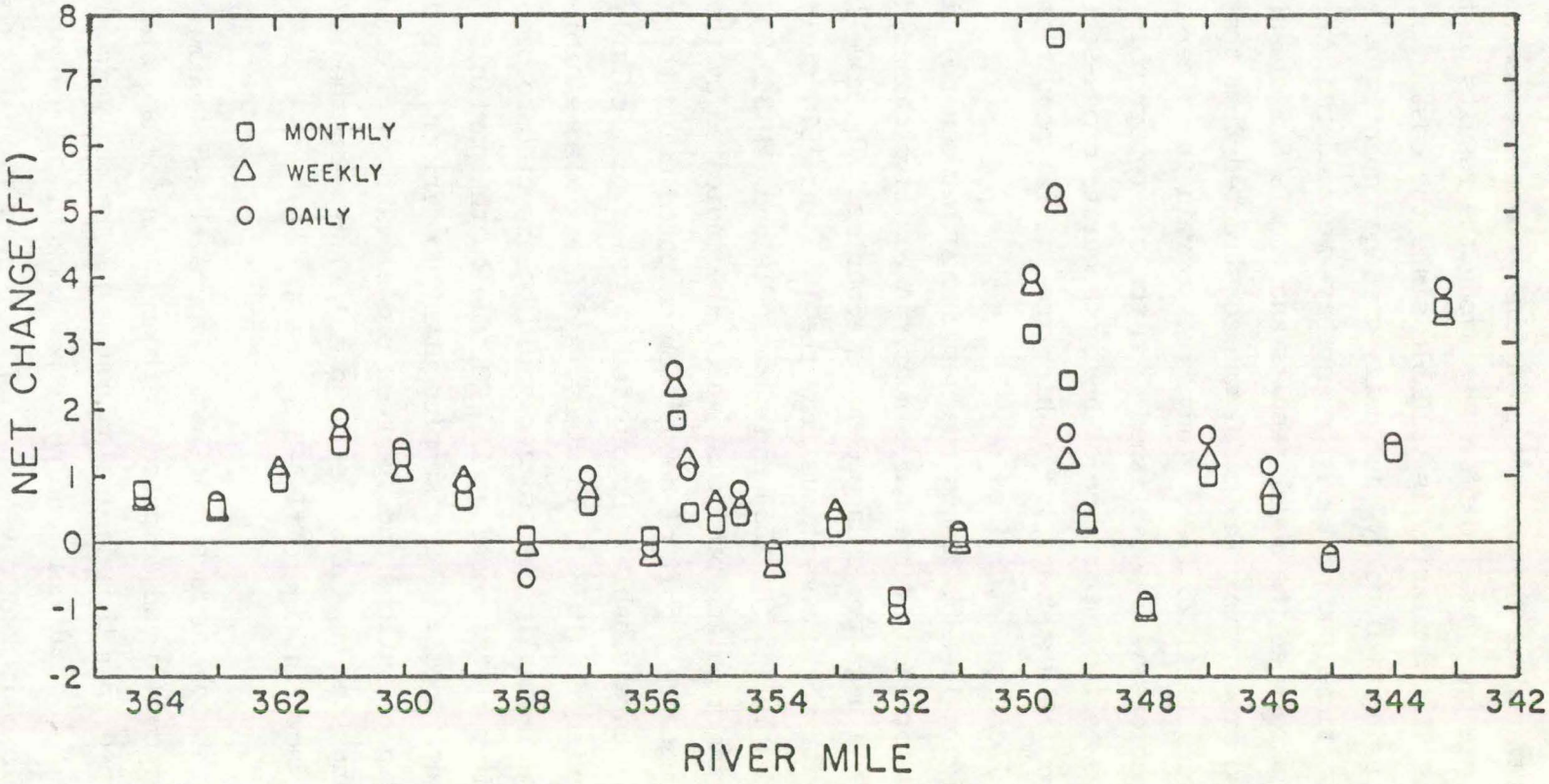

Figure II-A-5.2 Comparison of computed net bed-elevation changes

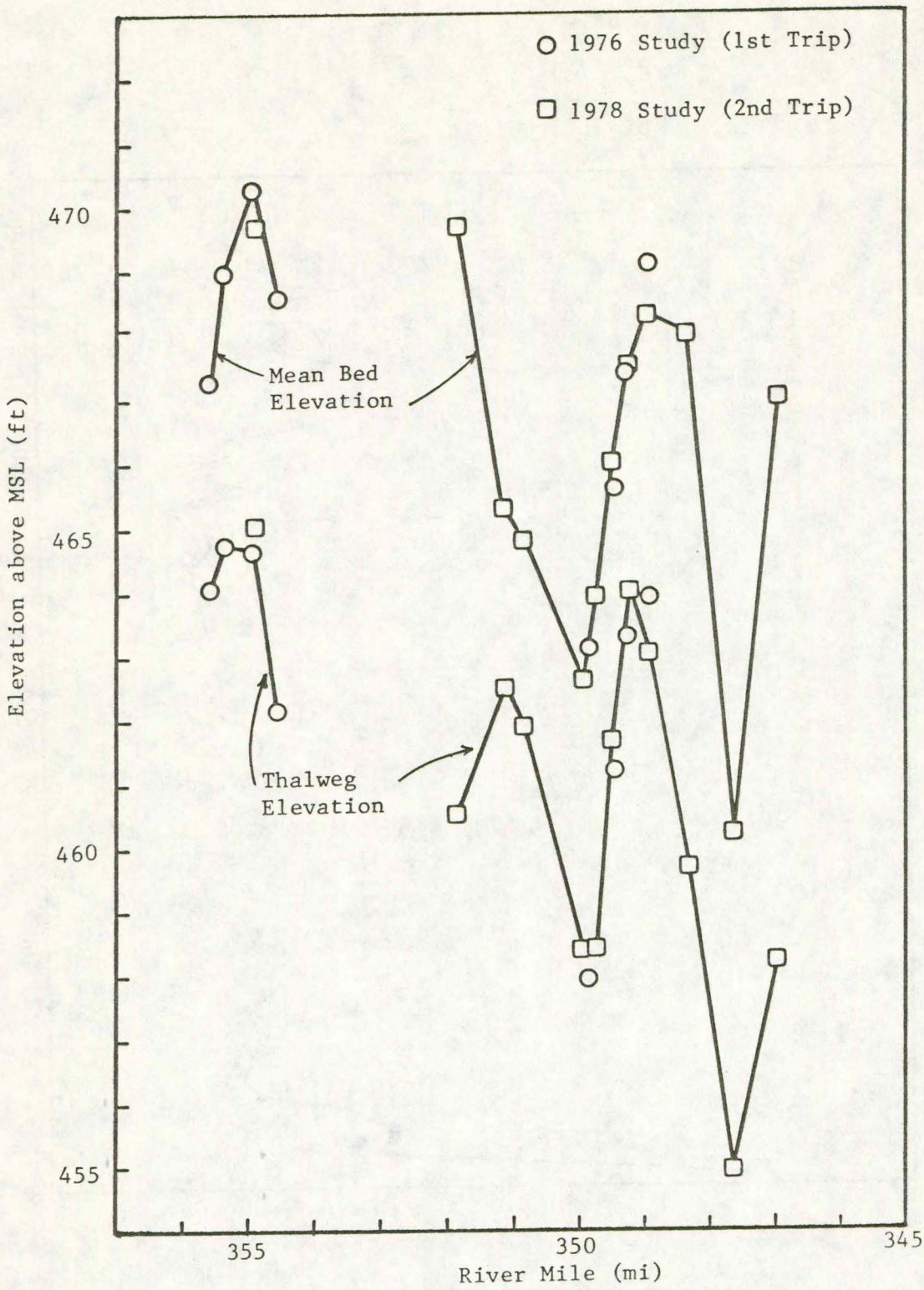

Figure II-A-5.3 Comparison of 1976 and 1978 field-study results

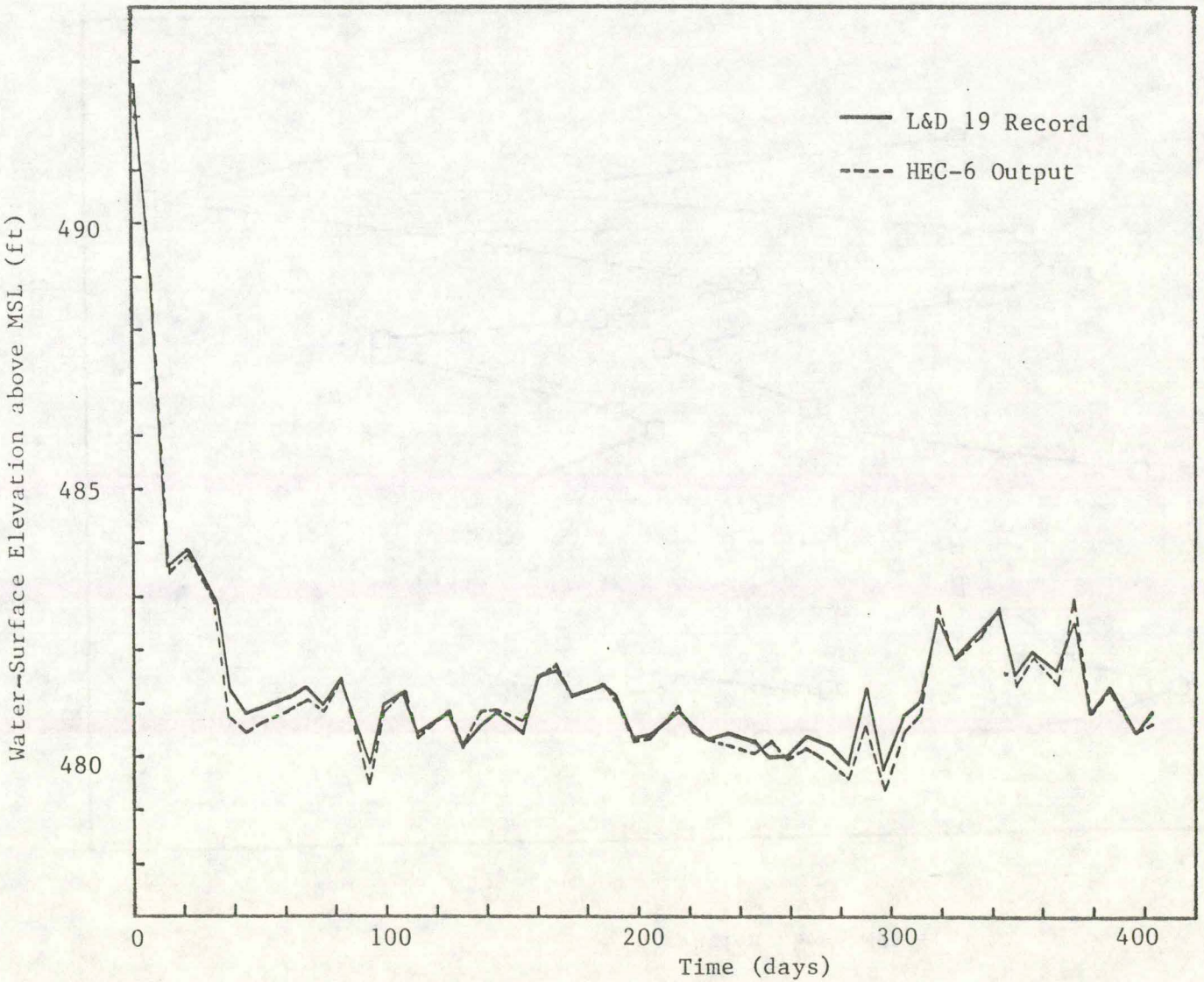

Figure II-A-5.4 Comparison of computed and recorded stage elevations at L&D 19

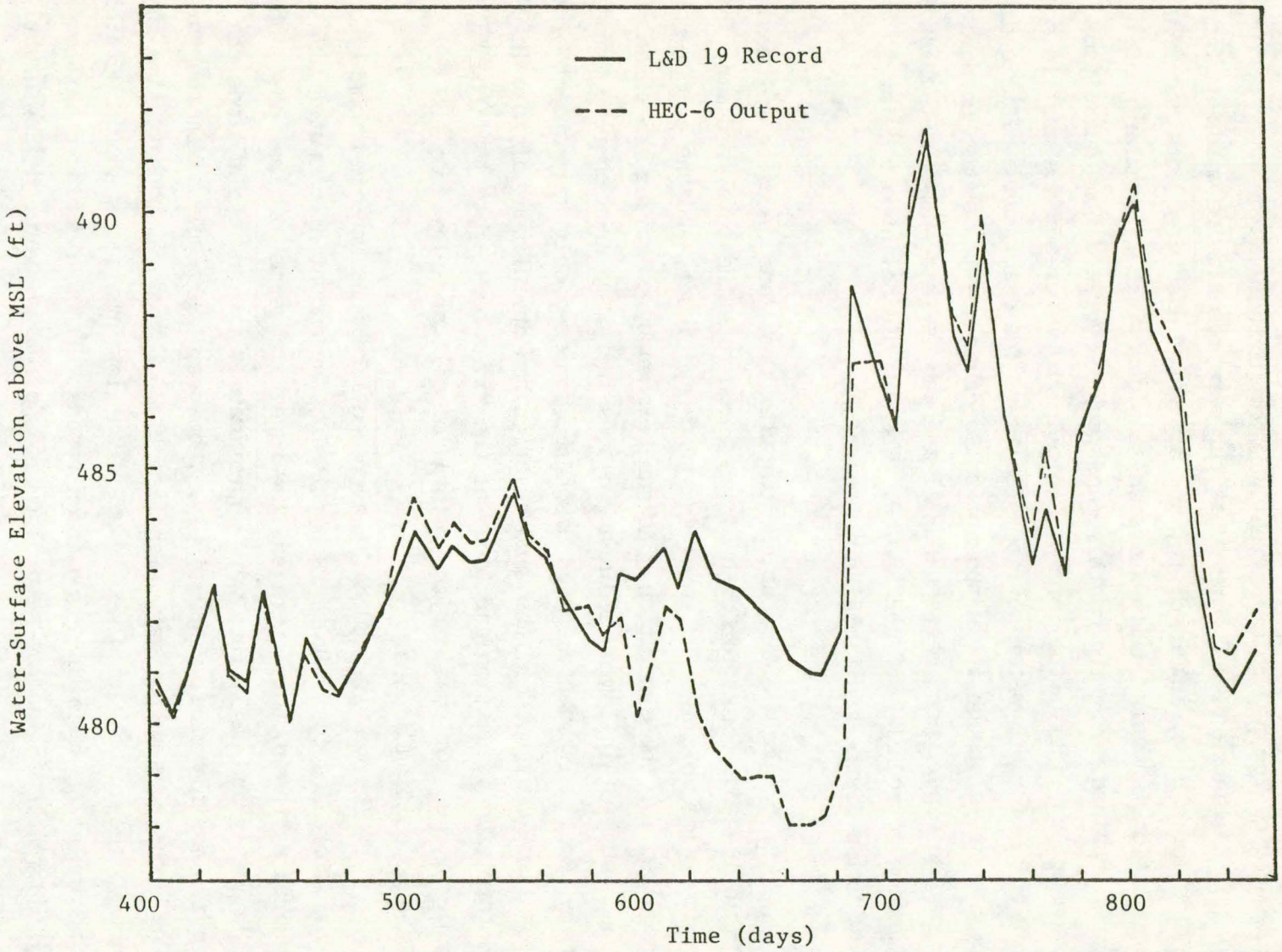

Figure II-A-5.4 Cont'd

its free-surface level. Consequently, a larger storage volume is required in the upstream reach of the pool, thus causing the actual recorded water surface elevation at L&D 19 to be much higher than would be normally expected for these flow conditions. The overall agreement demonstrates the adequacy of the n-Q relation that was formulated.

Figure II-A-5.5 presents three representative water-surface profiles for a high, intermediate, and low water discharge obtained from a simulation run using daily-averaged flow quantities. Similar profiles were obtained using the monthly- and weekly-averaged flow quantities. As seen in the figure, the form of a dip in the water-surface profile occured at RM 356 for all water-surface profiles. The exact cause of this dip is not known, although it is thought to be caused by the sudden channel contraction experienced between RM 357 and 356, with a subsequent channel expansion between RM 356 and 355.59. The dip did not appear prior to the inclusion of the additional cross sections.

c. Trap efficiencies, computer time, and dredging volumes. Table II-A-5.1 lists for each of the three runs the total sediment inflow and outflow volumes, the resulting trap efficiency, and the computer time required for the simulation. As can be seen by comparing the three runs, the amount of inflowing sediment volumes increased when shorter time steps were used. Although the sand discharge composed only ten percent of the total sediment volume, the sand fraction had an influential role in determining deposition and scour of the river bed. Note that the HEC-6 program does not consider the removal of silt and clay from the bed once deposition occurs.

The weekly- and daily-averaged flow runs required roughly one-third more and four times, respectively, the amount of computer time required by the monthly-averaged-flow runs. In terms of final cost, however, the weekly and daily runs were approximately two and eight times the cost of the monthly runs, respectively. However, the results from the three different runs do not vary significantly. Therefore, to save time and money, the monthly- and weekly-averaged flow quantities should suffice in simulating scour and deposition trends, although during peak flows it is advisable to include several periods of daily-averaged flow quantities.

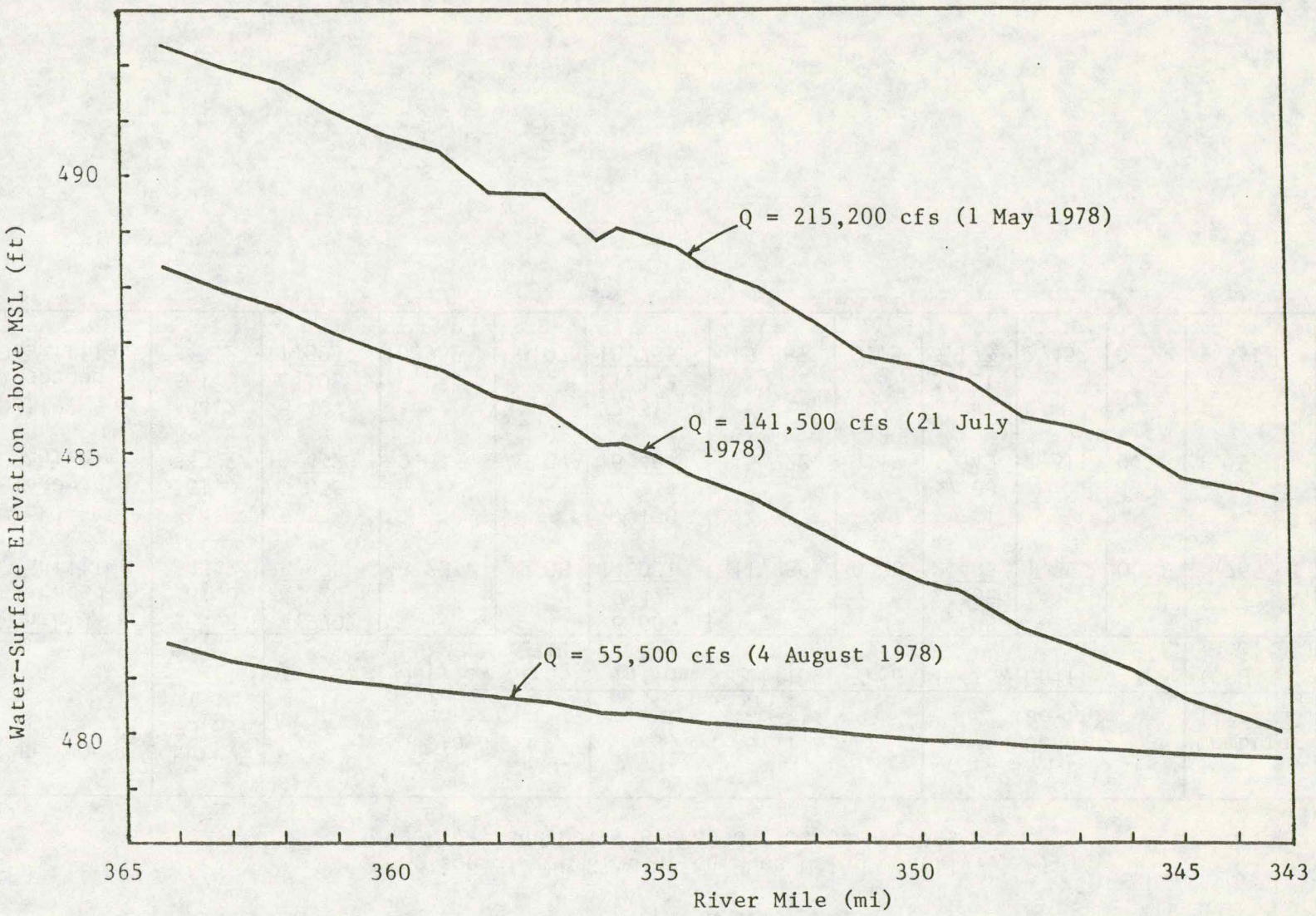

Figure II-A-5.5 Representative water-surface profiles obtained using daily-averaged flow quantities

Table II-A-5.1

Comparison of the Simulation Runs Using Monthly-, Weekly-, and Daily-Averaged Flow Quantities

Run Type	Entry Point	Clay (ac-ft)			Silt (ac-ft)			Sand (ac-ft)			Computer Time
		Inflow	Outflow	Trap Eff.	Inflow	Outflow	Trap Eff.	Inflow	Outflow	Trap Eff.	(CPU sec)
Monthly-	364.2	4,970			6,609			38			
Averaged	361.0	4,020			7,422			2,368			
Quantities	343.2	8,990	8,233	0.08	14,031	11,286	0.20	2,406	1,895	0.21	765
Weekly-	364.2	5,376			7,150			41			
Averaged	361.0	5,056			9,334			3,008			
Quantities	343.2	10,432	9,673	0.07	16,484	13,722	0.17	3,049	2,311	0.24	1,053
Daily-	364.2	5,497			7,311			42			
Averaged	361.0	6,198			11,442			3,731			
Quantities	343.2	11,695	10,932	0.07	18,753	15,887	0.15	3,773	2,452	0.35	3,331

d. Bed-material profiles. The bed-material profiles are probably the most difficult river characteristic to simulate and to compare with profiles derived from field studies. The size distribution of bed material can vary significantly across a section, where deposition may be occurring in one area, while another area may be undergoing scour. Numerous samples were taken at a cross section in an attempt to obtain a representative composite bed-material profile. The HEC-6 program is able to incorporate a full bed-material profile at each cross section. However, table II-A-5.2 shows how much variation can be expected in the fundamental bed-material parameters over time and distance. The data representing the three sampling trips made during the 1976 field study indicate the variations that can be expected due to: (1) the changes that the bed-material composition undergoes with time (in this case, the four-month period from May to September, 1976) and, (2) the changes resulting from the different locations of sampling sites at a particular channel cross section. The columns labeled HEC-6 denote the resulting parameters of the three 28-month simulation runs. The last two columns represent the results of the 1978 field study. Ideally, one would expect the HEC-6 results to be similar to the 1978 field-study results, although the slightly different cross-section locations could cause a difference. Overall, these results demonstrate the difficulty in modeling and comparing the various bed-material parameters, which have been shown to vary with time and location.

One final point worth mentioning refers to differences obtained from the use of different computer systems and languages. Running an identical sample program supplied by the HEC on an IBM 370 system yielded slightly different results than those obtained by the HEC. Also, the use of standard FORTRAN and Minnesota FORTRAN gave slightly different results. However, the variations found were of the order of ± 2 percent, and thus are not considered to be significant.

B. The CSU Mathematical Models.

1. General model description. Two mathematical simulation models, developed at Colorado State University (CSU), Fort Collins, Colorado (Chen and Simons, 1980), have been applied to the Pool 20 study reach at the request of the IIHR to investigate the effectiveness of the models

Table II-A-5.2

Comparison of Bed-Material Properties

Parameter	River Mile (mi)		1976 Study			Run Results (HEC-6)			1978 Study	
	1976 Study	1978 Study	1st Trip	2nd Trip	3rd Trip	Monthly	Weekly	Daily	1st Trip	2nd Trip
Median Particle Size D_{50} (mm)	354.93		0.65	0.60	0.52	0.66	0.66	0.66		
		354.89							0.65	0.58
	349.82		0.38	0.45	0.60	0.43	0.43	0.43		
		349.75							0.54	0.49
		349.50							0.61	0.50
	349.45		0.50	0.43	0.44	0.35	0.42	0.42		
	349.29		0.54	0.74	0.57	0.48	0.50	0.48		
		349.24							0.52	0.49
		348.98							0.53	0.46
	348.96		0.45	0.43	0.57	0.44	0.42	0.42		
Geometric Mean Particle Size D_g (mm)	354.93		0.74	0.66	0.59	0.70	0.68	0.68		
		354.89							0.80	0.70
	349.82		0.41	0.46	0.66	0.36	0.33	0.34		
		349.75							0.56	0.53
		349.50							0.70	0.60
	349.45		0.70	0.46	0.43	0.23	0.27	0.26		
	349.29		0.60	0.89	0.64	0.44	0.54	0.50		
		349.24							0.57	0.61
		348.98							0.61	0.53
	348.96		0.50	0.52	0.67	0.48	0.47	0.46		
Geometric Standard Deviation of Particle Size σ_g	354.93		1.86	1.87	1.70	1.94	1.99	1.99		
		354.89							2.16	2.07
	349.82		2.79	1.65	1.69	3.09	3.02	2.95		
		349.75							1.71	2.14
		349.50							2.12	1.81
	349.45		2.20	1.77	1.97	3.92	3.82	4.05		
	349.29		1.81	2.29	1.84	2.26	1.86	2.00		
		349.24							1.79	2.64
		348.98							1.98	1.85
	348.96		1.77	1.83	1.93	1.82	1.85	1.90		

in simulating flow conditions and phenomena. The first model, a one-dimensional uncoupled-unsteady water and sediment routing model (UUWSR Model) employs an implicit numerical method for water routing to solve the water continuity and momentum equations assuming a fixed bed. The sediment continuity equation for sediment routing is then solved at the same time step. The UUWSR model has been applied previously to Pools 4 through 8 in the Upper MR system (Simons et al., 1979). The second model, a one-dimensional steady-uncoupled sediment routing model (SUSR Model) also assumes a fixed bed, then computes the backwater profile for a step discharge by solving the energy equation. The bed-elevation changes are determined at the end of the time step by solving the sediment continuity equation. The SUSR model has been applied to the Yazoo River Basin (Simons et al. 1978) and has been found to be excellent in studying long-term changes in a complex river system.

As seen with the HEC-6 model, the first objective was to use historical records in addition to data collected from the 1976 field study (Nakato and Kennedy, 1977) to establish the initial conditions for the models. Simulation runs were then carried out through the time of completion of the 1978 field study (Vadnal, 1979), thereby allowing a comparison between the field results and those obtained from the model predictions.

Section 2 reports on the construction of the two models using the available geometric, sediment, and hydrologic data, while section 3 discusses the calibration of the models. Section 4 analyzes the sensitivities of the two models, and section 5 evaluates the performance of the two models and the results obtained.

2. Construction of the models.

a. Data availability. Field data from the two field studies conducted by the IIHR were used along with historical records to compile the input conditions for the models. Geometric data were obtained from the 1977 report for cross sections in the problem shoaling area, while the other model cross sections were obtained from a 1945 survey conducted by COE(RI). Water and sediment inflows for the DMR were obtained from records and measurements at St. Francisville, Missouri. Hydrologic data (water discharge and stage elevations) for L&D 19 and L&D 20 were compiled from discharge and stage hydrographs. Sediment-discharge relationships

at L&D 19 were obtained from measurements taken there. A preliminary relationship was derived for the study reach using the previously discussed HEC-6 program (U.S. Army Corps of Engineers, 1977). Details of dredging operations performed during the model study period (May 1976 through August 1978) also were available.

b. Model construction. The Pool 20 river reach was divided into 27 cross sections with space intervals ranging from 0.2 mi in the Fox Island shoaling area to 1.2 mi at L&D 19. Figure II-A-1.1 displays the locations of the chosen cross sections and a map of the study area.

Since the wash loads typical in the MR are generally considered to be transported continually throughout the main flow, only the bed-material discharges affect the river-bed-elevation changes. Consequently, only the bed-material discharges were considered in the models for sediment routing. However, the 1976 field study found that roughly 10 percent of the suspended-load samples collected near the shoaling areas was in the sand-size range, while roughly 1 percent of the suspended-load samples collected near L&D 19 was in the sand-size range, and approximately 25 percent of similar samples taken in the DMR contained sand-size particles. Thus, bed-material-transport relationships were derived from the available data which incorporated the appropriate fraction of the sand-sized particles found in suspension. The relation for the general study reach is

$$g_{BM} = 9.82 \times 10^{-6} V^{3.58} \qquad (2.8)$$

where g_{BM} is the unit width bed-material discharge in cfs/ft, and V is the mean flow velocity in ft/s. This equation was used in both the UUWSR and SUSR models to obtain the sediment-transport rate in Pool 20 by multiplying g_{BM} by the top channel width.

For the sediment input from L&D 19,

$$g_{BM(LD19)} = 8.42 \times 10^{-7} V^{3.5} \qquad (2.9)$$

where $g_{BM(LD19)}$ is the unit width bed-material discharge at L&D 19 in cfs/ft, and V is the mean flow velocity in ft/s.

For the sediment input from the DMR,

$$Q_{BM(DMR)} = 5.7 \times 10^{-8} Q^{1.74} \qquad (2.10)$$

where $Q_{BM(DMR)}$ is the bed-material discharge in cfs, and Q is the flow discharge in cfs for the DMR.

The preliminary n-Q relationship for Pool 20 obtained by the HEC-6 program was given previously as:

$$n = 9.502 \times 10^{-8} Q + 0.01 \quad \text{for } Q \leq 118{,}000 \text{ cfs} \qquad (2.4)$$

$$n = 0.0213 \quad \text{for } Q \geq 118{,}000 \text{ cfs} \qquad (2.5)$$

However, the UUWSR and SUSR models require a power relation of the form:

$$n = n_o(aQ^b) \qquad (2.11)$$

Thus, (2.4) was approximated by

$$n = 0.0213\ (0.0324)Q^{0.29} \qquad (2.12)$$

At the beginning of the calibration procedure (2.5) and (2.12) were used, but were later modified to obtain better agreement between measured and computed stage elevations at L&D 19.

3. Calibration of the models. A calibrated mathematical model should be able to simulate flow characteristics and geomorphic changes in the modeled study reach. Three important factors for simulation are:

(1) The water discharge and water-surface elevation at computational cross sections,
(2) The cross-sectional changes, and
(3) The sediment-transport rates.

a. Calibration of the UUWSR model. The relations involving n were modified to obtain better agreement between the measured and computed stage hydrographs at the upstream boundary, L&D 19, from 1 May 1976 to 31 August 1976. The modifications yielded:

$$n = 0.0213\ (0.211)Q^{0.13} \quad \text{for } Q \leq 180{,}000 \text{ cfs} \qquad (2.13)$$

$$n = 0.0219 \quad \text{for } Q \geq 180{,}000 \text{ cfs} \qquad (2.14)$$

The utilization of these relations gave differences in stage elevation at the upstream boundary typically less than 1 ft, except during the period from December 1977 to March 1978 where ice-jam effects caused larger differences.

Cross-sectional changes were computed at one Fox Island location and at four locations near Buzzard Island. The model was calibrated to reproduce the geomorphic changes at these locations. The results of the computations at the five locations are shown in figures II-B-3.1 through II-B-3.5 together with the cross-sectional shapes found at the completion of the field study in August 1978. Note that for this one-dimensional model, the overall bed-area changes were computed at each cross section, and then distributed according to relative conveyance to compute the new cross-section shapes shown in the figures. This sediment-distribution method is described by Simons and Chen (1979).

Modifications of the sediment-transport relations, (2.8); (2.9); and (2.10), to produce a better calibrated model were not attempted due to the lack of more recent detailed information regarding cross-section shapes, and the fact that the 1976 and 1978 field studies surveyed different cross sections. However, correct trends in the thalweg elevations were predicted by the model in the recurrent shoaling areas near Fox Island and Buzzard Island, as can be seen in figure II-B-3.6. Thus, it appears that the calibrated model does adequately simulate geomorphic changes over the study reach.

b. Calibration of the SUSR model. A similar procedure to that described for the UUWSR Model was used in the modifications of the relations:

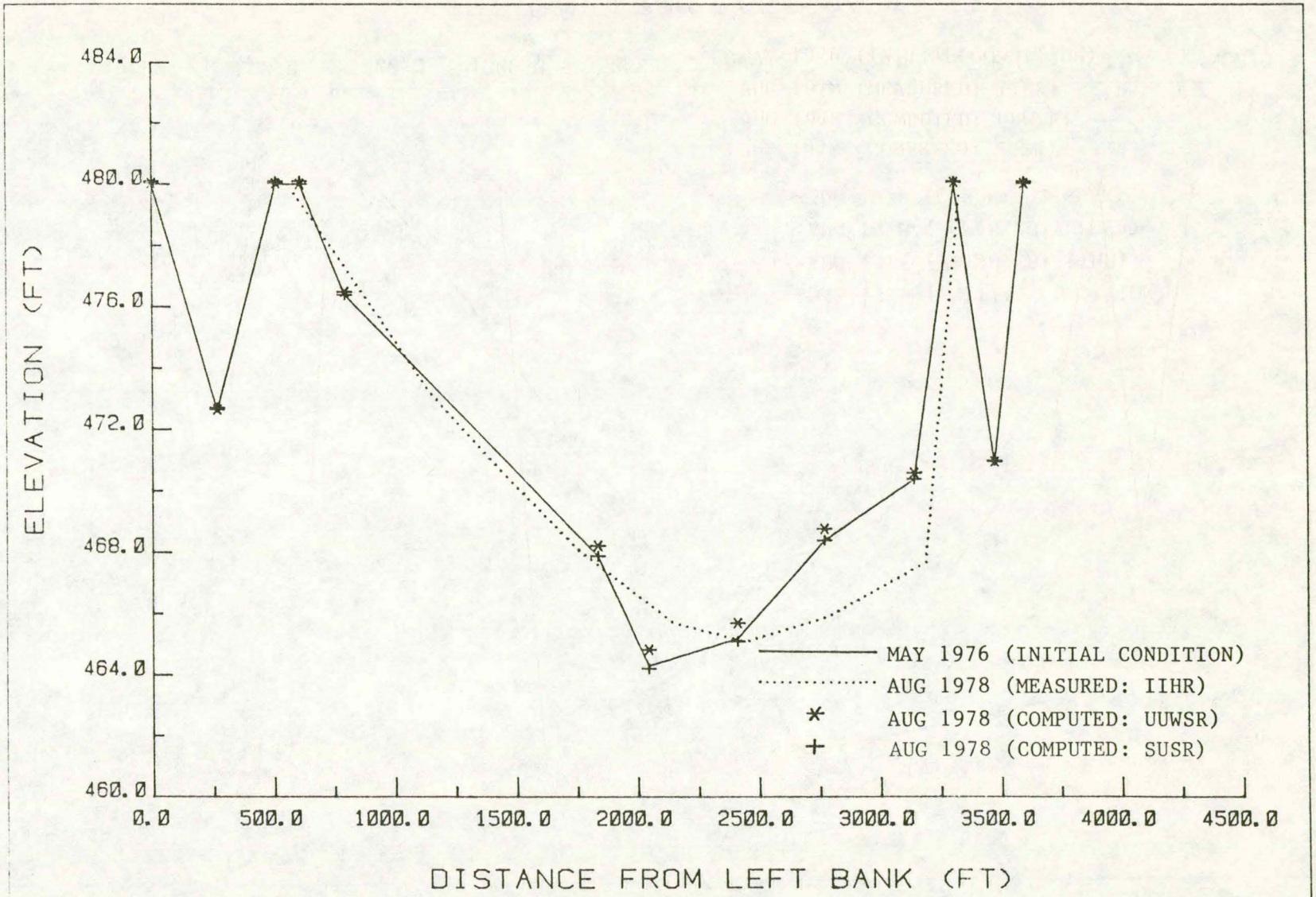

Figure II-B-3.1 Measured and computed cross-section profiles at RM 354.93

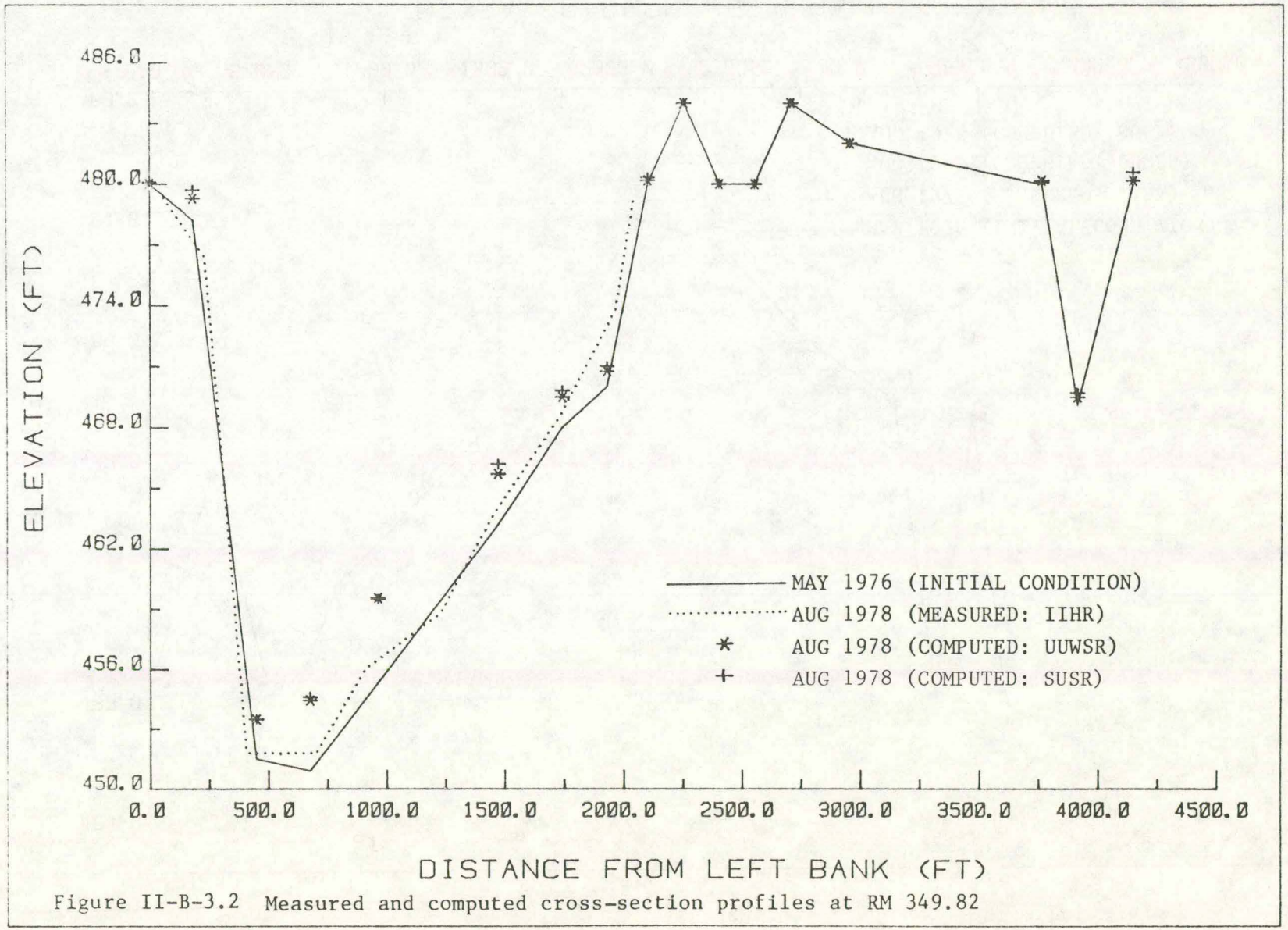

Figure II-B-3.2 Measured and computed cross-section profiles at RM 349.82

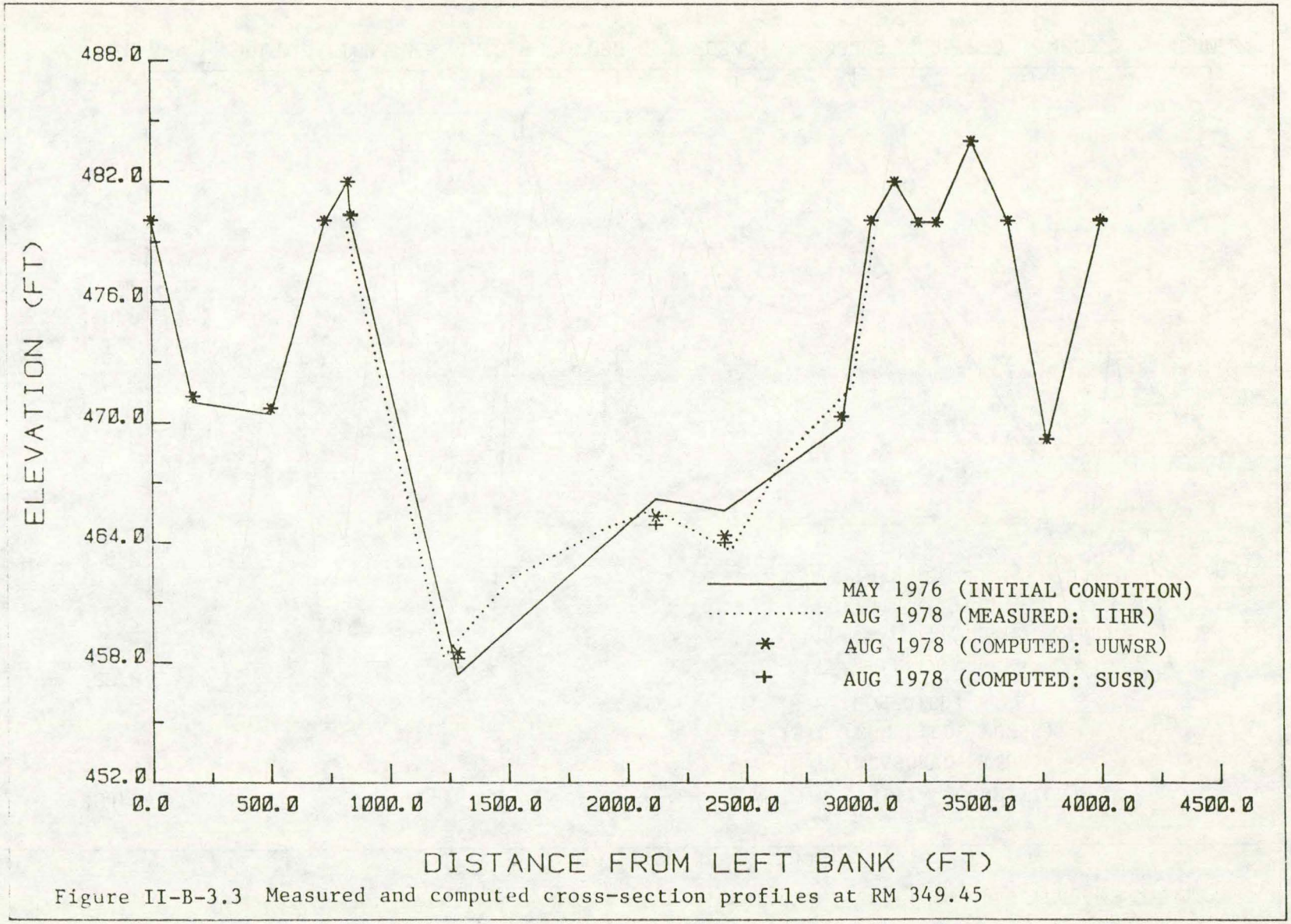

Figure II-B-3.3 Measured and computed cross-section profiles at RM 349.45

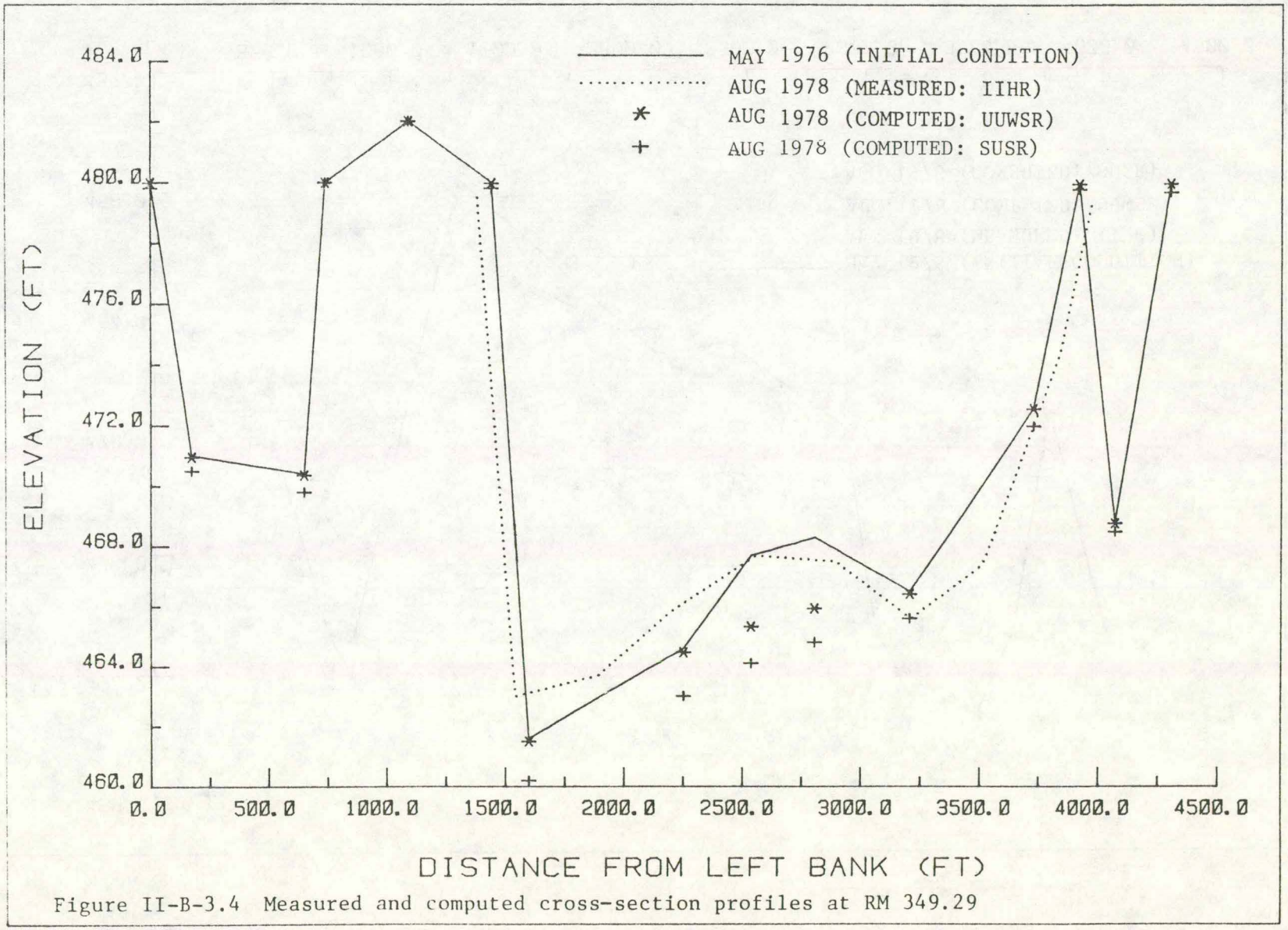

Figure II-B-3.4 Measured and computed cross-section profiles at RM 349.29

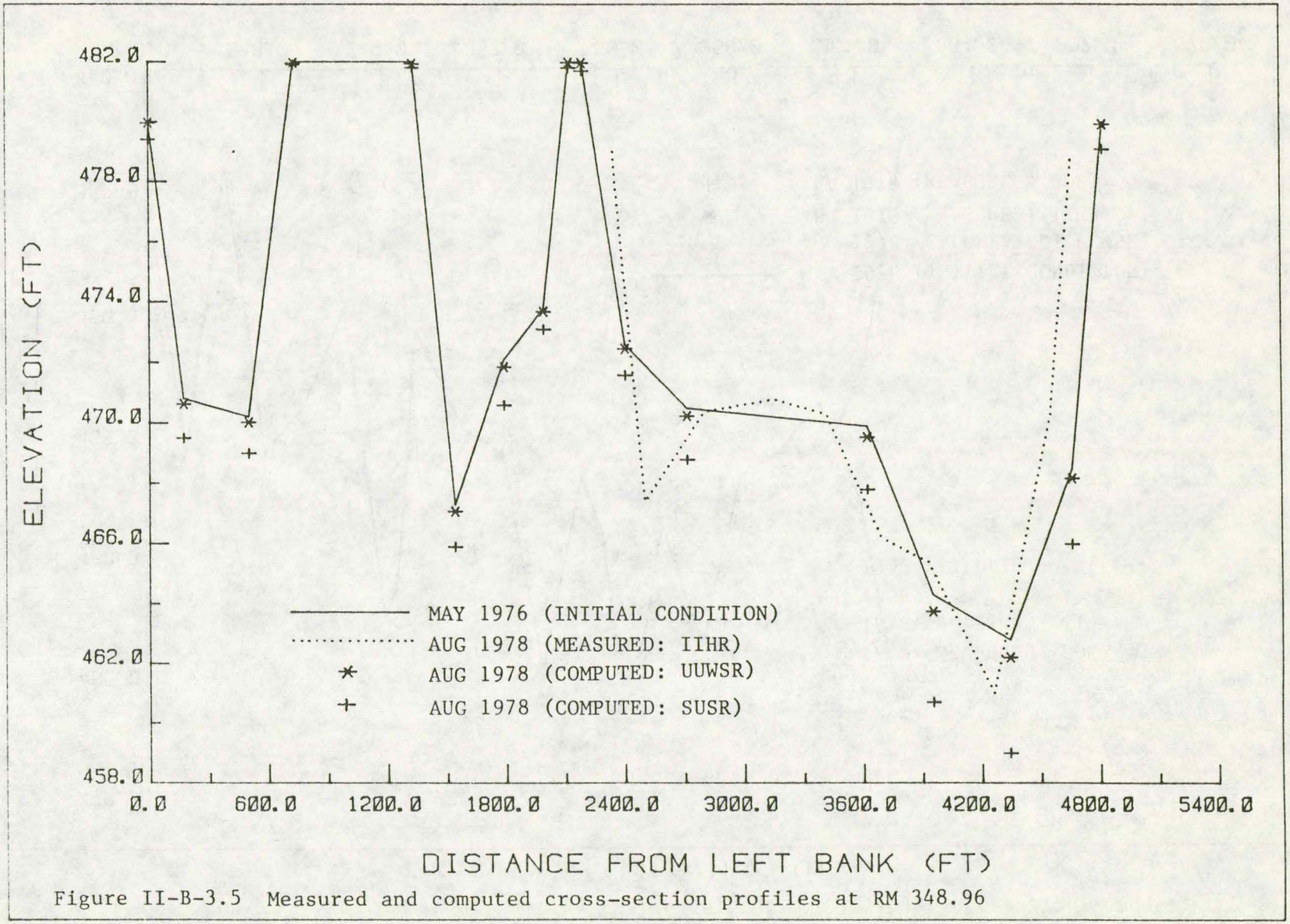

Figure II-B-3.5 Measured and computed cross-section profiles at RM 348.96

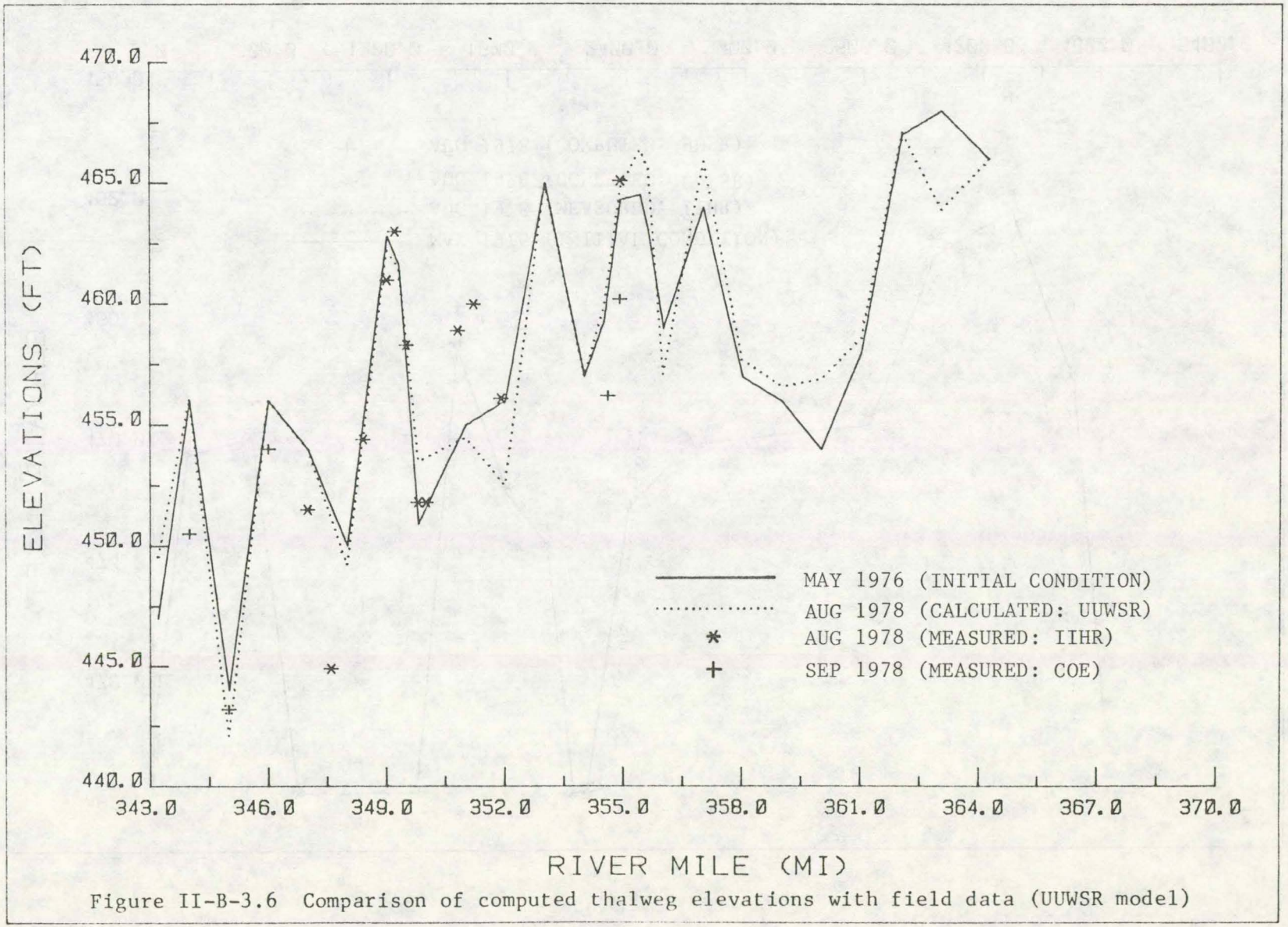

Figure II-B-3.6 Comparison of computed thalweg elevations with field data (UUWSR model)

involving n. The revised formulas are given by

$$n = 0.0213\ (0.211)\ Q^{0.14} \quad \text{for } Q \leq 133{,}000 \text{ cfs} \qquad (2.15)$$

$$n = 0.0234 \quad \text{for } Q \geq 133{,}000 \text{ cfs} \qquad (2.16)$$

These values calculated for n using (2.15) and (2.16) are about 7 percent larger than those values calculated using (2.13) and (2.14) in the UUWSR model. The difference is due to:

(1) The SUSR model uses an energy equation for backwater computations, while the unsteady water-continuity and momentum equations are used in the UUWSR model.

(2) The SUSR model approximates the geometric properties at a computational cross section using a power relation, while the UUWSR model uses linear interpolation of stages versus geometric variables (cross-sectional area, top width, and conveyance).

As with the UUWSR model, differences between the recorded and computed stage elevations at L&D 19 for the study period were typically less than 1 ft, although ice-jam effects caused larger differences between December 1977 and March 1978.

Cross-sectional shapes that were computed using the SUSR model are also displayed in figures II-B-3.1 through II-B-3.5, and they were compared to the final shapes determined during the 1978 field study. As discussed earlier, no further alterations were made to the sediment-transport equations to obtain a better calibrated model. However, figure II-B-3.7 shows that the SUSR model also correctly predicted general aggradation trends in the vicinity of the recurrent shoaling area near Fox Island. Hence, it appears that the SUSR model also may be used to simulate geomorphic changes over the study reach.

4. Sensitivity analysis.

a. Spatial design. Spatial design refers to a model's representation of the physical characteristics of a river system, including such information as the location of tributaries and data on channel properties. In sediment studies, the spacing of cross sections can be estimated in terms of a particle settling length which is given by

$$x = \frac{D}{w} V \qquad (2.17)$$

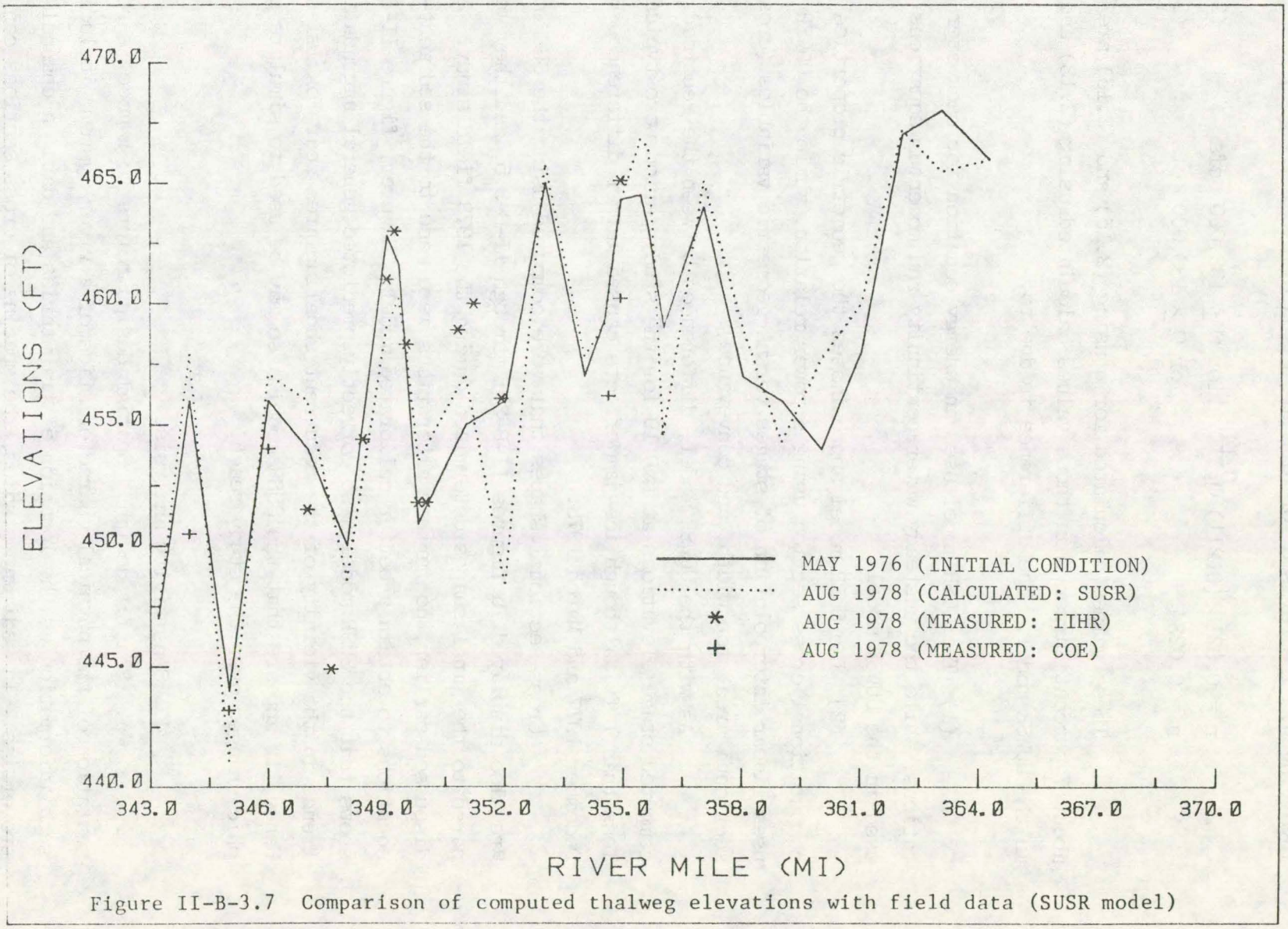

Figure II-B-3.7 Comparison of computed thalweg elevations with field data (SUSR model)

where x is the particle settling length; D is the depth of flow; V is the velocity of flow; and w is the fall velocity of the median bed-material sediment size, D_{50}. Since the largest amounts of sediment are transported during high flows, typical high-flow values should be used in (2.17). Using a recommended spacing from 1x to 10x (Simons et al., 1979a), the spacing of 0.2 mi to 1.2 mi employed in the models was found to be adequate, although effects from varying the cross-section spacing were not investigated. Note, however, that cross sections should be located in areas of interest, at control points, and at places of sudden changes in water-surface profiles.

b. Temporal design and operational discharge. Temporal design refers to a model's ability to simulate changes in the water and sediment inputs to a river system with time, as well as representing the changes in the water and sediment discharges that occur throughout the river system. Temporal variations are generally mild in the Pool 20 study reach of the MR, and since discharge hydrographs are given on a daily basis, the use of a basic one-day time step was considered sufficient and convenient for the model. However, because changes occurring along the river bed are minimal during low flows when sediment-transport rates are small, larger time steps may be used or smaller discharges can be bypassed to increase the effectiveness of the model. As a result of an analysis performed on the absolute values of the changes in thalweg elevations with various discharges, those portions of the discharge hydrograph having flows less than 40,000 cfs were bypassed.

c. Effects of time steps. The average of the absolute values of the differences between the computed and recorded stage elevations at L&D 19 were compared for four different time intervals (1 day, 3 days, 5 days, and 10 days). The results indicated that the maximum time step that can be used in the UUWSR model without losing significant accuracy is about 5 days. Similar results were obtained when the absolute cumulative changes of the computed thalweg elevations at each cross section versus time were compared for the different time intervals.

Similar comparisons were made using the SUSR model, but with time intervals of 1 day, 5 days, 10 days, and 30 days. Computed results

were poor when the 30-day time interval was used. However, the utilization of a variable time step employing longer intervals for smaller discharges and shorter intervals for larger discharges produced good agreement with the results from a 1-day time step. Hence, it was shown that the SUSR model could adequately use a variable time step and still produce accurate results. It should be noted that the SUSR model required less computer time than the UUWSR model.

5. Discussion of results. Both the UUWSR and SUSR models show promise in their ability to predict river changes in Pool 20 of the Upper MR. The UUWSR model provided a better stage-elevation prediction, and both models calculated comparable bed-elevation changes. The SUSR model was able to use a longer time step and required less computer time, implying that the SUSR model is better suited than the UUWSR model for studying long-term impacts.

C. The CHAR2 Mathematical Model.

1. General model description. A one-dimensional mathematical model, CHAR2, was developed by Sogreah, a consulting firm in Grenoble, France (Cunge and Perdreau, 1972; Sogreah, 1981). The model consists of a one-dimensional steady-flow equation and a sediment-continuity equation:

$$\frac{\partial}{\partial x}\left(\frac{\partial Q}{\partial A^2} + gy\right) + g\frac{Q|Q|}{D^2} = 0 \qquad (2.18)$$

$$(1 - p)\frac{\partial z}{\partial t} + \frac{1}{b}\frac{\partial G}{\partial x} = 0,\ G = G(y,z,b,d,\ldots) \qquad (2.19)$$

where $Q = Q(x)$ = flow discharge; $A = A(x)$ = cross-sectional area; $y = y(x,t)$ = water-surface elevation; $z = z(x,t)$ = river-bed elevation; D = conveyance factor; p = porosity of river-bed sediment; b = river-bed width associated with a movable bed; $G = G(x,t)$ = sediment discharge; d = sediment characteristics; and g = gravitational acceleration. It is assumed that flow celerities are much greater than bed-form movement, and the flow resistance is given by the Manning roughness coefficient which is considered constant in time. The bed material is assumed to be homogeneous. The model considers only bed-load transport, allowing the use of one of the Meyer-Peter, Engelund-Hansen, DuBoys, or Einstein-Brown formulas. The numerical scheme utilized

to solve the system of nonlinear hyperbolic partial differential equations is an implicit finite-difference method with a double-sweep procedure developed by Cunge and Perdreau (1972).

2. CHAR2 model construction. Application of the CHAR2 model for Pool 20 of the MR first required a general model layout which is shown in figure II-C-2.1. The reach between RM 348 and RM 357, which includes two major shoaling area, used a spatial interval of 0.5 mile, while the spatial interval for the rest of the reach ranged from 0.8 mile to 1.5 mile. The input data and boundary conditions utilized were as follows:

(1) Input data. At each computational point, the main-channel cross-section geometry was constructed such that the cross-section profile varied laterally in a stepwise manner. Note that only main-channel cross sections were used in the model construction. At each subsection, median bed-material size and bed elevation were given using available data. The porosity of river-bed sediment (0.49) and the kinematic viscosity of water (1.08×10^{-5} ft^2/s) were assumed to be constant throughout the model calibration period. The constant value of $n = 0.023$ $ft^{-1/3}s$ was adopted; this value was based on the calibration result of the HEC-6 program. The Einstein-Brown formula was used to model bed load.

(2) Boundary conditions. The following boundary conditions were given for the model construction:

a. At L&D 19 (upstream boundary), the monthly-averaged MR discharge, Q, was given as a function of time, t, for the model calibration period. Since L&D 19 trapped most of the coarse sediments, no sediment input at this upstream boundary was considered (note that the CHAR2 program considers only bed-load transport).

b. At the DMR mouth, the monthly-averaged DMR discharge was given. Total sediment input, Q_T, from the DMR was calculated as a sum of partial suspended-load discharge, Q_S, and bed-load discharge, Q_B:

$$Q_T \cong Q_B + 0.25\, Q_S \tag{2.20}$$

in which the factor of 0.25 was employed since approximately 25 percent of the suspended load in the DMR contains sand materials. The quantities Q_S

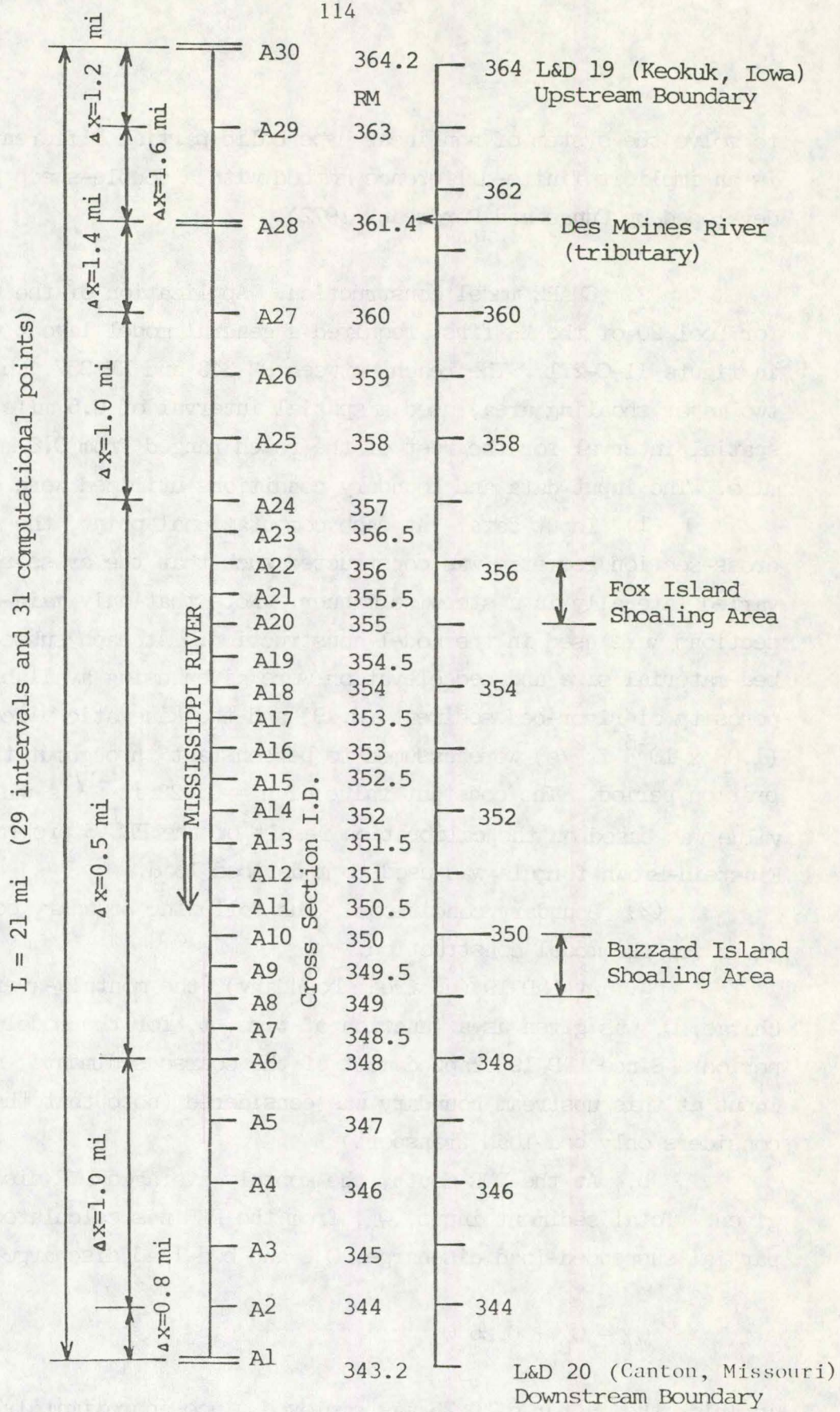

Figure II-C-2.1 Schematic outline of the CHAR2 model cross sections

and Q_B were determined as functions of Q based on the USGS and the IIHR field data:

$$Q_S = 3.10 \times 10^{-3} Q^{1.66} \quad (2.21)$$

and

$$Q_B = 1.19 \times 10^{-8} Q^{2.59} \quad (2.22)$$

where Q is in units of cfs, and Q_S and Q_B are in units of tons/day.

c. At L&D 20 (downstream boundary), the monthly-averaged pool elevation, y, was given as a function of t.

3. Results of the CHAR2 model calibration. The computer simulation was conducted by Sogreah for the time period from 1 May 1976 to 31 August 1978 (28 months). As described in the preceding section, monthly-averaged input data were employed. The computer run utilized a temporal computation interval ranging between 6 hrs. and 5 days. The computer printout provided information on water-surface and thalweg elevations, mean velocity, flow discharge, and sediment-transport rate at each cross section of the study reach. Figure II-C-3.1 illustrates the initial longitudinal thalweg profile and calculated water-surface profile. The observed water-surface elevation at the upstream boundary (RM 364.2) agrees very well with the calculated value. Note that the water-surface elevation at the downstream end was given as a boundary condition. Figures II-C-3.2 and II-C-3.3 show similar plots for t = 185 days and t = 543 days, respectively. Since there are no field data available on thalweg elevations for these days, it is difficult to judge the accuracy of the longitudinal bed-profile prediction. However, the overall prediction of the water-surface profiles seems to be quite satisfactory. Figure II-C-3.4 provides both the initial and calculated (t = 850 days) thalweg elevations at all computation points as well as those which were measured by IIHR and COE. Although the model considered only the bed-load-transport rate, the overall prediction of the thalweg elevation seems to be satisfactory except at certain computational points. A rough comparison was made between the MR bed-load discharges computed from the CHAR2 program and the approximately equivalent bed-load discharges from the 1978 field study, computed by summing the measured bed-load discharges:

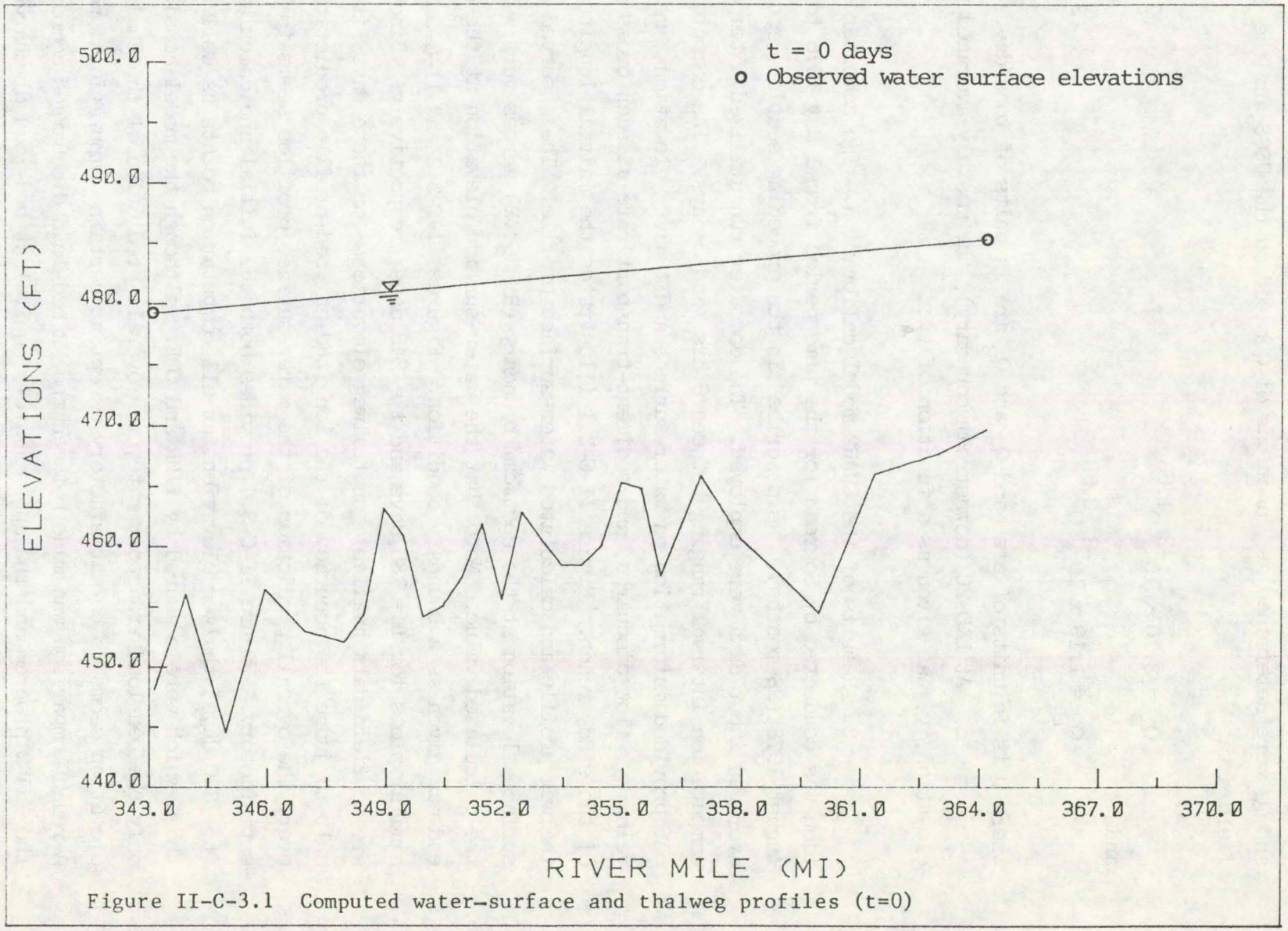

Figure II-C-3.1 Computed water-surface and thalweg profiles (t=0)

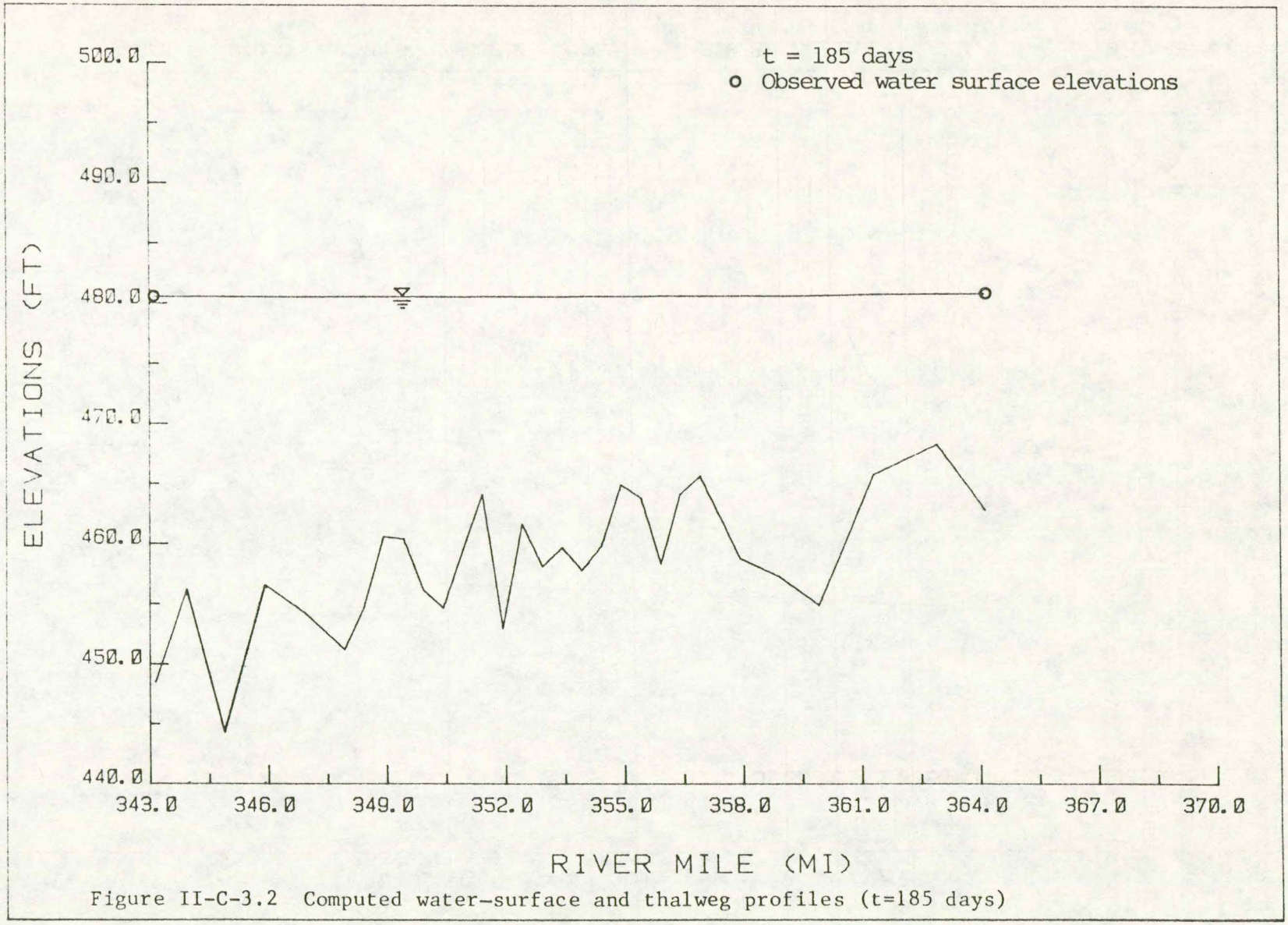

Figure II-C-3.2 Computed water-surface and thalweg profiles (t=185 days)

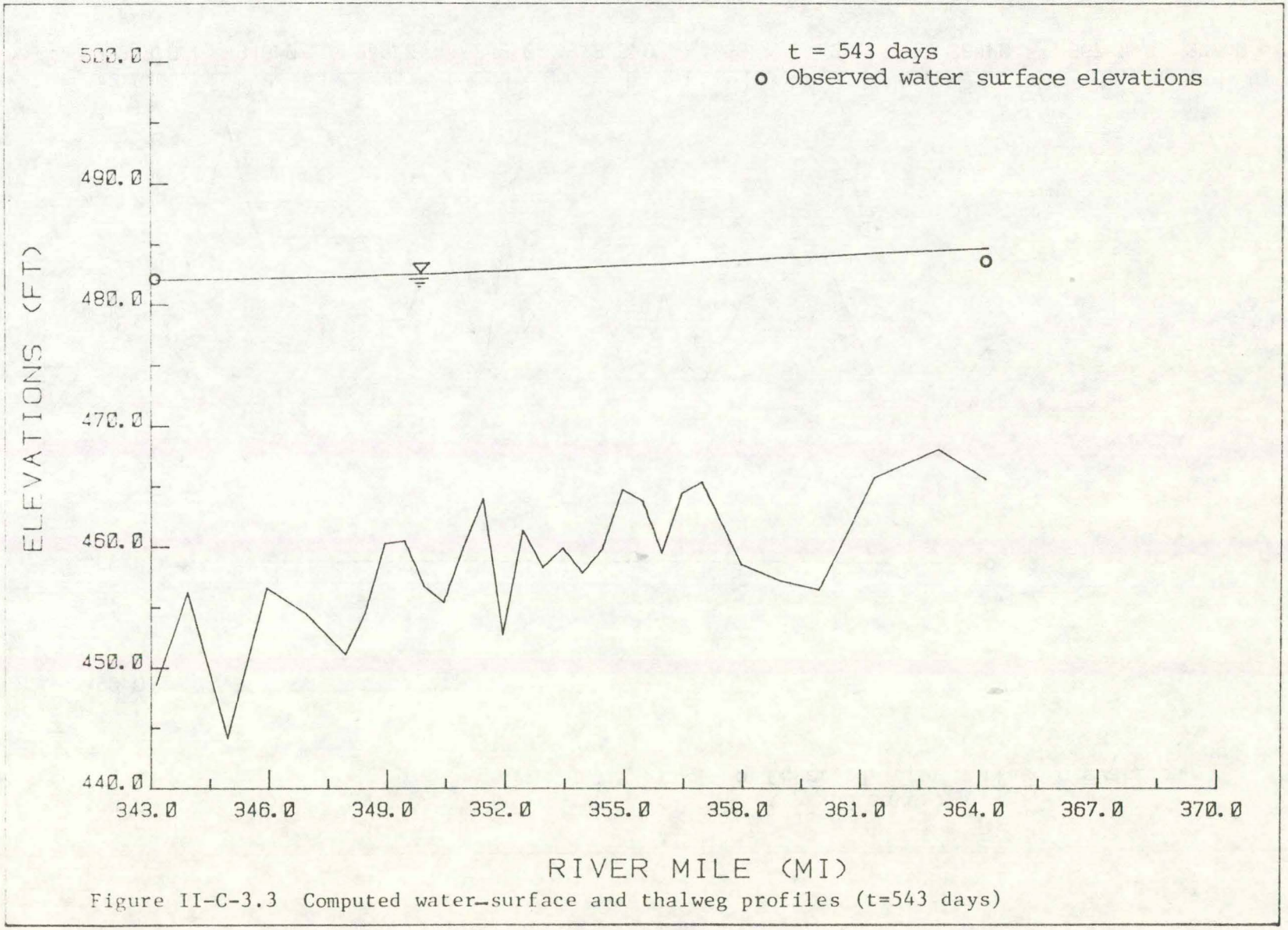

Figure II-C-3.3 Computed water-surface and thalweg profiles (t=543 days)

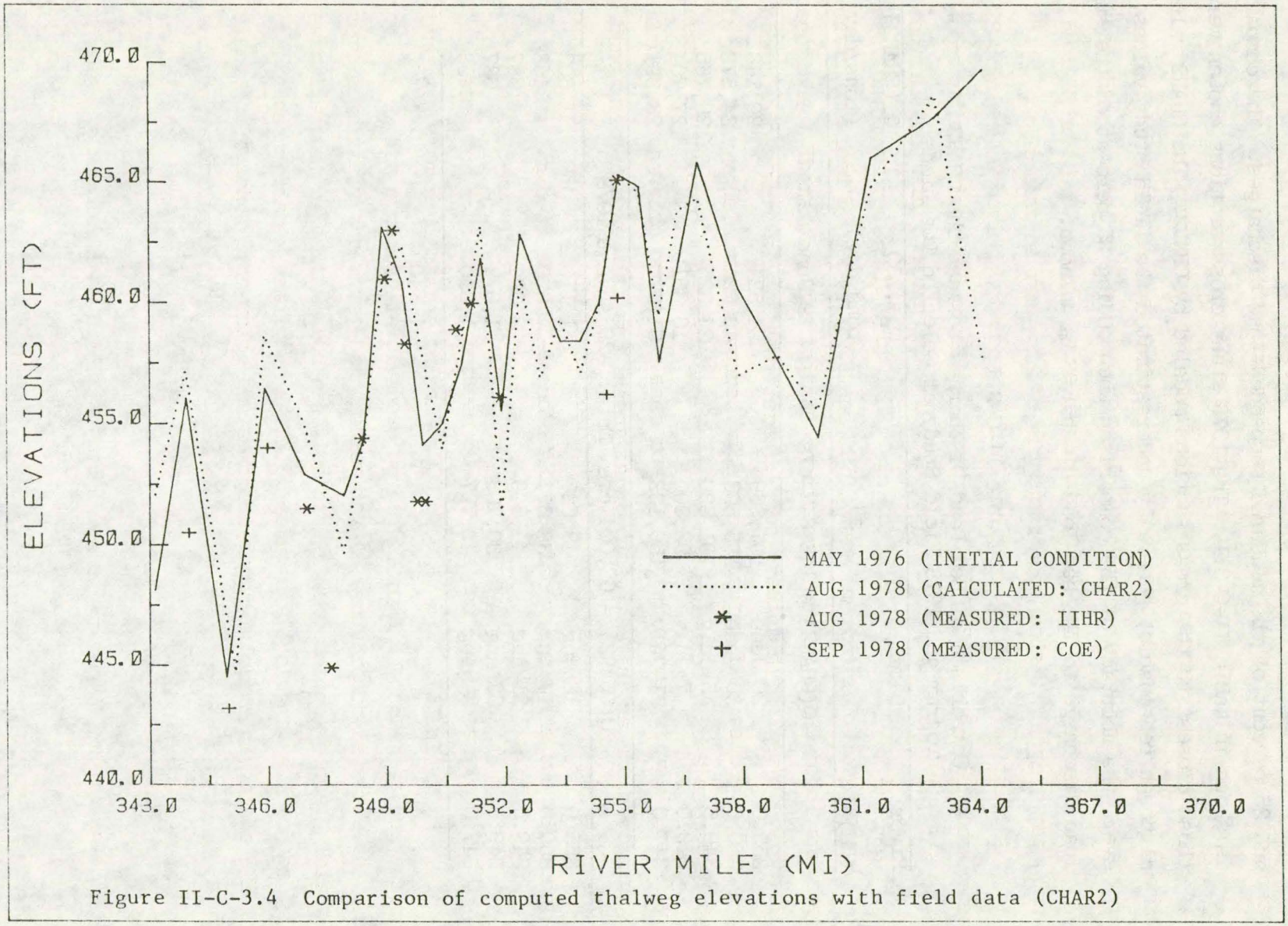

Figure II-C-3.4 Comparison of computed thalweg elevations with field data (CHAR2)

and 25 percent of the measured suspended-load discharges. The comparison is shown in table II-C-3.1. The 1978 study cross sections chosen were those closest to the cross sections modeled by CHAR2. The CHAR2 values, although reasonable, generally underestimated the field study values. However, the accuracy of the comparison when adding 25 percent of the suspended-load discharge to the bed-load discharge is unknown.

Table II-C-3.1

Comparison of Bed-Load Discharges between the CHAR2 Program and 1978 Field Study at Selected Locations

River Mile (RM)	Date	Q (cfs)	$Q_B+.25Q_s$ (tons/day)	Q_B(CHAR2) (tons/day)
	Q(CHAR2) = 148,842 cfs Date: 29 June 1978			
355.0	26 June	107,869	24,524	20,148
350.0	30 June	135,596	40,024	34,573
349.5	5 July	101,830	24,325	29,765
349.0	7 July	96,800	16,361	27,704
347.0	11 July	159,183	51,077	28,391
	Q(CHAR2) = 62,004 cfs Date: 29 August 1978			
355.0	16 Aug	48,687	1,115	1,603
350.0	17 Aug	38,077	696	458
349.5	21 Aug	44,509	3,394	687
349.0	22 Aug	30,703	1,072	687
347.0	24 Aug	42,727	1,050	458

D. Summary and Recommendations. The present study consisted of two principal parts. PHASE A of the investigation included two campaigns to collect and analyze detailed field data in the Pool 20 study reach of the Mississippi River (MR) between RM 347 and 355 and in the Des Moines River (DMR) near its mouth. These data were used to make diagnoses of the recurrent shoaling problems in the vicinities of Fox Island and Buzzard Island. The empirical flow-sediment-discharge relationships formulated using the data enabled the determination of approximate increases in sediment-transport capacity when side channels were closed to abate shoaling activities of the main channel. The data were also utilized to calibrate various numerical models in PHASE B of the study.

PHASE B included testing of the HEC-6 model (Hydrologic Engineering Center, Corps of Engineers), the UUWSR and SUSR models (Colorado State University), and the CHAR2 model (Sogreah). The HEC-6 program was run at The University of Iowa, and the other three models were run by the developers using the basic initial and boundary input data model constructed by the Iowa Institute of Hydraulic Research (IIHR). Although each one-dimensional model has its own numerical model characteristics, accurate prediction of a longitudinal river-bed profile required them to have in common the following four major factors: (1) accurate initial conditions, including a cross-section profile and bed-material size distributions at each computational cross section; (2) accurate boundary conditions such as water and sediment inflows along the model boundaries, quantitative expressions of suspended- and bed-load discharges and information on the size of the sediment inputs, and stage hydrographs at the upstream and downstream boundaries; (3) bed-roughness characteristics at each computational point; and (4) reliable sediment-transport formulas which describe the sediment-transport characteristics in the study reach. It is extremely important to understand the interrelationship between these factors; an accurate estimate of sediment-transport rate depends entirely on accurate estimates of river-flow characteristics which require detailed geometric information as well as on information concerning bed roughness, which adjusts itself according to the sediment-transport rate. The interaction between the flow and the movable river bed is a continual, dynamic activity. Therefore, the exclusion of even one item listed above can lead to serious errors in computer simulations. However, since one can hardly be provided with a complete set of

input data in a practical numerical application, a number of assumptions often have to be made to close the gap in the input information.

Unfortunately, the study reach lacked certain input data in varying degrees; the most serious one was a lack of information on geometric configurations of the initial MR bed profiles, sediment-inflow rates from the DMR, and bed-material size distributions along the river.

Simulation runs of the aforementioned models all were made for a 28-month time period between May 1976 and August 1978. The initial longitudinal river-bed profiles for the HEC-6, UUSWR, and SUSR models were constructed mainly using COE's 1945 topographic maps, except for the cross sections measured in 1976 by IIHR. In the CHAR2 model, more recent topographic data, obtained by COE in 1974 and 1976, were incorporated for several sections. Therefore, the initial conditions for the CHAR2 model and the other models were slightly different. The predicted thalweg elevations by the four models were compared with the measured 1978 values. The degree of agreement between the computed and measured values seems to be almost of the same order for each model. Better agreement was generally found in the areas with sufficient input data. As far as the averaging period for the input data was concerned, monthly-averaged input data were sufficient in both the HEC-6 and CHAR2 models; whereas the two CSU models required a 5-day time step for a flow discharge over 100,000 cfs, a 10-day time step for a discharge between 50,000 cfs and 100,000 cfs, and a 30-day time step for a discharge below 50,000 cfs.

The application of these numerical models to predict and evaluate more accurately the river-bed changes in the study reach requires the establishment of initial bed profiles at all computation points. This task can be accomplished easily by detailed soundings including side channels along the reach. Concerning the sediment-input information in the DMR, sediment sampling should be continued at St. Francisville, Missouri, to establish a meaningful and reliable flow-sediment rating curve since the DMR is the major source of sediment responsible for the recurrent shoaling. With these simple, supplementary data the calibration of one-dimensional models will certainly become more reliable, and the long-term effect of side channel closures recommended in Chapter I can be tested. Although a two-dimensional model has been recently developed by CSU and tested for

Pool 4 of the MR, the future of such models is still in the dark because of the lack of sufficient field data to calibrate (note here that there are not sufficient input data for even a ONE-DIMENSIONAL model) and the high cost of computation. It should be emphasized that numerical modeling technology is such that it could predict accurately changes in movable river-bed profiles only if sufficiently accurate input data were given.

Based on the present study, several recommendations concerning the applicability of the tested models to the GREAT-II study reach can be made. First, the usage of CHAR2 is not practical because the program is not readily available (a contract with the Sogreah is necessary). However, the CHAR2 model is attractive because of the simplicity of its model construction, requiring the least input information among those models tested, and its economic advantages. Second, the CSU models should be used in predicting local shoaling areas because of their capability to predict lateral changes in river-bed elevations which neither CHAR2 nor HEC-6 is able to provide. Third, HEC-6 should also be used for its capability of analyzing river-bed armoring processes, although it cannot predict lateral changes of bed elevations. Finally, it is strongly recommended that these models be retested for Pool 20 upon compilation of a new set of detailed cross-section data.

LIST OF REFERENCES

Chen, Y.H., & Simon, D.B., "Construction and Calibration of the CSU One-Dimensional Water and Sediment Routing Models of Pool 20 in the Upper Mississippi River System," Prepared for the Iowa Institute of Hydraulic Research, The University of Iowa, Iowa City, Iowa, June, 1980.

Cunge, J.A., & Perdreau, J.A., "Mobile Bed Fluvial Mathematical Models," La Houille Blanche No. 7-1973, 1973.

Guy, H.P., "Laboratory Theory and Methods for Sediment Analysis," U.S. Geological Survey, Techniques of Water-Resources Investigations, Book 5, Chapter C1, 1969.

Guy, H.P., & Norman, V.W., "Field Methods for Measurement of Fluvial Sediment," U.S. Geological Survey, Techniques of Water-Resources Investigations, Book 3, Chapter C2, 1970.

Jennings, M.E., & Land, L.F., "Simulation Studies of Flow and Sediment Transport Using a Mathematical Model, Atchafalaya River Basin, Louisiana," U.S. Geological Survey, Gulf Coast Hydroscience Center, National Space Technology Laboratories, Bay St. Louis, Mississippi, Water-Resources Investigation 77-14, May, 1977.

Nakato, T., & Kennedy, J.F., "Field Study of Sediment Transport Characteristics of the Mississippi River Near Fox Island (RM 355-6) and Buzzard Island (RM 349-50)," IIHR Report No. 201, Iowa Institute of Hydraulic Research, The University of Iowa, Iowa City, Iowa, April, 1977.

Simons, D.B. et al., "Environmental Inventory and Assessment of Navigation Pools 24, 25, and 26, Upper Mississippi and Lower Illinois Rivers--A Geomorphic Study--," Contract Report Y-75-3, U.S. Army Engineer Waterways Experiment Station, July, 1975.

Simons, D.B. & Chen, Y.H., "A Mathematical Model of the Lower Chippewa River Network System," Prepared for the U.S. Army Corps of Engineers, St. Paul District, St. Paul, Minnesota, Report No. CER 78-79 DBS-YHC-58, June, 1979.

Simons, D.B. et al., "Sedimentation Study of the Yazoo River Basin, User Manual for Program KUWASER," prepared for the U.S. Army Corps of Engineers, Vicksburg District, Vicksburg, Mississippi, Report No. CER79-80DBS-RML-GOB6, 1979a.

Sogreah, "Modeling of River Longitudinal Profile: Evolution Using the CHAR2 System," Consulting Firm in France, October, 1978.

U.S. Corps of Engineers, "Scour and Deposition in Rivers and Reservoirs," Computer Program HEC-6, Hydrologic Engineering Center, Davis, California, March, 1976.

Vadnal, J.L., "Field Study of Sediment Transport Characteristics of the Mississippi River Near Buzzard Island (RM 347-55)," M.S. Thesis, The University of Iowa, Iowa City, Iowa, December, 1979.

Vanoni, V.A., "Sedimentation Engineering," ASCE Manuals and Reports on Engineering Practices--No. 54, 1975.

Williams, D.T., "Effects of Dam Removal: An Approach to Sedimentation," Technical Paper No. 50, The Hydrologic Engineering Center, U.S. Army Corps of Engineers, Davis, California, October, 1977.

Appendix A Bed-Material Size Distributions

Table A1 Results of Particle-Size Analyses of Bed-Material Samples

Sec. & Trip No.	Dist. from R.B. (m)	Sieve Size (mm) & Sample Weight Retained (gm)										
		16	8	4	2	1	0.5	0.25	0.125	0.062	PAN	TOTAL
1-1-1	48			0.4	5.0	23.4	64.5	81.0	19.1	3.2	150.1	203.1
1-2-1	162			5.9	12.9	30.7	133.3	163.5	13.1	0.4	0.2	360.0
1-2-1	271		3.0	16.5	47.4	75.8	113.6	86.3	16.4	0.9	0.3	360.2
1-2-1	473		20.3	48.1	44.1	70.4	109.0	62.8	7.8	0.3	0.1	359.9
1-2-1	696			0.6	5.1	43.0	191.3	114.7	5.1	0.1	0.1	360.0
1-3-1	50			0.3	0.4	2.1	78.7	359.1	22.4	0.1		463.1
1-3-1	72			4.3	7.9	23.3	147.1	271.6	8.9	0.1		463.2
2-1-1	174		0.8	1.7	3.5	18.3	84.4	112.1	8.9	0.1		229.8
2-1-1	227			2.3	16.7	59.0	99.4	44.0	8.1	0.3		229.8
2-1-1	440			0.8	2.9	15.6	97.5	105.3	7.5	0.1		229.7
2-1-1	627				0.7	5.0	57.7	152.7	13.6	0.1	0.1	229.9
3-1-1	107			0.6	6.5	40.3	191.7	109.3	9.3	3.9	4.5	366.1
3-2-1	150		1.4	17.7	34.7	56.4	127.0	161.9	13.6	0.5	0.2	413.4
3-2-1	353			0.4	1.0	6.5	183.9	211.4	10.0	0.2		413.4
3-2-1	442			2.4	1.8	10.6	158.1	221.5	18.6	0.3		413.3
3-2-1	623			1.3	1.7	3.2	34.9	202.0	152.1	17.8	0.4	413.4
4-1-1	115			14.1	50.5	94.7	149.7	144.6	39.1	2.6	0.9	496.2
4-1-1	183			6.1	5.9	9.3	49.7	327.2	93.9	3.7	0.4	496.2
4-1-1	373		2.2	13.1	23.6	65.8	209.1	172.4	9.8	0.2		496.2
4-1-1	527	116.5		33.7	33.1	56.0	132.9	111.9	11.5	0.7		496.3
5-1-1	122			0.5	1.2	4.3	84.1	356.1	31.1	0.6	0.1	478.0
5-1-1	260		3.1	7.9	21.3	59.6	168.8	185.7	30.0	1.3	0.4	478.1
5-1-1	346			2.4	3.5	35.5	257.3	164.9	13.3	0.9	0.2	478.0

Appendix A Cont'd

Table A1 (cont'd)

Sec. & Trip No.	Dist. from R.B. (m)	Sieve Size (mm) & Sample Weight Retained (gm)										
		16	8	4	2	1	0.5	0.25	0.125	0.062	PAN	TOTAL
5-1-1	515	322.4	59.1	22.6	5.8	6.1	16.0	31.1	13.1	1.2	0.5	477.9
6-1-1	61		2.5	3.2	7.7	20.1	106.2	262.5	25.9	1.2	0.2	429.5
6-1-1	132		5.5	23.1	46.4	57.3	88.1	169.5	36.7	2.4	0.5	429.5
6-1-1	206			2.6	8.6	51.4	171.6	170.5	22.7	1.7	0.3	429.4
6-1-1	298	6.3	10.1	8.1	10.6	42.9	252.3	84.1	11.9	2.6	0.7	429.6
6-1-1	353		3.9	6.8	16.6	38.6	181.3	172.2	9.7	0.3		429.4
6-1-1	449		0.9	0.5	1.0	18.1	261.9	141.5	4.2	0.5	1.0	429.6
6-1-1	531		9.2	12.4	4.7	3.4	15.5	76.4	43.2	4.0	260.7	429.5
6-1-1	615			0.6	0.2	0.3	1.4	58.7	170.2	43.6	154.5	429.5
7-1-1	36		1.1	0.8	1.1	6.4	25.2	56.4	11.6	4.2	240.3	347.1
7-1-1	111			1.6	5.7	23.8	89.2	202.3	21.9	1.3	1.4	347.2
7-1-1	210			3.4	1.8	8.2	51.3	258.3	23.3	0.8	0.1	347.2
7-1-1	302		0.9	15.5	34.1	48.6	108.2	125.5	13.9	0.4		347.1
7-1-1	385		2.1	10.8	37.2	84.2	143.1	63.5	5.6	0.5	0.1	347.1
7-1-1	468		11.0	25.8	45.2	61.9	132.8	66.3	3.7	0.3		347.0
7-1-1	543			4.8	17.0	66.6	164.3	91.0	3.2	0.1	0.1	347.1
7-1-1	629		4.8	8.3	36.0	110.7	142.1	34.1	6.1	1.1	3.9	347.1
7-2-1	125			0.1	1.9	12.7	116.1	296.6	56.1	3.0	1.3	487.8
8-1-1	54			1.0	5.2	6.1	78.5	359.1	39.3	4.6	0.9	494.7
8-2-1	63		0.4	1.2	4.4	23.4	122.0	284.0	37.1	1.5	0.2	474.2
8-2-1	151			1.2	9.7	50.3	174.3	215.4	22.3	0.9	0.2	474.3
8-2-1	228		0.9	11.6	37.8	64.2	122.6	202.6	33.2	1.1	0.1	474.1
8-2-1	349		0.7	1.6	8.3	37.6	173.6	230.4	21.3	0.8		474.3

Appendix A Cont'd

Table A1 (cont'd)

Sec. & Trip No.	Dist. from R.B. (m)	Sieve Size (mm) & Sample Weight Retained (gm)										
		16	8	4	2	1	0.5	0.25	0.125	0.062	PAN	TOTAL
8-2-1	437		2.3	14.1	41.5	85.5	177.1	129.4	21.7	2.2	0.5	474.3
8-2-1	550		3.6	9.2	26.5	92.2	241.5	98.1	3.1			474.2
8-2-1	661			2.2	3.0	20.4	212.4	229.6	6.5	0.1	0.1	474.3
8-2-1	751			1.1	1.4	4.6	99.8	250.1	17.6	2.1	97.4	474.1
9-1-1	44				0.8	14.0	104.6	303.0	64.6	7.5	0.9	495.4
9-1-1	141	9.9	33.6	47.3	23.1	40.4	137.9	134.1	36.6	7.3	25.2	495.4
9-1-1	228			0.8	7.9	40.9	162.9	249.5	32.4	1.0		495.4
9-1-1	327		0.4	9.6	18.6	45.6	114.6	224.5	79.0	3.0	0.1	495.4
9-1-1	339	3.2		4.8	14.2	50.0	184.6	206.8	31.1	0.8		495.5
9-1-1	417			5.2	24.9	73.0	156.3	190.1	43.7	2.0	0.1	495.3
9-1-1	495			2.3	2.8	36.7	265.2	176.2	11.7	0.5	0.1	495.5
9-1-1	597		2.3	24.5	89.7	138.0	147.1	81.6	11.8	0.5		495.5
9-1-1	676			8.0	48.2	115.2	179.1	133.4	11.1	0.5	0.1	495.6
9-2-1	101		2.1	20.9	34.2	72.6	203.1	172.5	7.4	0.1	0.1	513.0
10-1-1	36			0.9	14.0	66.9	223.7	165.1	12.9	1.8	1.9	487.2
10-1-1	107	74.1	99.1	60.4	37.0	24.3	52.5	107.2	29.5	2.3	0.7	487.1
10-1-1	215			5.1	10.9	39.0	145.2	273.3	12.8	0.8	0.1	487.2
10-1-1	289	0.7		2.2	13.9	55.7	193.4	181.7	37.2	2.3	0.1	487.2
10-1-1	378			12.8	23.7	68.8	243.3	122.8	14.8	0.7	0.2	487.1
10-1-1	479		10.2	32.6	54.1	85.5	156.3	127.7	18.3	2.2	0.3	487.2
10-1-1	572		0.4	7.6	28.6	84.9	181.7	166.3	11.6	5.9	0.2	487.2
10-1-1	660		1.0	3.5	12.1	48.6	153.6	209.5	55.9	2.7	0.3	487.2
11-1-1	30			3.6	5.8	41.6	321.3	110.9	2.2	0.2		485.6

Appendix A Cont'd

Table A1 (cont'd)

Sec. & Trip No.	Dist. from R.B. (m)	Sieve Size (mm) & Sample Weight Retained (gm)										
		16	8	4	2	1	0.5	0.25	0.125	0.062	PAN	TOTAL
11-1-1	83		0.9	3.8	16.8	54.5	220.7	185.4	3.1	0.3	0.1	485.6
11-1-1	146			2.3	8.2	30.0	143.0	260.6	39.2	2.3	0.1	485.7
11-1-1	196			0.6	1.5	13.4	217.7	222.2	28.3	1.8	0.3	485.8
11-1-1	254			0.9	1.9	12.3	76.1	126.5	55.9	13.1	199.0	485.7
11-1-1	296					0.6	2.3	114.9	46.8	43.0	278.0	485.6
11-1-1	344					1.0	77.9	77.9	69.3	58.4	201.1	485.6
11-1-1	396				0.2	5.0	10.0	20.3	102.5	270.1	77.4	485.5
11-2-1	77			2.1	19.2	58.3	163.2	136.9	15.5	0.7	0.1	396.0
11-2-1	267		15.9	26.9	31.2	51.5	126.5	133.5	10.0	0.3	0.1	395.9
11-2-1	449		4.0	11.9	27.1	54.1	165.3	125.8	7.4	0.2	0.1	395.9
12-1-1	52				0.1	20.4	72.0	35.7	27.0	15.6	70.5	241.3
12-1-1	161		3.1	8.9	21.0	36.2	91.4	77.2	3.1	0.2	0.2	241.3
12-1-1	294			3.5	3.1	7.1	56.0	153.3	16.8	1.3	0.2	241.3
12-1-1	405		0.7	3.2	8.0	20.5	80.3	111.1	16.9	0.6		241.3
12-1-1	490			0.5	3.7	18.0	75.1	108.2	15.4	2.9	17.7	241.5
12-1-1	602		0.5	8.7	14.6	28.3	77.0	97.0	14.5	0.5	0.1	241.2
12-1-1	700			2.0	5.5	12.4	66.9	130.3	23.1	1.0	0.1	241.3
12-1-1	816			0.7	2.3	11.2	64.7	125.2	36.0	1.0	0.1	241.2
13-1-1	34		14.0	45.2	100.1	119.4	69.3	31.8	4.4	1.7	0.8	386.7
13-1-1	99		2.5	11.9	35.8	74.5	96.5	107.6	38.4	17.7	1.9	386.8
13-1-1	136		0.8	3.5	12.6	75.4	202.0	73.1	11.7	6.0	1.6	386.7
13-1-1	95			3.5	11.0	53.2	178.7	196.7	32.3	2.9	0.6	478.9
13-1-1	45		2.1	13.7	35.3	84.4	185.0	152.1	8.3	2.8	13.6	497.3

Table A1 (cont'd)

Sec. & Trip No.	Dist. from R.B. (m)	Sieve Size (mm) & Sample Weight Retained (gm)										
		16	8	4	2	1	0.5	0.25	0.125	0.062	PAN	TOTAL
13-1-1	80		23.0	28.5	55.6	97.1	141.7	125.6	14.4	2.4	9.0	497.3
13-1-1	136		6.6	7.4	17.0	76.3	255.3	103.5	13.2	2.8	15.1	497.2
1-1-2	51				0.7	6.5	48.2	129.1	38.0	1.0	0.2	223.7
1-2-2	46			5.5	4.7	8.2	66.9	161.5	22.5	0.9	0.1	270.3
1-2-2	170		0.8	6.5	23.1	43.8	69.2	80.7	44.1	1.9	0.1	270.2
1-2-2	273			3.2	9.0	24.7	93.5	129.0	10.8	0.1		270.3
1-2-2	364		18.0	40.9	18.8	23.7	61.7	83.9	22.2	0.8	0.2	270.2
1-2-2	482			10.8	43.8	85.0	82.6	39.5	8.3	0.3	0.1	270.4
1-2-2	566		8.2	16.8	15.8	30.0	127.3	65.3	6.7	0.1		270.2
1-2-2	668			2.8	20.7	49.5	114.0	70.9	12.3	0.1		270.3
1-2-2	779				2.1	21.7	129.4	107.8	9.0	0.2		270.2
1-3-2	72			1.2	3.6	11.1	93.9	163.6	5.4			278.8
2-1-2	56			2.6	12.8	48.5	137.0	47.7	1.1	0.2		249.9
2-1-2	128		3.8	0.5	1.8	13.2	100.3	123.1	7.0	0.2		249.9
2-1-2	214			5.2	20.0	39.4	98.0	74.1	12.8	0.3	0.1	249.9
2-1-2	335			0.2	0.6	5.3	98.8	130.2	14.5	0.3		249.9
2-1-2	436				1.8	25.7	117.5	97.6	7.0	0.2		249.8
2-1-2	526		1.0	1.1	10.5	21.6	69.8	129.7	15.9	0.3		249.9
2-1-2	621			2.2	9.8	33.2	118.5	80.9	5.2	0.1		249.9
2-1-2	716			2.4	16.4	49.8	105.1	70.0	6.1	0.1		249.9
3-1-2	96			4.0	37.7	80.8	92.6	79.9	23.5	2.2	0.7	321.4
3-2-2	59		4.7	18.2	7.8	10.6	79.1	119.4	13.0	1.0	0.2	254.0
3-2-2	155		2.9	18.4	12.2	9.7	53.2	143.2	12.8	1.4	0.2	254.0

Appendix A Cont'd

Table A1 (cont'd)

Sec. & Trip No.	Dist. from R.B. (m)	Sieve Size (mm) & Sample Weight Retained (gm)										
		16	8	4	2	1	0.5	0.25	0.125	0.062	PAN	TOTAL
3-2-2	262		5.5	9.9	5.8	2.7	34.0	165.4	29.5	1.2	0.1	254.1
3-2-2	364			0.4	0.7	5.6	77.7	136.6	32.1	0.8	0.1	254.0
3-2-2	461			0.4	1.5	11.5	77.2	139.9	23.2	0.4		254.1
3-2-2	568			0.5	4.5	27.3	114.1	95.2	12.3	0.2		254.1
3-2-2	667		1.2	7.3	8.1	16.7	87.1	123.8	9.4	0.4	0.1	254.1
3-2-2	729		1.3	2.3	3.8	5.9	53.2	160.6	26.0	0.9	0.1	254.1
4-1-2	37			0.1	2.6	3.2	10.9	65.1	34.9	2.9	0.5	120.2
4-1-2	117			1.0	7.6	14.4	35.2	56.9	4.9	0.2	0.1	120.3
4-1-2	221			0.5	2.8	12.0	46.7	49.2	8.8	0.2		120.2
4-1-2	305		1.4	5.1	9.3	19.2	40.6	38.6	5.7	0.3	0.1	120.3
4-1-2	365			2.7	1.8	7.4	47.4	56.6	4.2	0.2		120.3
4-1-2	432				1.6	6.7	34.0	69.5	8.1	0.3	0.1	120.3
4-1-2	526			1.7	0.8	4.0	39.6	66.1	8.0	0.1		120.3
4-1-2	634				0.4	8.0	46.4	61.8	3.6			120.2
5-1-2	23		4.6	8.7	4.1	4.7	13.8	53.9	106.2	54.0	11.4	261.4
5-1-2	93		1.0	1.9	5.9	4.6	68.7	158.7	20.1	0.3	0.1	261.3
5-1-2	180		2.2	14.3	41.9	65.4	75.0	52.3	9.3	0.8	0.2	261.4
5-1-2	246		0.6	12.0	27.0	52.5	95.4	57.6	14.8	1.2	0.2	261.3
5-1-2	342			0.4	4.2	25.1	109.8	112.2	8.6	1.1		261.4
5-1-2	407		0.9	0.2	5.0	29.7	130.4	92.8	2.1			261.1
5-1-2	496	87.4	63.8	37.0	11.8	6.3	9.4	26.8	16.5	1.6	0.8	261.4
5-1-2	550					0.2	1.0	21.3	145.2	85.7	8.0	261.4
6-1-2	43			1.1	2.4	10.5	55.7	122.0	16.4	0.2	0.1	208.4

Table A1 (cont'd)

Sec. & Trip No.	Dist. from R.B. (m)	Sieve Size (mm) & Sample Weight Retained (gm)										
		16	8	4	2	1	0.5	0.25	0.125	0.062	PAN	TOTAL
6-1-2	127			0.4	3.6	17.4	80.4	95.8	10.5	0.2		208.3
6-1-2	188		2.1	12.2	39.2	50.8	49.9	42.6	11.2	0.4	0.1	208.5
6-1-2	277		5.1	4.3	5.9	18.4	63.9	87.4	22.3	1.0		208.3
6-1-2	358		4.4	15.2	18.0	40.3	72.9	53.2	3.9	0.3	0.1	208.3
6-1-2	438			0.1	1.8	58.9	123.0	23.6	0.8	0.1		208.3
6-1-2	524			0.1	0.4	7.1	58.8	134.2	6.7	0.8	0.1	208.2
6-1-2	592					0.4	2.8	21.9	147.9	33.8	1.6	208.4
7-1-2	31			2.7	0.7	1.0	2.7	7.2	4.4	1.4	232.2	252.3
7-1-2	119				1.0	14.8	88.7	136.1	11.3	0.2	0.1	252.2
7-1-2	190		1.3	3.8	0.6	3.2	35.3	162.5	42.0	3.0	0.5	252.2
7-1-2	289		1.7	25.3	26.3	28.8	59.1	91.1	18.1	0.9	1.0	252.3
7-1-2	358			1.3	5.8	17.5	100.9	120.8	5.6	0.2		252.1
7-1-2	472		5.8	7.9	8.3	25.5	125.2	74.3	4.8	0.3		252.1
7-1-2	560			0.1	2.3	12.6	79.0	150.2	7.8	0.1		252.1
7-1-2	641		5.7	35.9	37.8	42.7	63.0	45.2	18.0	3.6	0.3	252.2
7-2-2	120				0.4	1.6	38.4	163.0	41.1	1.0	0.2	245.7
8-1-2	50			2.8	17.6	36.2	93.1	96.9	18.7	2.2	0.7	268.2
8-2-2	41				0.2	3.8	25.4	111.3	40.4	0.3	0.3	181.7
8-2-2	141			2.6	6.1	18.1	39.9	14.4	98.9	1.5	0.2	181.7
8-2-2	233			1.4	6.0	21.7	51.2	86.8	14.4	0.2		181.7
8-2-2	329			0.2	0.9	11.8	53.5	96.6	18.4	0.3		181.7
8-2-2	432		1.6	8.7	29.7	48.3	52.6	31.7	8.4	0.6	0.1	181.7
8-2-2	543			7.1	18.5	29.0	70.7	50.6	5.6	0.1		181.6

Appendix A Cont'd

Table A1 (cont'd)

Sec. & Trip No.	Dist. from R.B. (m)	Sieve Size (mm) & Sample Weight Retained (gm)										
		16	8	4	2	1	0.5	0.25	0.125	0.062	PAN	TOTAL
8-2-2	634	37.8	39.5	21.4	10.2	7.6	25.4	35.4	4.2	0.2		181.7
8-2-2	741				1.7	17.2	54.0	29.0	79.6	0.1	0.1	181.7
9-1-2	36			0.2	2.0	12.8	67.1	106.8	17.0	0.5	0.2	206.6
9-1-2	124		11.4	54.1	34.5	22.7	22.8	24.4	31.1	4.9	0.7	206.6
9-1-2	224			0.6	3.9	10.8	47.4	116.0	27.5	0.5		206.7
9-1-2	297		0.9	2.4	9.1	20.0	45.7	78.1	48.1	2.2	0.2	206.7
9-1-2	380			0.8	6.1	22.4	81.3	83.1	12.6	0.3	0.1	206.7
9-1-2	461			0.5	4.6	13.5	61.3	103.9	22.6	0.3		206.7
9-1-2	567				0.8	12.5	88.9	97.2	7.2	0.1		206.7
9-1-2	660			0.1	2.3	10.0	53.9	128.9	11.3	0.1		206.6
9-2-2	90				0.2	8.4	151.9	143.8	3.0	0.1		307.4
10-1-2	44	7.1	19.0	10.8	7.1	8.9	45.2	69.6	8.8	2.7	1.4	180.6
10-1-2	149		1.2	5.2	4.6	13.0	59.0	85.9	11.1	0.6	0.1	180.7
10-1-2	208		4.6	4.6	4.5	17.5	63.9	70.1	12.7	2.3	0.4	180.6
10-1-2	290		0.7	3.2	4.9	10.6	41.1	86.4	32.1	1.6	0.1	180.7
10-1-2	376			0.2	3.1	16.0	61.9	74.8	23.2	1.1	0.1	180.4
10-1-2	488			4.2	10.0	18.2	57.0	75.3	15.3	0.5	0.1	180.6
10-1-2	573			2.4	19.1	29.8	53.2	60.3	14.8	0.8	0.1	180.5
10-1-2	651				3.2	28.0	66.4	57.6	23.5	1.6	0.2	180.5
11-1-2	19	164.7	7.1	0.7	2.2	0.7	3.7	26.3	17.4	2.7	0.7	226.2
11-1-2	82	143.9	27.1	11.6	6.4	3.6	9.4	21.3	2.5	0.6		226.4
11-1-2	142			1.2	3.6	17.8	66.9	116.0	20.1	0.7	0.1	226.4
11-1-2	193				0.1	2.7	51.3	139.9	32.0	0.4	0.1	226.5

Table A1 (cont'd)

Sec. & Trip No.	Dist. from R.B. (m)	Sieve Size (mm) & Sample Weight Retained (gm)										
		16	8	4	2	1	0.5	0.25	0.125	0.062	PAN	TOTAL
11-1-2	237					4.8	67.3	124.5	29.0	0.7	0.1	226.4
11-1-2	291				1.3	5.1	25.6	47.7	25.2	1.9	119.5	226.3
11-1-2	338					0.2	2.2	14.7	63.3	16.7	129.2	226.3
11-2-2	54				1.9	5.0	83.2	147.3	12.5	0.1		250.0
11-2-2	235			0.2	1.5	19.8	100.8	120.7	6.8	0.1		249.9
11-2-2	446		4.0	9.7	12.8	27.6	98.9	89.3	7.4	0.2	0.1	250.0
12-1-2	45				0.1	0.6	2.1	4.2	4.6	2.1	201.1	214.8
12-1-2	156		1.1	2.8	18.4	44.5	106.6	39.9	1.2	0.3	0.1	214.9
12-1-2	291	43.6	52.0	21.6	17.2	13.3	13.5	34.7	16.3	2.4	0.2	214.8
12-1-2	397				0.4	5.1	68.3	124.5	16.4	0.1		214.8
12-1-2	507			0.1	2.1	18.8	137.8	50.7	5.2	0.1		214.8
12-1-2	574		0.3	1.6	3.4	17.7	72.0	99.6	19.5	0.7		214.8
12-1-2	654			0.9	5.4	17.9	86.7	95.7	8.0	0.2		214.8
12-1-2	753				4.9	20.6	69.8	98.0	20.5	0.8	0.2	214.8
13-1-2	54		7.1	8.9	20.1	54.5	115.2	77.0	2.9	0.4	0.2	286.3
13-1-2	86			1.8	18.0	42.1	85.2	115.8	18.0	3.2	2.2	286.3
13-1-2	127			0.8	2.7	16.6	104.8	128.1	24.6	5.8	2.8	286.2
13-1-2	42			0.5	3.5	10.5	21.7	14.4	1.2	7.2	209.6	268.6
13-1-2	82			0.6	3.5	17.9	65.6	115.7	14.3	6.5	44.4	268.5
13-1-2	127			2.7	8.6	46.7	111.2	72.8	18.4	5.1	3.0	268.5

Appendix B Sample HEC-6 Input and Output Formats

Input

```
T1       IOWA INSTITUTE OF HYDRAULIC RESEARCH (G323)                    IIHR001     PAGE 0001


T1       IOWA INSTITUTE OF HYDRAULIC RESEARCH (G323)                    IIHR001
T2       APPLICATION OF HEC-6 TO POOL20, MISSISSIPPI RIVER (KEOKUK-CANTON)
T3       ONLY TRIBUTARY = DES MOINES RIVER :T.NAKATO,J.VADNAL, S.WU  JANUARY 1980
NC   0.06     0.06    .0213
NV      4 -0.0213   200000   0.0213   118246 .016146    64000 .011015    10000
X1 343.2       12        0     2500
GR   480        0      457      750      459     1000      456     1150      459     1200
GR   457     1500      451     1900      447     2000      457     2200      461     2400
GR   466     2450      480     2500
H  343.2                 100     2450
X1 344.0       13        0     3500     4224     4224     4224
GR   480        0      469      100      473      400      471      800      465     1950
GR   460     2050      464     2250      456     2700      461     2800      463     2950
GR   460     3000      467     3250      480     3500
H  344.0                  50     3400
X1 345.0       11        0     2100     5280     5280     5280
GR   480        0      477      150      451      200      444      350      446      450
GR   463      850      469     1400      470     1600      473     1700      474     1850
GR   480     2100
H  345.0                 150     2050
X1 346.0       12        0     3000     5280     5280     5280
GR   480        0      464      300      462      450      466      550      474     1100
GR   459     1950      460     2300      456     2400      462     2650      462     2750
GR   475     2850      480     3000
H  346.0                 100     2900
X1 347.0       12        0     2900     5280     5280     5280
GR   480        0      468      100      462      200      468      400      466      600
GR   463      650      454      800      474     2450      475     2600      473     2700
GR   474     2800      480     2900
H  347.0                  50     2850
X1 348.0       13        0     2100     5280     5280     5280
GR   480        0      476       50      473      500      469      550      472      900
GR   468      950      469     1100      465     1350      454     1600      450     1900
GR   452     1950      477     2050      480     2100
H  348.0                  50     2050
X1348.96       17        0     4825     5069     5069     5069
GR 480.0        0    470.8      174    470.2      505    482.0      738    482.0     1338
GR 467.3     1544    472.1     1797    473.8     2000    482.0     2135    482.0     2200
GR 472.6     2410    470.5     2719    469.9     3627    464.3     3956    462.8     4343
GP 468.5     4661    480.0     4825
H 348.96                 1338     4825
X1349.29       15        0     4302     1742     1742     1742
GR 480.0        0    471.0      174    470.4      650    480.0      738    482.0     1088
GR 480.0     1438    461.6     1599    464.6     2252    467.7     2537    468.3     2806
GR 466.5     3206    472.6     3725    480.0     3915    468.8     4069    480.0     4302
H 349.29                 1438     3915              466.4     3265     3515     3515
X1349.45       18        0     4010      845      845      845
GR 480.0        0    471.0      174    470.4      505    480.0      738    482.0      838
GR 480.0      848    457.4     1286    466.2     2126    465.6     2415    469.8     2913
GR 480.0     3048    482.0     3148    480.0     3248    480.0     3323    484.0     3473
GR 480.0     3623    469.0     3777    480.0     4010
H 349.45                  848     3048              464.9     2478     2728     2728
X1349.82       17        0     4137     1954.    1954     1954
GR 480.0        0    478.2      183    451.5      449    450.9      675    455.3      961
GR 463.2     1469    468.0     1738    470.0     1925    480.0     2096    484.0     2246
GR 480.0     2396    480.0     2546    484.0     2696    482.0     2946    480.0     3750
GP 469.1     3904    480.0     4137
H 349.82                    0     2096
X1 351.0       12        0     1900     6230     6230     6230
GR   480        0      472      100      468      400      458      550      455      650
```

Appendix B Cont'd

Input

T1 IOWA INSTITUTE OF HYDRAULIC RESEARCH (G323) IIHR001 PAGE 0002

GR 460	850	457	1000	464	1150	467	1450	469	1500
GR 469	1600	480	1900						
H 351.0		100	1800						
X1 352.0	12	0	2400	5280	5280	5280			
GR 480	0	479	200	469	250	473	700	471	750
GR 475	800	470	1650	464	1750	456	2100	458	2200
GR 477	2300	480	2400						
H 352.0		200	2300						
X1 353.0	15	0	2500	5280	5280	5280			
GR 480	0	470	150	469	250	465	350	471	550
GR 466	600	468	1000	466	1500	468	1550	466	1650
GR 466	2100	468	2150	467	2400	469	2450	480	2500
H 353.0		100	2450						
X1 354.0	12	0	2400	5280	5280	5280			
GR 480	0	477	50	476	300	477	950	470	1250
GR 468	1450	462	1500	457	2100	460	2200	458	2250
GR 459	2300	480	2400						
H 354.0		50	2350						
X1354.54	17	0	3630	2851	2851	2851			
GR 480.0	0	471.6	269	480.0	515	484.0	615	484.0	765
GR 480.0	865	477.3	915	480.0	965	483.0	1090	480.0	1215
GR 477.3	1363	475.8	1658	470.6	2036	464.9	2885	460.5	3174
GR 459.3	3515	480.0	3630						
H 354.54		1215	3630						
X1354.93	13	0	3607	2059	2059	2059			
GR 480.0	0	472.6	269	480.0	515	480.0	615	476.4	798
GR 467.9	1838	464.3	2045	465.2	2412	468.4	2773	470.4	3144
GR 480.0	3318	470.9	3476	480.0	3607				
H 354.93		615	3318						
X1355.39	15	0	3640	2429	2429	2429			
GR 480.0	0	476.7	128	473.2	390	471.9	682	468.0	942
GR 466.0	1565	464.5	1844	465.5	2398	472.0	2677	480.0	2792
GR 488.0	2842	488.0	3292	480.0	3342	468.2	3500	480.0	3631
H 355.39		0	2792						
X1355.59	17	0	3380	1056	1056	1056			
GR 480.0	0	470.4	63	463.1	266	466.4	791	465.1	1024
GR 466.1	1519	465.8	1700	469.6	1998	475.2	2218	480.0	2297
GR 469.5	2425	474.4	2593	480.0	2691	488.0	2891	480.0	3091
GR 475.1	3249	480.0	3380						
H 355.59		0	2297						
X1 356.0	7	0	1800	2165	2165	2165			
GR 480	0	478	50	460	200	459	350	478	1550
GR 478	1750	480	1800						
H 356.0		50	1700						
X1 357.0	18	0	3000	5280	5280	5280			
GR 480	0	474	50	472	200	478	350	473	450
GR 477	600	474	900	477	1000	466	1950	464	2000
GR 468	2050	467	2200	465	2250	467	2400	466	2450
GR 467	2750	473	2900	480	3000				
H 357.0		50	2950						
X1 358.0	9	0	1300	5280	5280	5280			
GR 479	0	471	200	473	250	465	350	464	450
GR 459	750	461	800	457	1250	471	1300		
H 358.0		50	1300						
X1 359.0	10	0	2300	5280	5280	5280			
GR 480	0	471	300	474	450	472	1200	470	1250
GR 472	1350	465	1700	456	1950	469	2200	480	2300
H 359.0		100	2250						
X1 360.0	9	0	1300	5280	5280	5280			
GR 480	0	460	200	454	400	457	600	457	950

Appendix B Cont'd

Input

```
T1      IOWA INSTITUTE OF HYDRAULIC RESEARCH (G323)                    IIHR001     PAGE 0003


GR    460     1100      458     1150      473     1200      480     1300
H   360.0               50     1250
X1  361.0       10        0     1800     5280     5280     5280
GR    481        0      476      150      478      200      479      350      471      500
GR    458     1100      467     1650      466     1700      471     1750      481     1800
H   361.0              400     1800
QT
X1  362.0       10        0     2900     5280     5280     5280
GR    480        0      471     1200      472     1500      471     1750      475     1800
GR    467     1950      470     2150      470     2650      467     2750      480     2900
H   362.0             1200     2880
X1  363.0        8        0     2400     5280     5280     5280
GR    480        0      471      850      470     1000      469     1200      468     1500
GR    470     1950      472     2200      480     2400
H   363.0              850     2400
X1  364.2       14        0     2100     6336     6336     6336
GR    480        0      474      950      474     1050      473     1150      474     1250
GR    473     1350      472     1450      466     1550      466     1600      470     1700
GR    469     1850      473     1950      475     2050      490     2100
H   364.2              950     2050
EJ
T4        MODEL INCLUDES CLAY, SILT, SAND, AND GRAVEL. TOTAL SEDIMENT LOAD INPUT
T5        AT L&D19 INCLUDES ONLY CLAY, SILT, AND VFS. BUT, DES MOINES RIVER SED.
T6        INPUT HAS CLAY, SILT, VFS, FS, MS, CS, VCS, VFG, AND FG.
T7        TOFFALETI FORMULA IS USED. MODEL UTILIZES WEEKLY  AVERAGED DISCHARGES
T8        FOR WATER AND SEDIMENT.
I1
I2    CLAY
I3    SILT                3        3
I4    SAND                         7
L     Q       10000     50000    150000    200000
L     CLAY       35      1790     26080     52620
L     SILT      102      5150     75180    151694
L     VFS      0.83        42       611      1233
L      FS       0.0       0.0       0.0       0.0
L      MS       0.0       0.0       0.0       0.0
L      CS       0.0       0.0       0.0       0.0
L     VCS       0.0       0.0       0.0       0.0
L     VFG       0.0       0.0       0.0       0.0
L      FG       0.0       0.0       0.0       0.0
N   343.2               0.052     0.026     0.996                0.005     0.005     0.004     0.075
N           0.475     0.303     0.079     0.034     0.016
N   344.0               0.052     0.026     0.996                0.005     0.005     0.004     0.075
N           0.475     0.303     0.079     0.034     0.016
N   345.0               0.052     0.026     0.996                0.005     0.005     0.004     0.075
N           0.475     0.303     0.079     0.034     0.016
N   346.0               0.052     0.026     0.996                0.005     0.005     0.004     0.075
N           0.475     0.303     0.079     0.034     0.016
N   347.0               0.052     0.026     0.996                0.005     0.005     0.004     0.075
N           0.475     0.303     0.079     0.034     0.016
N   348.0               0.052     0.026     0.999                0.001     0.002     0.003     0.101
N           0.477     0.288     0.089     0.028     0.010
N 348.96                0.052     0.026     0.999                0.001     0.002     0.003     0.101
N           0.477     0.288     0.089     0.028     0.010
N 349.29                0.052     0.026     0.999                0.000     0.000     0.001     0.048
            0.409     0.361     0.129     0.039     0.012
N 349.45                0.052     0.026     0.978                0.000     0.001     0.001     0.051
            0.444     0.279     0.091     0.066     0.045
N 349.82                0.052     0.026     0.993                0.047     0.047     0.034     0.166
N           0.331     0.192     0.084     0.056     0.036
```

Appendix B Cont'd

Input


```
N  351.0          0.052   0.026   0.993           0.000   0.000   0.001   0.038
N          0.335  0.335   0.179   0.083   0.022
N  352.0          0.052   0.026   0.993           0.000   0.000   0.001   0.038
N          0.335  0.335   0.179   0.083   0.022
N  353.0          0.052   0.026   0.993           0.000   0.000   0.001   0.038
N          0.335  0.335   0.179   0.083   0.022
N  354.0          0.052   0.026   0.993           0.000   0.000   0.001   0.038
N          0.335  0.335   0.179   0.083   0.022
N 354.54          0.052   0.026   0.993           0.000   0.000   0.001   0.038
N          0.335  0.335   0.179   0.083   0.022
N 354.93          0.052   0.026   0.992           0.000   0.000   0.001   0.020
N          0.284  0.444   0.158   0.059   0.026
N 355.39          0.052   0.026   0.988           0.000   0.001   0.001   0.018
           0.331  0.432   0.134   0.049   0.022
N 355.59          0.052   0.026   0.903           0.000   0.000   0.001   0.020
N          0.295  0.331   0.129   0.065   0.061
N  356.0          0.052   0.026   0.903           0.000   0.000   0.001   0.020
N          0.295  0.331   0.129   0.065   0.061
N  357.0          0.052   0.026   0.903           0.000   0.000   0.001   0.020
N          0.295  0.331   0.129   0.065   0.061
N  358.0          0.052   0.026   0.903           0.000   0.000   0.001   0.020
N          0.295  0.331   0.129   0.065   0.061
N  359.0          0.052   0.026   0.903           0.000   0.000   0.001   0.020
N          0.295  0.331   0.129   0.065   0.061
N  360.0          0.052   0.026   0.903           0.000   0.000   0.001   0.020
N          0.295  0.331   0.129   0.065   0.061
N  361.0          0.052   0.026   0.903           0.000   0.000   0.001   0.020
N          0.295  0.331   0.129   0.065   0.061
N  362.0          0.104   0.026   0.723           0.007   0.008   0.010   0.065
N          0.233  0.097   0.076   0.097   0.130
N  363.0          0.104   0.026   0.723           0.007   0.008   0.010   0.065
N          0.233  0.097   0.076   0.097   0.130
N  364.2          0.104   0.026   0.723           0.007   0.008   0.010   0.065
N          0.233  0.097   0.076   0.097   0.130
$TRIB
L    Q        200     300     5000    10000   20000   30000
L    CLAY    0.41    1.09     936     4939   26066   68974
L    SILT    1.65    4.37    3743    19754  104263  275898
L    VFS     0.68    1.82    1559     8231   43443  114957
L    FS    0.0001   .0004    1.46     10.9    80.5     260
L    MS    0.0007   .0022    7.33     54.3     403    1300
L    CS    0.0042    .013    45.8      339    2516    8122
L    VCS   0.0021   .0069    23.4      174    1288    4159
L    VFG   0.0008   .0027    9.34     69.3     513    1657
L    FG    0.0004   .0012    4.21     31.2     232     747
$HYD
*     B  RUN 1, MAY 1976 --- 1 (STARTING N = .0213) TEST RUN!!
Q 187200   20611
R  482.6
T      63
W       7
$$END
```

Appendix B Cont'd

1 Output

```
*************************************************
* HEC-6   PROGRAM NUMBER 723-X6-L2470           *
* SCOUR AND DEPOSITION IN RIVERS AND RESERVOIRS *
* VERSION 2.7                 1 NOVEMBER 1976   *
*************************************************
T1       IOWA INSTITUTE OF HYDRAULIC RESEARCH (G323)                    IIHR001
T2       APPLICATION OF HEC-6 TO POOL20, MISSISSIPPI RIVER (KEOKUK-CANTON)
T3       ONLY TRIBUTARY = DES MOINES RIVER :T.NAKATO,J.VADNAL, S.WU  JANUARY 1980
     ALER       ASEL         CE          CC          LFA         NR        TAN        CRL
P    .050000  0.000000  1.000000  1.000000            1
     ALER       ASEL         CE          CC          LFA         NR        TAN        CRL
                       1.000000  1.000000
SEC NO.    343.200
SEC NO.    344.000
SEC NO.    345.000
SEC NO.    346.000
SEC NO.    347.000
SEC NO.    348.000
SEC NO.    349.000
SEC NO.    350.000
SEC NO.    351.000
SEC NO.    352.000
SEC NO.    353.000
SEC NO.    354.000
SEC NO.    355.000
SEC NO.    356.000
SEC NO.    357.000
SEC NO.    358.000
SEC NO.    359.000
SEC NO.    360.000
SEC NO.    361.000
TRIBUTARY ENTRY POINT      0. OCCURRS AT X-SECTION  NO.    20
SEC NO.    362.000
SEC NO.    363.000
SEC NO.    364.200
NO. OF CROSS SECTIONS READ IN =   22
NO. OF INPUT DATA MESSAGES=    0
END OF GEOMETRIC DATA
;
T4       MODEL INCLUDES CLAY, SILT, SAND, AND GRAVEL. TOTAL SEDIMENT LOAD INPUT
T5       AT LAD19 INCLUDES ONLY CLAY, SILT, AND VFS. BUT, DES MOINES RIVER SED.
T6       INPUT HAS CLAY, SILT, VFS, FS, MS, CS, VCS, VFG, AND FG.
T7       TOFFALETI FORMULA IS USED. MODEL UTILIZES MONTHLY AVERAGED DISCHARGES
T8       FOR WATER AND SEDIMENT.
BASIC BACKWATER TAPE
IOWA INSTITUTE OF HYDRAULIC RESEARCH (G323)                    IIHR001
APPLICATION OF HEC-6 TO POOL20, MISSISSIPPI RIVER (KEOKUK-CANTON)
ONLY TRIBUTARY = DES MOINES RIVER :T.NAKATO,J.VADNAL, S.WU  JANUARY 1980
SEDIMENT PARAMETER DATA
        SPI       IBG       MNQ      SPGF      ACGR
I1       0.         0         1     1.000    32.174
        MTCL                         SPGC      DTCL      STCD      PUCD      UWCL      CCCD
I2         1                         2.650      .020      .020    78.000    30.000    16.000
        MTCL     IASL      LASL      SGSL      DTSL      STSD      PUSD      UWSD      CCSD
I3         1        3         3     2.650      .020      .020    82.000    65.000     5.700
        MTC      IASA      LASA      SPGS       GSF      BSAE       PSI       UWD
I4         1         1         7     2.650      .667      .500    30.000    93.000
FOLLOWING GRAIN SIZES UTILIZED
CLAY SIZE=        .000013
```

Appendix B Cont'd

Output

```
SILT SIZES=      .000101
SAND SIZES UP=   .000288   .000580   .001160   .002319   .004639   .009279   .018560
SIGS RATING TABLE
L    G        10000.000   50000.000  150000.000  200000.000
L    CLAY        35.000    1790.000   26080.000   52620.000
L    SILT       102.000    5150.000   75180.000  151694.000
L    VFS          .830      42.000     611.000    1233.000
L     FG         0.000       0.000       0.000       0.000
L    VFG         0.000       0.000       0.000       0.000
L    VCS         0.000       0.000       0.000       0.000
L     CS         0.000       0.000       0.000       0.000
L     MS         0.000       0.000       0.000       0.000
L     FS         0.000       0.000       0.000       0.000
VOLUME VS DEPTH OF DEPOSITS
                VOLUME      MOVEABLE    %              ELEVATIONS
  SEC NO.  SHAPE FACTOR   BED WIDTH  % LEFT SIDE   RIGHT SIDE      THALWEG
    343.20                   2100.0       457.00       466.00       447.00
    344.00                   3325.0       469.00       467.00       456.00
    345.00                   1900.0       477.00       474.00       444.00
    346.00                   2775.0       484.00       475.00       454.00
    347.00                   2800.0       468.00       474.00       454.00
    348.00                   2050.0       476.00       477.00       460.00
    349.00                   2200.0       471.00       464.00       459.00
    350.00                   1575.0       452.00       465.00       451.00
    351.00                   1700.0       472.00       469.00       455.00
    352.00                   2250.0       479.00       477.00       456.00
    353.00                   2400.0       470.00       485.00       465.00
    354.00                   2325.0       477.00       468.00       457.00
    355.00                   2350.0       472.00       468.00       454.00
    356.00                   1625.0       479.00       472.00       459.00
    357.00                   2925.0       474.00       473.00       464.00
    358.00                   1200.0       471.00       471.00       457.00
    359.00                   2100.0       471.00       469.00       456.00
    360.00                   1150.0       460.00       473.00       454.00
    361.00                   1375.0       471.00       481.00       458.00
    362.00                   2225.0       471.00       467.00       467.00
    363.00                   1975.0       471.00       480.00       468.00
    364.20                   1600.0       474.00       475.00       466.00
INACTIVE BED, GRAIN SIZE DISTRIBUTION BY SIZE FRACTION,(N-CARDS)
N  343.2      0.000        .052         .026         .996         0.000        .005         .005         .004         .075
                .475         .303         .079         .034         .016
N  344.0      0.000        .052         .026         .996         0.000        .005         .005         .004         .075
                .475         .303         .079         .034         .016
N  345.0      0.000        .052         .026         .996         0.000        .005         .005         .004         .075
                .475         .303         .079         .034         .016
N  346.0      0.000        .052         .026         .996         0.000        .005         .005         .004         .075
                .475         .303         .079         .034         .016
N  347.0      0.000        .052         .026         .996         0.000        .005         .005         .004         .075
                .475         .303         .079         .034         .016
N  348.0      0.000        .052         .026         .999         0.000        .001         .002         .003         .101
                .477         .288         .089         .028         .010
N  349.0      0.000        .052         .026         .999         0.000        .001         .002         .003         .101
                .477         .288         .089         .028         .010
N  350.0      0.000        .052         .026         .993         0.000        .047         .047         .034         .166
                .331         .192         .084         .056         .036
N  351.0      0.000        .052         .026         .993         0.000        0.000        0.000        .001         .038
                .335         .335         .179         .083         .022
N  352.0      0.000        .052         .026         .993         0.000        0.000        0.000        .001         .038
                .335         .335         .179         .083         .022
N  353.0      0.000        .052         .026         .993         0.000        0.000        0.000        .001         .038
```

Output

	.335	.335	.179	.083	.022				
N 354.0	0.000	.052	.026	.993	0.000	0.000	0.000	.001	.038
	.335	.335	.179	.083	.022				
N 355.0	0.000	.052	.026	.992	0.000	0.000	0.000	.001	.020
	.284	.444	.158	.059	.026				
N 356.0	0.000	.052	.026	.993	0.000	0.000	0.000	.001	.020
	.295	.331	.129	.065	.061				
N 357.0	0.000	.052	.026	.993	0.000	0.000	0.000	.001	.020
	.295	.331	.129	.065	.061				
N 358.0	0.000	.052	.026	.993	0.000	0.000	0.000	.001	.020
	.295	.331	.129	.065	.061				
N 359.0	0.000	.052	.026	.993	0.000	0.000	0.000	.001	.020
	.295	.331	.129	.065	.061				
N 360.0	0.000	.052	.026	.993	0.000	0.000	0.000	.001	.020
	.295	.331	.129	.065	.061				
N 361.0	0.000	.052	.026	.993	0.000	0.000	0.000	.001	.020
	.295	.331	.129	.065	.061				
N 362.0	0.000	.104	.026	.723	0.000	.007	.008	.010	.065
	.233	.097	.076	.097	.130				
N 363.0	0.000	.104	.026	.723	0.000	.007	.008	.010	.065
	.233	.097	.076	.097	.130				
N 364.2	0.000	.104	.026	.723	0.000	.007	.008	.010	.065
	.233	.097	.076	.097	.130				

ACTIVE DEPOSITS, VOL. IN TONS
NONE SPECIFIED, ASSUMED ZERO
TRIBUTARY INFLOW DATA
G-GS RATING TABLE

L G	300.000	5000.000	10000.000	20000.000
L CLAY	1.260	465.000	1994.000	8550.000
L SILT	5.050	1857.000	7963.000	34137.000
L VFS	2.110	773.000	3316.000	14215.000
L FS	.001	1.000	4.000	26.000
L MS	.002	4.000	22.000	131.000
L CS	.015	23.000	136.000	821.000
L VCS	.008	12.000	70.000	420.000
L VFG	.003	5.000	28.000	167.000
L FG	.001	2.000	13.000	76.000

NO. OF INPUT DATA MESSAGES= 0
END OF SEDIMENT DATA
* B RUN 1,
DOWNSTREAM BOUNDARY DATA
WATER DISCHARGE= 112797.00
ELEVATION= 479.20
TEMPERATURE= 63.00
FLOW DURATION(DAYS) 31.00

ACCUMULATED AC-FT BY ENTRY		CLAY			SILT			SAND		
DAYS	POINT	INFLOW	OUTFLOW	TRAP EFF	INFLOW	OUTFLOW	TRAP EFF	INFLOW	OUTFLOW	TRAP EFF
31.00	364.200	421.27			560.05			3.19		
	361.000	266.36			490.86			157.82		
TOTAL=	343.200	687.63	687.63	-.00	1050.91	1050.91	0.00	161.00	156.17	.03

SECTION ID NO	BED CHANGE FEET	WS ELEV FEET	THALWEG EL FEET	Q CFS	SEDIMENT LOAD IN TONS/DAY CLAY	SILT	SAND
364.200	-.05	485.71	465.95	96427.	8679.	25576.	553.
363.000	-.03	485.37	467.97	96427.	8879.	25576.	1015.
362.000	-.02	485.17	466.98	96427.	8879.	25576.	1418.
361.000	-.05	484.86	457.95	112797.	14493.	47993.	12312.
360.000	.08	484.62	454.08	112797.	14493.	47993.	11619.

Output

359.000	-.05	484.39	455.05	112797.	14493.	47993.	12529.
358.000	-.11	483.93	456.89	112797.	14493.	47993.	13560.
357.000	.04	483.75	464.04	112797.	14493.	47993.	12574.
356.000	-.13	483.12	458.87	112797.	14493.	47993.	14079.
355.000	.18	482.95	454.18	112797.	14493.	47993.	10982.
354.000	-.06	482.58	456.94	112797.	14493.	47993.	12056.
353.000	-.02	482.29	464.98	112797.	14493.	47993.	12411.
352.000	-.14	481.76	455.86	112797.	14493.	47993.	14863.
351.000	.12	481.28	455.12	112797.	14493.	47993.	13192.
350.000	.11	481.05	451.11	112797.	14493.	47993.	11867.
349.000	-.14	480.77	458.86	112797.	14493.	47993.	14269.
348.000	.03	480.31	450.03	112797.	14493.	47993.	13824.
347.000	.05	480.11	454.05	112797.	14493.	47993.	12062.
346.000	.02	479.87	456.02	112797.	14493.	47993.	12309.
345.000	-.00	479.49	444.00	112797.	14493.	47993.	12329.
344.000	.01	479.31	456.01	112797.	14493.	47993.	12045.
343.200	.28	479.20	447.28	112797.	14493.	47993.	10204.

* B RUN 2.
DOWNSTREAM BOUNDARY DATA
WATER DISCHARGE= 55150.00
ELEVATION= 479.40
TEMPERATURE= 72.00
FLOW DURATION(DAYS) 30.00

ACCUMULATED AC-FT BY ENTRY		CLAY			SILT			SAND		
DAYS	POINT	INFLOW	OUTFLOW	TRAP EFF	INFLOW	OUTFLOW	TRAP EFF	INFLOW	OUTFLOW	TRAP EFF
61.00	364.200	491.81			653.77			3.72		
	361.000	326.38			601.49			192.44		
TOTAL=	343.200	818.19	752.46	.08	1255.26	1051.13	.16	196.16	196.73	.20

SECTION ID NO	BED CHANGE FEET	WS ELEV FEET	THALWEG EL FEET	Q CFS	SEDIMENT LOAD IN TONS/DAY CLAY	SILT	SAND
364.000	-.05	481.06	465.85	46971.	1536.	4423.	36.
363.000	-.03	480.87	467.97	46971.	1536.	4423.	36.
362.000	.16	480.76	467.16	46971.	1439.	2305.	37.
361.000	.21	480.64	458.21	55150.	2662.	5526.	2499.
360.000	.28	480.59	454.28	55150.	2595.	4291.	2596.
359.000	.06	480.50	456.06	55150.	2499.	2951.	2764.
358.000	-.11	480.38	456.89	55150.	2499.	2951.	2771.
357.000	.12	480.31	464.12	55150.	2368.	1726.	3081.
356.000	-.13	480.10	458.87	55150.	2368.	1726.	3093.
355.000	.30	480.08	454.30	55150.	2275.	1163.	1881.
354.000	-.04	479.97	456.96	55150.	2204.	846.	2124.
353.000	.03	479.91	465.03	55150.	2088.	496.	2095.
352.000	-.13	479.78	455.87	55150.	2018.	354.	2422.
351.000	.14	479.69	455.14	55150.	1954.	256.	2497.
350.000	.25	479.66	451.25	55150.	1892.	196.	954.
349.000	-.13	479.61	458.87	55150.	1809.	119.	1169.
348.000	.03	479.53	450.03	55150.	1756.	89.	1305.
347.000	.11	479.52	454.11	55150.	1659.	50.	243.
346.000	.03	479.48	456.03	55150.	1570.	29.	156.
345.000	-.00	479.42	444.00	55150.	1526.	22.	327.
344.000	.03	479.41	456.03	55150.	1439.	12.	84.
343.200	.30	479.40	447.30	55150.	1412.	10.	38.